

TE  
662  
.A3  
no.  
FHWA-  
RD-  
78-68

Report No. FHWA-RD-78-68

# STRUCTURE MECHANICS FOR BRIDGE DESIGN



DEPARTMENT OF  
TRANSPORTATION  
FEB 6 1979  
LIBRARY

**July 1977**  
**Final Report**

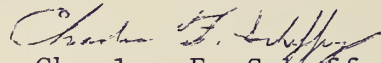
Document is available to the public through  
the National Technical Information Service,  
Springfield, Virginia 22161

**Prepared for**  
**FEDERAL HIGHWAY ADMINISTRATION**  
**Offices of Research & Development**  
**Washington, D. C. 20590**

## FOREWORD

This report, FHWA-RD-78-68, is the result of a study of fracture mechanics under the general direction of Professor Richard Roberts, Lehigh University, Bethlehem, Pennsylvania. It is intended as an aid to the highway bridge engineer in the application of fracture mechanics to the design of highway bridges. This report and accompanying Report FHWA-RD-78-69 have been used as course material for six seminars offered by the Federal Highway Administration on the subject of fracture mechanics for bridge design.

Sufficient copies of the report are being distributed to provide a minimum of one copy to each Regional office, one copy to each Division office, and two copies to each State highway agency. Direct distribution is being made to the Division offices.



Charles F. Scheffey  
Director, Office of Research  
Federal Highway Administration

## NOTICE

This document is disseminated under the sponsorship of the Department of Transportation in the interest of information exchange. The United States Government assumes no liability for its contents or use thereof.

The contents of this report reflect the views of the authors, who are responsible for the facts and the accuracy of the data presented herein. The contents do not necessarily reflect the official views or policy of the Office of Research. This report does not constitute a standard, specification, or regulation.

The United States Government does not endorse products or manufacturers. Trade or manufacturers' names appear herein only because they are considered essential to the object of this document.

1. Report No. <b>FHWA-RD-78-68</b>		2. Government Accession No.		3. Recipient's Catalog No.	
4. Title and Subtitle <b>Fracture Mechanics for Bridge Design</b>			5. Report Date <b>July 1977</b>		
			6. Performing Organization Code		
7. Author(s) <b>R. Roberts, J. M. Barsom, S. T. Rolfe, J. W. Fisher</b>			8. Performing Organization Report No.		
9. Performing Organization Name and Address <b>Coxe Lab., #32 Lehigh University Bethlehem, Pennsylvania 18015</b>			10. Work Unit No. (TRAIS)		
			11. Contract or Grant No. <b>P.O. No. 5-3-0209</b>		
12. Sponsoring Agency Name and Address <b>Department of Transportation Federal Highway Administration Washington, D. C. 20590</b>			13. Type of Report and Period Covered <b>Final Report</b>		
			14. Sponsoring Agency Code		
15. Supplementary Notes <b>Federal Highway Administration Contract Manager: C. H. McGogney (HRS-11)</b>					
16. Abstract  This report provides an introduction to the elements of fracture mechanics for bridge design. Fracture mechanics concepts are introduced and used as the basis for understanding fatigue and fracture in bridge structures. Various applications are cited.					
<div style="border: 1px solid black; padding: 10px; width: fit-content; margin: auto;"> <p>DEPARTMENT OF TRANSPORTATION</p> <p><b>FEB 6 1979</b></p> <p>LIBRARY</p> </div>					
17. Key Words <b>Fracture, Fatigue, Bridges, Bridge Safety, Bridge Design, Bridge Failure</b>			18. Distribution Statement <b>No restrictions. This document is available to the public through the National Technical Information Service, Springfield, Virginia 22161</b>		
19. Security Classif. (of this report) <b>Unclassified</b>		20. Security Classif. (of this page) <b>Unclassified</b>		21. No. of Pages <b>213</b>	22. Price

662  
 A3  
 FHWA  
 RD-  
 78-68

15

## ACKNOWLEDGMENTS

The assistance and guidance of Mr. Charles McGogney and Mr. Jerar Nishanian of the Office of Research of the Federal Highway Administration is gratefully acknowledged. The able assistance of Ms. Jone Svirzofsky in the preparation of the manuscript is also noted.

## PREFACE

Failure of the Point Pleasant Bridge in 1967 and subsequent bridge failures caused the various sectors of the bridge building industry to reevaluate existing codes and standards as related to bridge design, fabrication and overall safety. The traditional forum for such deliberations and evaluations by federal officials, state officials and private industry is the American Association of State Highway and Transportation Officials (AASHTO). This organization has recently put forward a set of fracture toughness requirements for bridge steels as well as modifying their existing fatigue standards so that the combination, the fatigue and fracture guidelines, reflect the best current thinking with respect to bridge safety. One purpose of this report is to examine the current AASHTO fatigue and fracture guidelines and to discuss the technical basis for them.

The material presented in this report was prepared by Dr. John Barsom, United States Steel Corporation, Monroeville, Pennsylvania, Dr. John Fisher, Lehigh University, Bethlehem, Pennsylvania, Dr. Richard Roberts, Lehigh University, Bethlehem, Pennsylvania, and Dr. Stanley Rolfe, University of Kansas, Lawrence, Kansas. Dr. Roberts served as overall coordinator for this project while major responsibility for the preparation of the individual chapters was as follows: Chapter 1, Rolfe; Chapter 2, Barsom; Chapter 3, Fisher; Chapter 4, Roberts; Chapter 5, Rolfe and Fisher. Financial support for this project was provided by the Office of Research of the Federal Highway Administration through Purchase Order No. 5-3-0209. This effort was monitored technically by Mr. C. McGogney of the Federal Highway Administration Office of Research.

The reader should keep in mind that the information presented here is of an elementary nature, intended to provide an introduction to the concepts of Fatigue and Fracture mechanics. As such, only the material considered essential to an introductory view has been chosen by the authors. To this end the report provides an introduction to Fracture Mechanics and discussions of how Fracture Mechanics is applied to fatigue and fracture requirements. The specific AASHTO specifications related to fatigue design and material toughness requirements are presented and discussed. Finally, a number of bridge failures are examined to highlight the use of Fracture Mechanics.

As a final note it is the authors' intent and understanding that the material in this report is intended for general information only, and should not be used in relation to any specific application without independent examination and verification of its applicability and suitability by professionally qualified personnel. Those making use thereof or relying thereon assume all risk and liability arising from such use or reliance.

## TABLE OF CONTENTS

Chapter	Page
DOT COVER SHEET . . . . .	i
ACKNOWLEDGMENTS . . . . .	ii
PREFACE . . . . .	iii
TABLE OF CONTENTS . . . . .	v
<b>1</b> INTRODUCTION AND OVERVIEW OF FRACTURE MECHANICS AS RELATED TO BRIDGE STRUCTURES. . . . .	1
1.1 Introduction . . . . .	1
1.2 Notch-Toughness Testing. . . . .	5
1.3 Brittle-Fracture Design Considerations . . . . .	10
1.4 Introduction to Fracture Mechanics . . . . .	13
REFERENCES. . . . .	19
FIGURES . . . . .	21
<b>2</b> CONCEPTS OF FRACTURE MECHANICS – FATIGUE AND FRACTURE CONTROL . . . . .	31
2.1 General Discussion . . . . .	31
2.2 Fracture-Mechanics Methodology . . . . .	31
2.3 Fatigue-Crack Initiation . . . . .	34
2.4 Fatigue-Crack Propagation. . . . .	38
2.5 Fracture Toughness . . . . .	42
2.6 Fracture-Control Plan. . . . .	47
REFERENCES. . . . .	53
FIGURES . . . . .	55
<b>3</b> FATIGUE BEHAVIOR OF WELDMENTS AND THE AASHTO REQUIREMENTS. . . . .	76
3.1 Introduction . . . . .	76
3.2 Fatigue of Welded Details. . . . .	77
3.3 AASHTO Fatigue Requirements. . . . .	84
REFERENCES. . . . .	90
TABLES. . . . .	91
FIGURES . . . . .	92

Chapter		Page
4	FRACTURE BEHAVIOR AND THE AASHTO FRACTURE REQUIREMENTS. . . . .	120
	4.1 Introduction . . . . .	120
	4.2 Fracture Appearance Tests. . . . .	122
	4.3 Fracture Energy Measurements . . . . .	124
	4.4 Fracture Mechanics Measurements. . . . .	124
	4.5 Bridge Steel Behavior. . . . .	127
	4.6 AASHTO Fracture Toughness Requirements . . . . .	130
	REFERENCES. . . . .	133
	TABLES. . . . .	135
	FIGURES . . . . .	136
5	BRIDGE FAILURE EXAMPLES . . . . .	155
	5.1 Introduction . . . . .	155
	5.2 A Fracture Mechanics Analysis of the Bryte Bend Bridge Fracture. . . . .	155
	5.3 Analysis of Crack Growth in the Quinipiac River Bridge . . . . .	163
	REFERENCES. . . . .	172
	FIGURES . . . . .	173



# CHAPTER 1. INTRODUCTION AND OVERVIEW OF FRACTURE MECHANICS AS RELATED TO BRIDGE STRUCTURES

## 1.1 INTRODUCTION

Brittle fracture is a type of catastrophic failure in structural steels that usually occurs without prior plastic deformation. Furthermore, once started the fracture processes proceed with such rapidity [i.e., the cracks travel at speeds approaching 7000 ft/sec (2134 m/sec)] that generally no time is available to take corrective action. The fracture is usually characterized by a flat fracture surface (cleavage) with little or no shear lips, as shown in Figure 1.1, and at average stress levels below those of general yielding. Brittle fractures are not so common as fatigue, yielding, or buckling failures, but when they do occur they may be more costly in terms of human life and/or property damage.<sup>1)\*</sup>

Although brittle fractures such as shown in Figures 1.1 and 1.2 have occurred in many types of structures,<sup>1-5)</sup> including bridges,<sup>6)</sup> the bridge-building industry did not pay particular attention to the possibility of brittle fractures in bridges until the failure of the Point Pleasant Bridge at Point Pleasant, West Virginia. On December 15, 1967, this bridge collapsed without warning, resulting in the loss of 46 lives. Photographs of this eyebar suspension bridge before and after collapse are shown in Figures 1.3 and 1.4.

---

\*See references.

An extensive investigation of the collapse was conducted by the National Transportation Safety Board (NTSB),<sup>7)</sup> and their conclusion was "that the cause of the bridge collapse was the cleavage fracture in the lower limb of the eye of eyebar 330 at joint C13N of the north eyebar suspension chain in the Ohio side span." Because the failure was unique in several ways, numerous investigations of the failure were made.

Extensive use of fracture mechanics was made by Bennett and Mindlin<sup>8)</sup> in their metallurgical investigation of the Point Pleasant Bridge and they concluded that

1. "The fracture in the lower limb of the eye of eyebar 330 was caused by the growth of a flaw to a critical size for fracture under normal working stress.
2. The initial flaw was due to stress-corrosion cracking from the surface of the hole in the eye. There is some evidence that hydrogen sulfide was the reagent responsible for the stress-corrosion cracking. (The final report indicates that the initial flaw was due to fatigue, stress-corrosion cracking and/or corrosion fatigue<sup>7)</sup>.)
3. The composition and heat treatment of the eyebar produced a steel with very low fracture toughness at the failure temperature.
4. The fracture resulted from a combination of factors; in the absence of any of these it probably would not have occurred: (a) the high hardness of the steel

which rendered it susceptible to stress-corrosion cracking; (b) the close spacing of the components in the joint which made it impossible to apply paint to the most highly stressed region of the eye, yet provided a crevice in this region where water could collect; (c) the high design load of the eyebar chain, which resulted in a local stress at the inside of the eye greater than the yield strength of the steel; and (d) the low fracture toughness of the steel which permitted the initiation of complete fracture from the slowly propagating stress-corrosion crack when it had reached a depth of only 0.12 in. (3.0 mm) (Figure 1.5)."

Since the time of the Point Pleasant bridge failure, other brittle fractures have occurred in steel bridges as a result of unsatisfactory fabrication methods, design details, or material properties.<sup>9,10)</sup> (These failures, as well as others, will be discussed in this short course.) These and other brittle fractures led to an increasing concern about the possibility of brittle fractures in steel bridges and resulted in the AASHTO (American Association of State Highway and Transportation Officials) Material Toughness Requirements being adopted in 1973.<sup>11)</sup>

The AASHTO toughness requirements were based on the science of fracture mechanics, which has shown that because of the *interrelation among materials, design, and fabrication*, brittle fractures cannot be eliminated in structures merely by using

materials with improved notch toughness. The designer still has fundamental responsibility for the overall safety and reliability of his structure. It is the objective of this course to show how fracture mechanics can be used in design to *prevent* brittle fractures and fatigue failures of bridge structures.

The science of *fracture mechanics* can be used to describe *quantitatively* the trade-offs among the three factors that control the susceptibility of a structure to fracture (stress, material toughness, and flaw size) so that the designer can determine the relative importance of each of them during *design* rather than during *failure analysis*. In general this will take the form

$$K_{Ic} = \sigma f(a)$$

where  $K_{Ic}$  is the plane strain fracture toughness which is a measure of a material's ability to resist brittle fracture,  $\sigma$  is the applied stress or load and  $f(a)$  represents the dependence on flaw size "a". Similar relationships will be examined in detail later.

As will be emphasized in this short course, fracture control, or fracture prevention in structures cannot be accomplished merely by specifying that the materials have a certain level of notch toughness. This approach is too simplistic and for those cases involving fatigue, it is inadequate. The designer should analyze all aspects of fracture control, and one of the primary purposes of this short course is to provide the designer with the necessary information to develop a safe, reliable bridge structure.

## 1.2 NOTCH-TOUGHNESS TESTING

In addition to the traditional mechanical property tests that measure strength, ductility, modulus of elasticity, etc., there are many tests available to measure some form of notch toughness. *Notch toughness* is defined as the ability of a material to absorb energy (usually when loaded dynamically) in the presence of a flaw, whereas *toughness* of a material is defined as the ability of a smooth member (unnotched) to absorb energy, usually when loaded slowly. Notch toughness is measured with a variety of specimens such as the Charpy V-Notch impact specimen, dynamic tear test specimen,  $K_{Ic}$ , precracked Charpy, etc., while toughness is usually characterized by the area under a stress-strain curve in a slow tension test. It is the presence of a notch or some other form of stress raiser that makes structural materials susceptible to brittle fracture under certain conditions.

Traditionally, the notch-toughness characteristics of low-and-intermediate-strength bridge steels have been described in terms of the transition from brittle to ductile behavior as measured by various types of impact tests. Most structural steels can fail in either a ductile or brittle manner depending on several conditions such as temperature, loading rate, and constraint. Ductile fractures are generally preceded by large amounts of plastic deformation and usually occur at  $45^\circ$  to the direction of the applied stress. Brittle or cleavage fractures generally occur with little plastic deformation and are usually normal to the direction of the principal stress. The transition

from one type of fracture behavior to the other generally occurs with changes in service conditions such as the state of stress, temperature, or strain rate.

This transition in fracture behavior can be related schematically to various fracture states, as shown in Figure 1.6. Plane-strain behavior refers to fracture under elastic stresses with little or no shear lip development, and it is essentially brittle. Plastic behavior refers to ductile failure under general yielding conditions accompanied usually, but not necessarily, with large shear lips. The transition between these two extremes is the elastic-plastic region, which is also referred to as the mixed-mode region.

For static loading, the transition region occurs at lower temperatures than for impact (or dynamic) loading. Thus, for structures subjected to static loading, the static transition curve should be used to predict the level of performance at the service temperature.

For structures subjected to some intermediate loading rate, an intermediate loading-rate transition curve should be used to predict the level of performance at the service temperature. Because the actual loading rates for many structures are not well defined, the impact loading curve (Figure 1.6) is often used to predict the service performance of structures even though the actual loading may be slow or intermediate. This practice is somewhat conservative and helps to explain why many structures that have low toughness as measured by impact tests have not

failed even though their service temperatures are well below an impact transition temperature. As noted in Figure 1.6, a particular notch-toughness value called the nil-ductility transition (NDT) temperature generally defines the upper limits of plane-strain behavior under conditions of impact loading.

One of the fundamental questions to be resolved regarding the interpretation of any particular toughness test for large structures is as follows: What level of material performance should be required for satisfactory performance in a particular structure? That is, as shown schematically in Figure 1.7 for impact loading, one of the following three general levels of material performance could be established at the service temperature of 32°F for a structural material.

1. Plane-strain behavior - steel 1.
2. Elastic-plastic behavior - steel 2.
3. Fully plastic behavior - steel 3.

Although fully plastic behavior would be a very desirable level of performance for structural materials, it may not be necessary or even economically feasible for many structures. That is, for a large number of structures, a reasonable level of elastic-plastic behavior (steel 2, Figure 1.7) is often satisfactory to prevent initiation of brittle fractures provided the design and fabrication are satisfactory.

The general purpose of the various kinds of notch-toughness tests is to model the behavior of actual structures so that the laboratory test results can be used to predict service

performance. In this sense many different tests have been used to measure the notch toughness of structural materials. These include Charpy V-notch (CVN) impact, drop weight NDT, dynamic tear (DT), wide plate, Battelle drop weight tear test (DWTT), pre-cracked Charpy, as well as many others. A description of most of these tests can be found in Chapter 4 of this text and References 1-3. Generally these notch-toughness tests were developed for specific purposes. For example, the CVN test is widely used as a screening test in alloy development as well as a fabrication and quality control test. In addition, because of correlations with service experience, the CVN test is often used in steel specifications for various structural, marine, and pressure-vessel applications. The NDT test is used to establish the minimum service temperature for various navy and marine applications, whereas the Battelle DWTT test was developed to measure the fracture appearance of line pipe steels as a function of temperature. The precracked Charpy test was developed by introducing a sharp crack into a CVN specimen to model the behavior in actual structures in which sharp cracks may be present.

All these notch-toughness tests generally have one thing in common, however, and that is to produce fracture in steels under carefully controlled laboratory conditions. Hopefully, the results of the test can be correlated with service performance to establish levels of performance, as shown in Figure 1.6, for various materials being considered for specific applications. In fact, the results of the above mentioned tests have been



extremely useful in many structural applications. Structural energy, deformation, and ability to absorb energy, etc., are all important structural parameters, and these tests have served as very good guidelines for the structural engineer.

However, even if correlations are developed for existing structures, they do not necessarily hold for certain designs, new operating conditions, or new materials because the results, which are expressed in terms of energy, fracture appearance, or deformation, cannot always be translated into structural design and engineering parameters such as stress and flaw size. Thus, a much better way to measure notch toughness is with principles of fracture mechanics. Fracture mechanics is a method of characterizing the fracture behavior in structural parameters that can be used directly by the engineer, namely stress and flaw size. Fracture mechanics is based on a stress analysis and thus does not depend on the use of extensive service experience to translate laboratory results into practical design information so long as the engineer can determine the material toughness, nominal stress, and flaw size in a particular structural member.

Fracture mechanics can account for the effect of temperature and loading rate on the behavior of structural members that have sharp cracks. It is becoming recognized that many large complex structures have discontinuities of some kind. Thus, the results of a fracture-mechanics analysis for a particular application (specimen size, service temperature, and loading rate) will yield the combinations of stress level and flaw size that would be

required to cause fracture. The engineer can then *quantitatively* establish allowable stress levels and inspection requirements so that fractures cannot occur. In addition, fracture mechanics can be used to analyze the growth of small cracks (for example, by fatigue loading or stress-corrosion) to critical size. Therefore, fracture mechanics has several very definite advantages compared with traditional notch-toughness tests and finally offers the designer a very definitive method of quantitatively designing to prevent brittle fracture in structures.

This is not to imply that the traditional notch-toughness tests are not still useful. In fact, there are many empirical correlations between fracture-mechanics values and existing toughness test results such as Charpy V-notch, dynamic tear, NDT, precracked Charpy, etc., that are extremely useful to the engineer. Because of the current limitations on test requirements for measuring  $K_{IC}$  as discussed in Chapter 4, existing notch-toughness tests must be used in many cases to help the designer estimate  $K_{IC}$  values for a particular material, as well as for quality-control or specification purposes such as the AASHTO toughness requirements.

### 1.3 BRITTLE-FRACTURE DESIGN CONSIDERATIONS

In addition to the catastrophic failures described in Section 1.1, there have been *numerous* "minor" failures of structures during construction or service that have resulted in delays, repairs, and inconveniences, some of which are very expensive. Nonetheless, compared with the total number of engineering

structures that have been built throughout the world, the number of catastrophic brittle fractures has been very small. As a result, the designer seldom concerns himself with the notch toughness of structural materials because the failure rate of most structures is very low. Nonetheless,

1. When designs become more complex,
2. When the use of high-strength thick welded plates becomes more common compared with the use of lower-strength thin riveted plates,
3. When the choice of construction practices becomes more dependent on minimum cost,
4. When the magnitude of loadings increases, and
5. When actual factors of safety decrease because of more precise computer designs,

the possibility of brittle fractures in large complex structures must be considered, and the designer must become more aware of available methods to prevent brittle failures.

The state-of-the-art *is* that fracture mechanics concepts *are* available that can be used in the design of structures to prevent brittle fractures.

Design codes often include this fact, and in the early 1970s, several design and materials specifications *based on concepts of fracture mechanics* were adopted by various engineering professions, including the American Association of State Highway and Transportation Officials-Notch Toughness Requirements for Bridge Steels. <sup>11)</sup>

The traditional design approach for most structures is generally based on the use of safety factors to limit the maximum calculated stress level to some percentage of either the yield or ultimate stress. It is suggested by Weck<sup>12)</sup> that this approach is somewhat outdated.

The factor of safety approach, by itself, does not always give the proper assurance of safety with respect to brittle fracture because large complex structures are not fabricated without some kind of discontinuities. Numerous failure investigations and inspections have shown this to be true. Research by Fisher and Yen<sup>13)</sup> has shown that discontinuities exist in practically all structural members, either from manufacture or from the process of fabricating the members by rolling, machining, punching, or welding. The sizes of these discontinuities range from very small microdiscontinuities (<0.01 in.) to several inches long.

In almost every brittle fracture that has occurred in structures, some type of discontinuity was present. These included very small arc strikes in some of the World War II ship failures, very small fatigue cracks (~0.07 in.) in the Comet airplane failures,<sup>14)</sup> and stress-corrosion or corrosion fatigue cracks (0.12 in.) in the critical eyebar of the Point Pleasant Bridge.<sup>7-8)</sup> Other failures, such as the 260-in.-diameter missile motor case that failed during hydrotest or the F-111 aircraft failure, had somewhat larger, but still undetected, cracks.<sup>1)</sup>

Bravenec<sup>15)</sup> has reviewed various brittle fractures during fabrication and testing and has shown that cracks have originated from torch-cut edges, mechanical gouges, corrosion pits, weld repairs, severe stress concentrations, etc. Dolan<sup>16)</sup> has made the flat statement that "*every structure* contains small flaws whose size and distribution are dependent upon the material and its processing. These may range from nonmetallic inclusions and microvoids to weld defects, grinding cracks, quench cracks, surface laps, etc."

The significant point is that discontinuities or cracks *are* present in many large fabricated structures even though the structure may have been "inspected." Methods of inspection or nondestructive testing are gradually improving, with the result that smaller and smaller discontinuities are becoming detectable. But the fact is that discontinuities are present regardless of whether or not they are discovered. In fact, the problem of establishing acceptable levels of discontinuities in welds is becoming somewhat of an economic problem since techniques that minimize the size and distribution of discontinuities are available if the engineer chooses to use them.

#### 1.4 INTRODUCTION TO FRACTURE MECHANICS

An overwhelming amount of research on brittle fracture in structures of all types has shown that numerous factors (e.g., service temperature, material toughness, design, welding, residual stresses, fatigue, constraint, etc.) can contribute to brittle fractures in large welded structures. However, the recent develop-

ment of fracture mechanics has shown that there are three *primary* factors that control the susceptibility of a structure to brittle fracture:

1. Material Toughness ( $K_C$ ,  $K_{IC}$ ,  $K_{Id}$ )

Material Toughness can be defined as the ability to carry load or deform plastically in the presence of a notch and can be described in terms of the critical stress-intensity factor under conditions of plane stress ( $K_C$ ) or plane strain ( $K_{IC}$ ) for slow loading and linear elastic behavior.  $K_{Id}$  is a measure of the critical material toughness under conditions of maximum constraint (plane strain) and impact or dynamic loading, also for linear elastic behavior. For elastic-plastic behavior (materials with higher levels of notch toughness than linear elastic behavior) the material toughness measured in terms of more appropriate elastic-plastic type parameters as discussed in Reference 1. In addition to metallurgical factors such as composition and heat treatment, the notch toughness of a steel also depends on the application temperature, loading rate, and constraint (state-of-stress) ahead of the notch.

2. Crack Size (a)

Brittle fractures initiate from discontinuities of various kinds. These discontinuities can vary

from extremely small cracks within a weld arc strike (as was the case in the brittle fracture of a T-2 tanker during World War II) to much larger weld or fatigue cracks. Complex welded structures are not fabricated without discontinuities (porosity, lack of fusion, toe cracks, mismatch, etc.), although good fabrication practice and inspection can minimize the original size and number of cracks. Thus, these discontinuities will be present in many welded structures even after all inspections and weld repairs are finished. Furthermore even though only "small" discontinuities may be present initially, these discontinuities can grow by fatigue or stress-corrosion, possibly to a critical size.

### 3. Stress Level ( $\sigma$ )

Tensile stresses (nominal, residual, or both) are necessary for brittle fractures to occur. These stresses are determined by conventional stress analysis techniques for particular structures.

These three factors are the primary ones that control the susceptibility of a structure to brittle fracture. All other factors such as temperature, loading rate, stress concentrations, residual stresses, etc., merely affect the above three *primary* factors.

Engineers have known these facts for many years and have reduced the susceptibility of structures to brittle fractures

by controlling the above factors in their structures *qualitatively*. That is, good design (e.g., adequate sections, minimum stress concentrations) and fabrication practices (decreased discontinuity size because of proper welding control and inspection), as well as the use of materials with good notch-toughness levels (e.g., as measured with a Charpy V-notch impact test), will minimize and have minimized the probability of brittle fractures in structures. However, the engineer has not had specified design guidelines to evaluate the relative performance and economic trade-offs among design, fabrication, and materials in a *quantitative* manner.

The recent development of fracture mechanics as an applied science has shown that all three of the above factors can be interrelated to predict (or to design against) the susceptibility of various structures to brittle fracture. Fracture mechanics is a method of characterizing fracture behavior in structural parameters familiar to the engineer, namely, stress and crack size. Linear-elastic fracture-mechanics technology is based on an analytical procedure that relates the stress-field magnitude and distribution in the vicinity of a crack tip to the nominal stress applied to the structure, to the size, shape, and orientation of the crack or crack-like discontinuity, and to the material properties. To establish methods of stress analysis for cracks in elastic solids, it is convenient to define three types of relative movements of two crack surfaces. These displacement modes in Figure 1.8 represent the local deformation in an infinitesimal element containing a crack front. The opening mode, Mode I, is characterized by local



displacements that are symmetric with respect to the  $x-y$  and  $x-z$  planes. The two fracture surfaces are displaced perpendicular to each other in opposite directions. Local displacements in the sliding or shear mode, Mode II, are symmetric with respect to the  $x-y$  plane and skew symmetric with respect to the  $x-z$  plane. The two fracture surfaces slide over each other in a direction perpendicular to the line of the crack tip. The tearing mode, Mode III, is associated with local displacements that are skew symmetric with respect to both  $x-y$  and  $x-z$  planes. The two fracture surfaces slide over each other in a direction that is parallel to the line of the crack front. Each of these modes of deformation corresponds to a basic type of stress field in the vicinity of crack tips.

Figure 1.9 shows the equations that describe the elastic-stress field in the vicinity of a crack tip in a body subjected to tensile stresses normal to the plane of the crack. The stress-field equations show that the distribution of the elastic-stress field in the vicinity of the crack tip is invariant in all structural components subjected to this type (Mode I) of deformation and that the magnitude of the elastic-stress field can be described by a single parameter,  $K_I$ , designated the stress-intensity factor. Consequently, the applied stress, the crack shape, size, and orientation, and the structural configuration associated with structural components subjected to this type of deformation affect the value of the stress-intensity factor but do not alter the stress-field distribution. Thus it is possible to translate laboratory results into practical design information without the use of extensive

service experience or correlations. Examples of some of the more widely used stress-flaw size relations are presented in Figure 1.10.

One of the underlying principles of fracture mechanics is that unstable fracture occurs when the stress-intensity factor at the crack tip reaches a critical value,  $K_{IC}$ . For Mode I deformation and for small crack-tip plastic deformation (plane-strain conditions), the critical-stress-intensity factor for fracture instability is designated  $K_{IC}$ .

The critical-stress-intensity factor,  $K_{IC}$ , represents the terminal conditions in the life of a structural component. The total useful life of the component is determined by the time necessary to initiate a crack and to propagate the crack from subcritical dimensions to the critical crack size,  $a_c$ . Crack initiation and subcritical crack propagation may be caused by cyclic stresses in the absence of an aggressive environment, by an aggressive environment under sustained load, or by the combined effects of cyclic stresses and an aggressive environment. Because all these modes of subcritical crack propagation are localized phenomena that depend on the boundary conditions at the crack tip, it is logical to expect the rate of subcritical crack propagation to depend on the stress-intensity factor,  $K_I$ , which serves as a single-term parameter representative of the stress conditions in the vicinity of the crack tip. Thus fracture mechanics theory can be used to analyze the behavior of a structure throughout its entire life as will be described in subsequent sessions.

## REFERENCES

1. S. T. Rolfe and J. M. Barsom, Fracture and Fatigue Control in Structures - Applications of Fracture Mechanics, Prentice Hall, New Jersey, 1976.
2. E. R. Parker, Brittle Behavior of Engineering Structures, prepared for the Ship Structure Committee under the general direction of the Committee on Ship Steel-National Academy of Sciences-National Research Council, Wiley, New York, 1957.
3. M. E. Shank, "A Critical Review of Brittle Failure in Carbon Plate Steel Structures Other than Ships," Ship Structure Committee Report, Serial No. SSC-65, National Academy of Sciences-National Research Council, Washington, D.C., Dec. 1, 1953 (also reprinted as Welding Research Council Bulletin).
4. H. G. Acker, "Review of Welded Ship Failures," Ship Structure Committee Report, Serial No. SSC-63, National Academy of Sciences-National Research Council, Washington, D.C., Dec. 15, 1953.
5. Marine Casualty Report, "Structural Failure of the Tank Barge I.O.S. 3301 Involving the Motor Vessel Martha R. Ingram on 10 January 1972 Without Loss of Life," Report No. SDCG/NTSB, March 74-1.
6. R. B. Madison & G. R. Irwin, "Fracture Analysis of Kings Bridge, Melbourne," Journal of the Structural Division, ASCE Vol. 97, No. ST 9, Proc. Paper 8377, Spet. 1971, pp 2229-2244.
7. "Collapse of U.S. 35 Highway Bridge, Point Pleasant, West Virginia," NTSB Report No. NTSB-HAR-71-1, Dec. 15, 1967.
8. J. A. Bennett and Harold Mindlin, "Metallurgical Aspects of the Failure of the Pt. Pleasant Bridge," Journal of Testing and Evaluation, March 1973, pp. 152-161.
9. "State Cites Defective Steel in Bryte Bend Failure," Engineering News Record, 185, No. 8, Aug. 20, 1970.
10. "Joint Redesign on Cracked Box Girder Cuts into Record Tied Arch's Beauty," Engineering News Record, 188, No. 13, March 30, 1972.
11. American Association of State Highway and Transportation Officials - Material Specifications, Association General Offices, Washington, D.C., 1974.
12. R. Weck, "A Rational Approach to Standards for Welded Construction," British Welding Journal, Nov. 1966.

13. J. W. Fisher and B. T. Yen, "Design, Structural Details, and Discontinuities in Steel, Safety and Reliability of Metal Structures," ASCE, Nov. 2, 1972.
14. T. Bishop, "Fatigue and the Comet Disasters," Metal Progress, May 1955, p. 79.
15. E. V. Bravenec, "Analysis of Brittle Fractures During Fabrication and Testing," ASCE, March 1972.
16. T. J. Dolan, "Preclude Failure: A Philosophy for Materials Selection and Simulated Service Testing," Wm. M. Murray Lecture, SESA Fall Meeting, Houston, Oct. 1969, published SESA Journal of Experimental Mechanics, Jan. 1970.

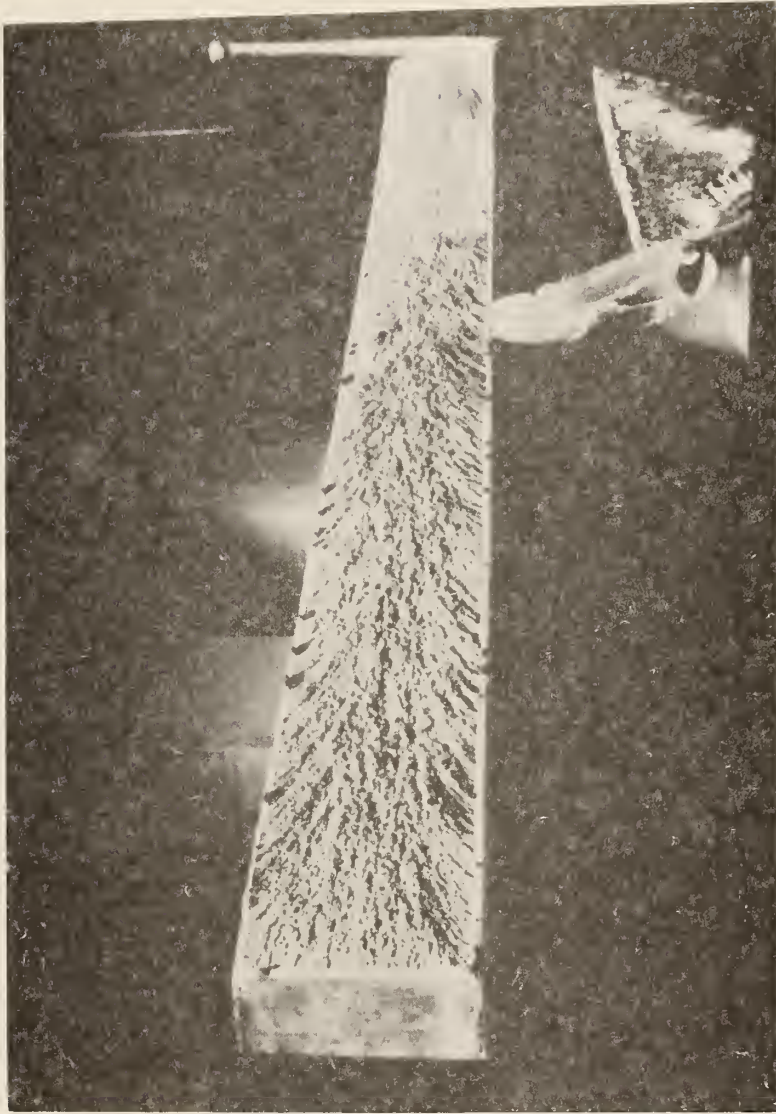


Figure 1-1 Photograph of typical brittle fracture surface in flange plate.

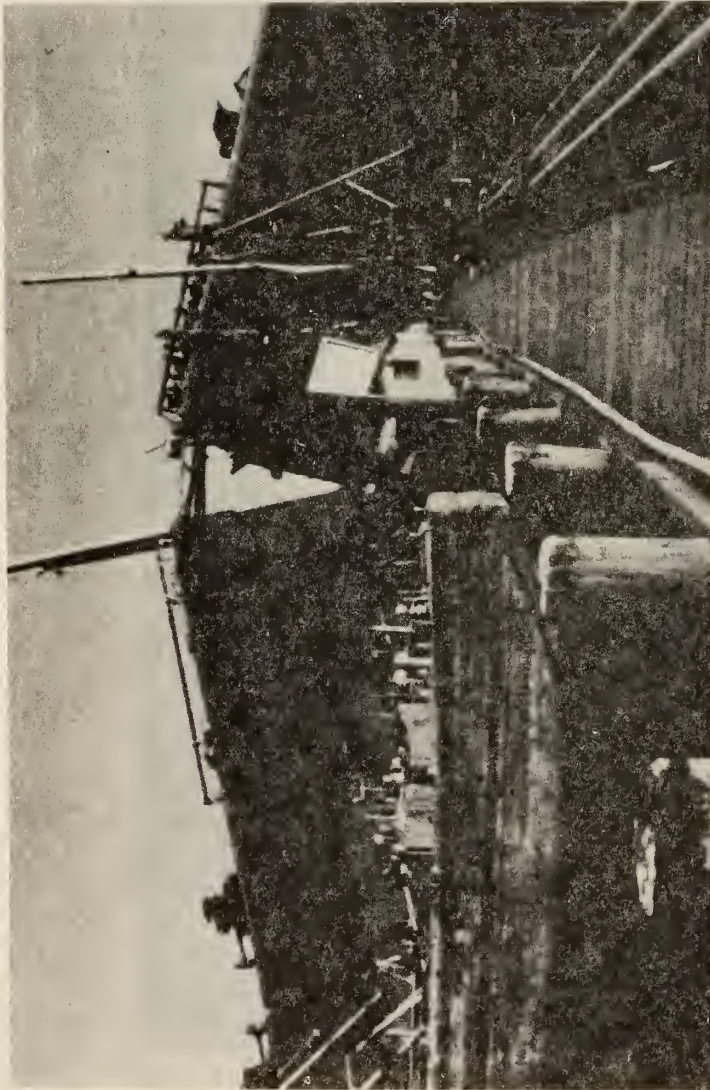


Figure 1-2 Brittle fracture of ship in 1972.



Figure 1-3 Photograph of St. Mary's Bridge similar to the Point Pleasant Bridge before collapse.

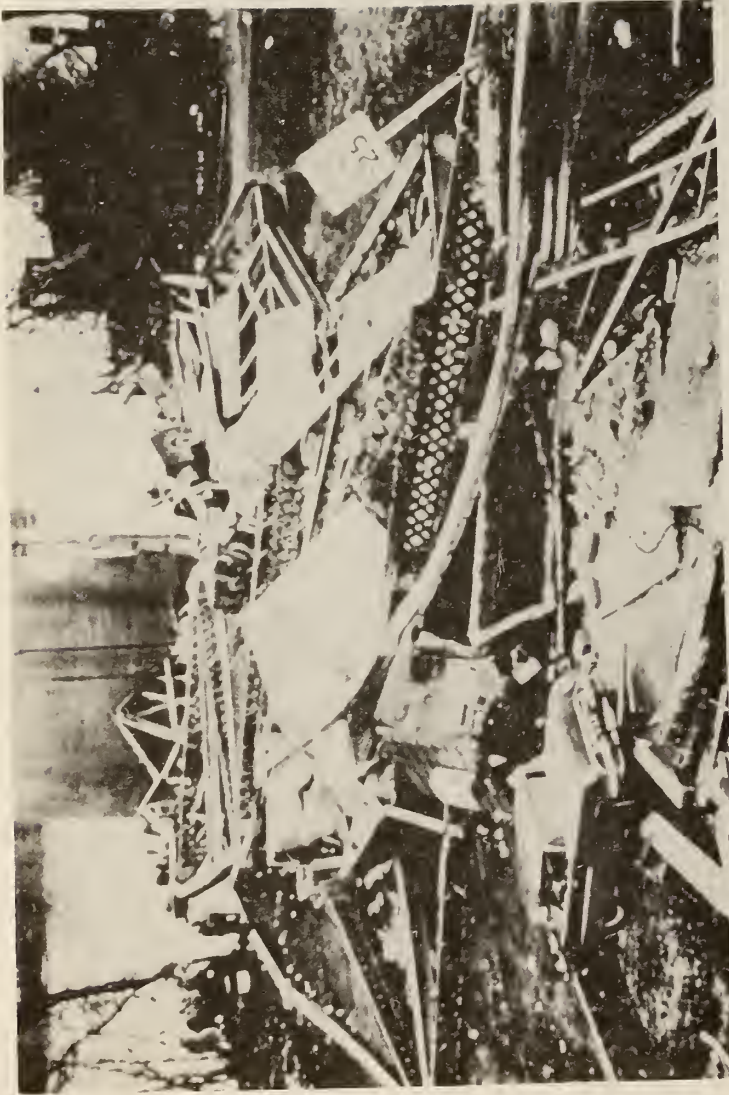


Figure 1-4 Photograph of Point Pleasant Bridge after collapse.



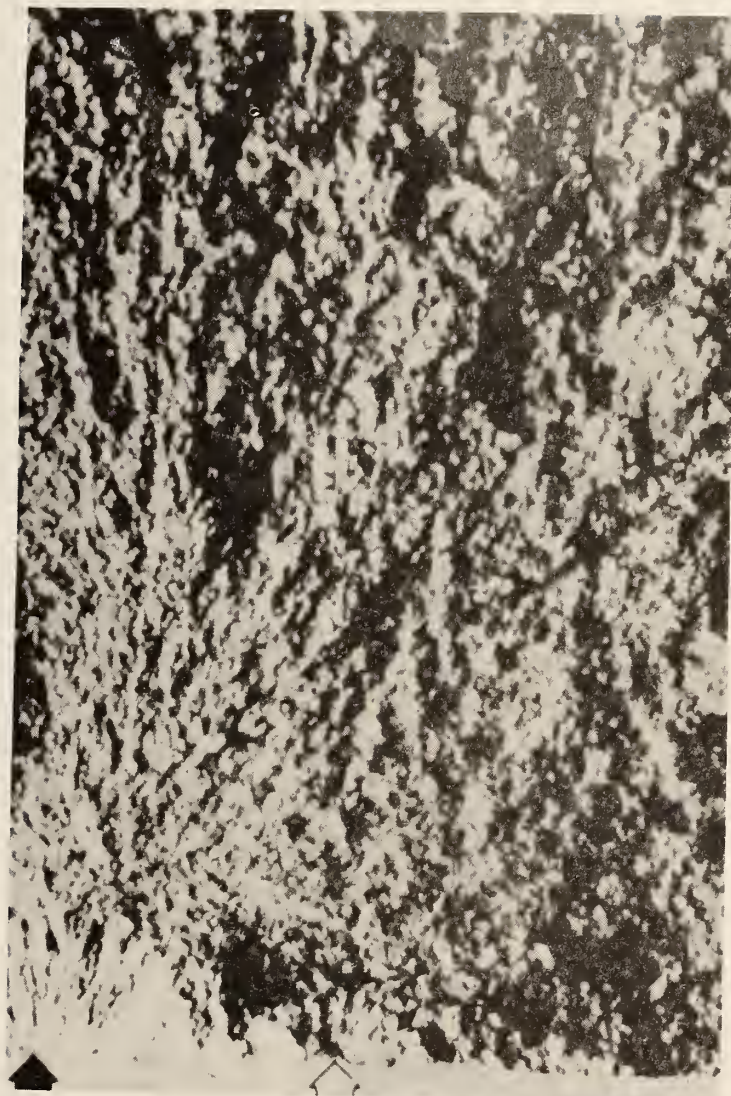


Figure 1-5 Photograph showing origin of failure in Point Pleasant Bridge.

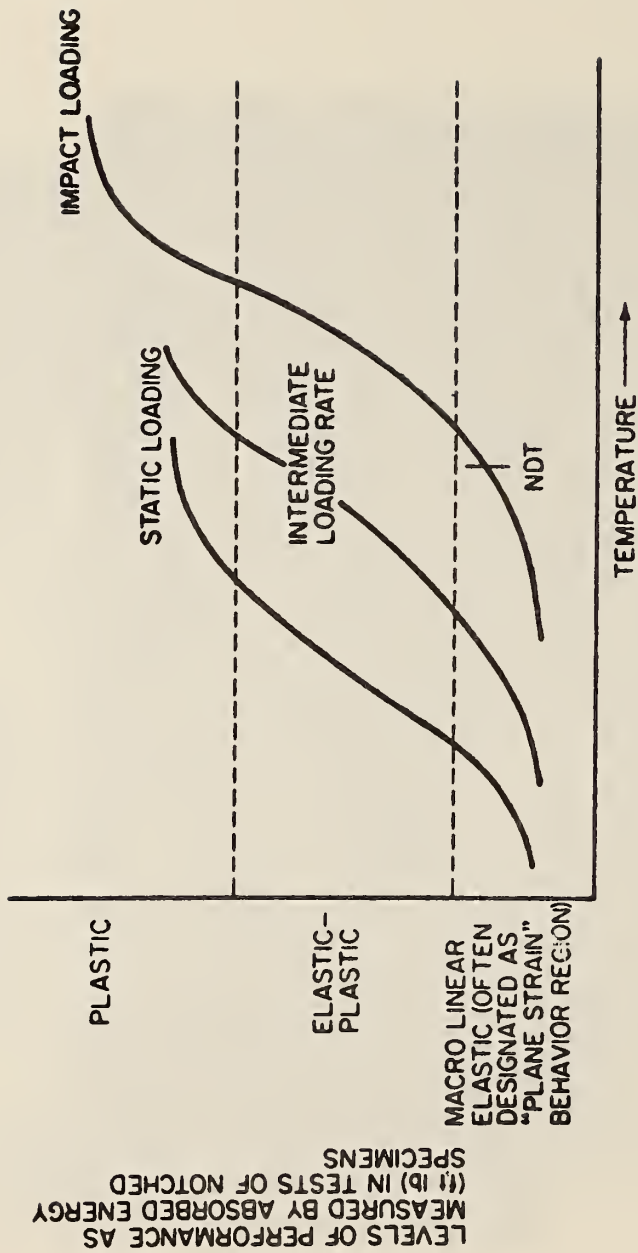


Figure 1-6 Schematic showing relation between notch-toughness test results and levels of structural performance for various loading rates.

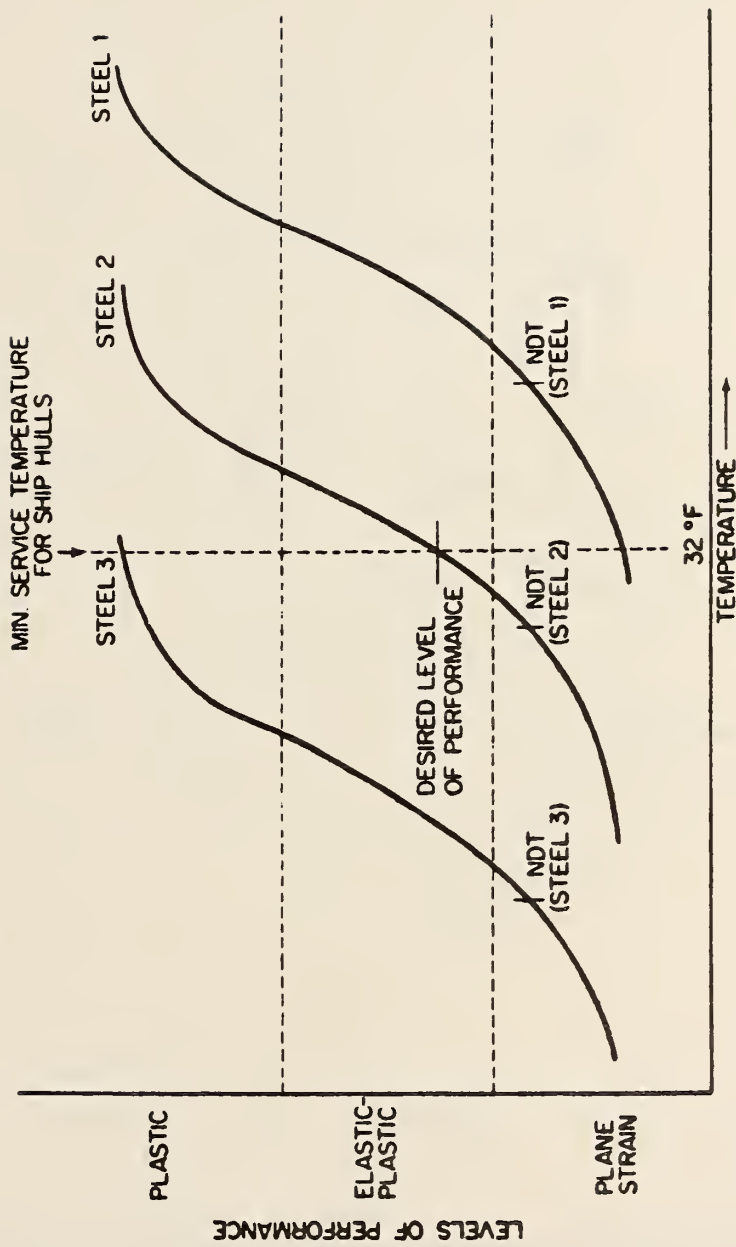


Figure 1-7 Schematic showing relation between level of performance and transition temperature for 3 arbitrary steels loaded under impact conditions.

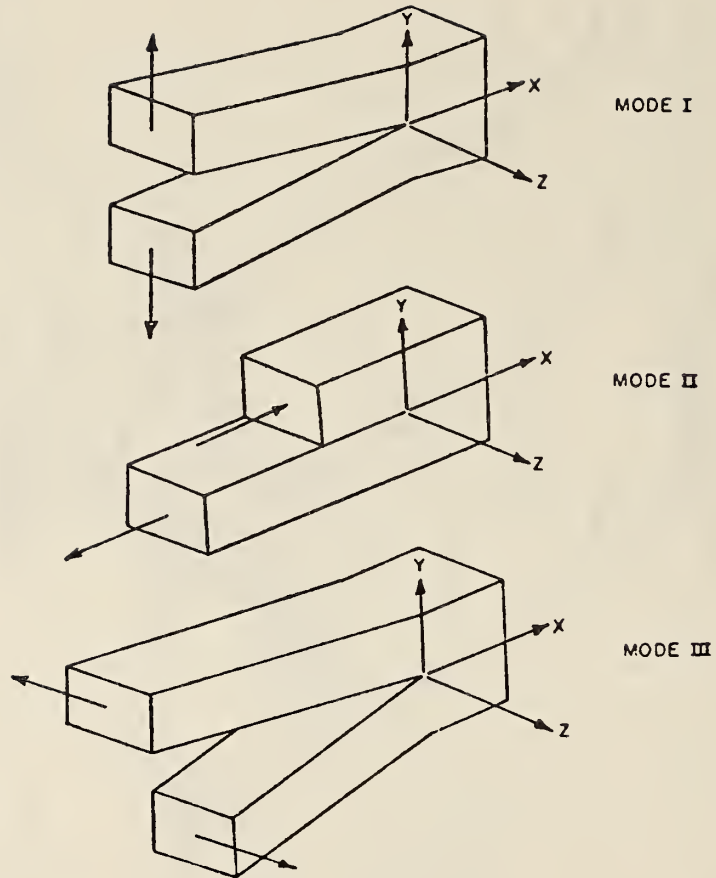


Figure I-8 The three basic modes of crack surface displacements.

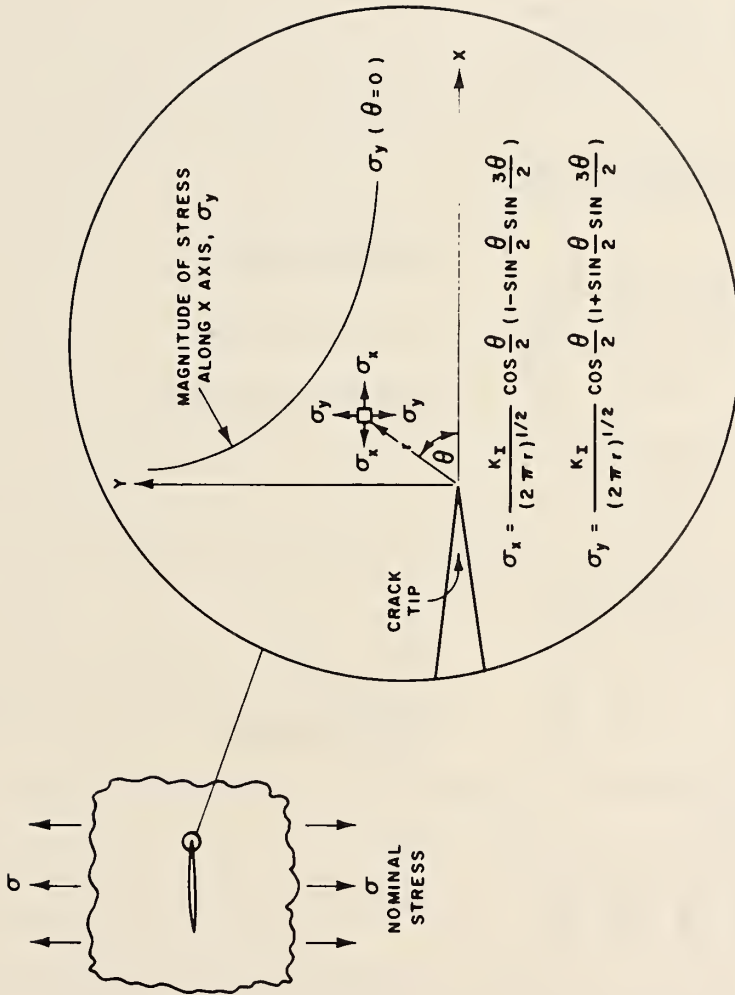
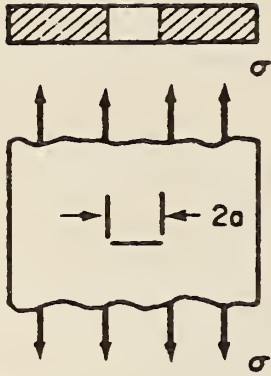
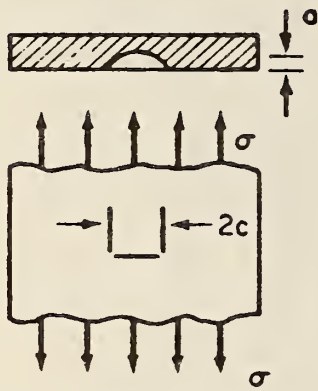


Figure 1-9 Elastic-stress-field distribution ahead of a crack.



THROUGH THICKNESS CRACK

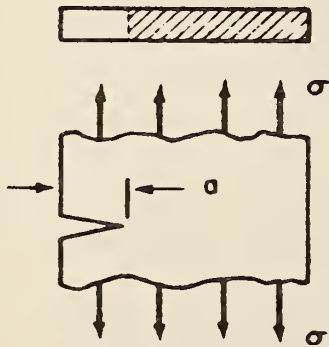
$$K_I = \sigma \sqrt{\pi a}$$



SURFACE CRACK

$$K_I = 1.12 \sigma \sqrt{\pi a / Q}$$

WHERE  $Q = f(a/2c, \sigma)$



EDGE CRACK

$$K_I = 1.12 \sigma \sqrt{\pi a}$$

Figure I-10  $K_I$  values for various crack geometries.

## CHAPTER 2. CONCEPTS OF FRACTURE MECHANICS - FATIGUE AND FRACTURE CONTROL

### 2.1 GENERAL DISCUSSION

Most engineering structures in existence perform safely and reliably. The safety and reliability of these structures have been achieved by improving the weak links that were observed during the life of each component in the system. Most present specifications on material, design, and fabrication are based on correlations with service experience. The comparatively few service failures in steel bridges indicate that the steel properties, design, and fabrication procedures used for bridges basically are satisfactory. However, the few service failures that have occurred indicated that some modifications in practices were needed. The identification of the specific modifications needed requires a thorough study of material properties, design, fabrication, inspection, erection, and service conditions. Fracture mechanics methodology has been of considerable help in this endeavor.

### 2.2 FRACTURE-MECHANICS METHODOLOGY

Fracture-mechanics methodology is very useful in designing to prevent crack initiation, subcritical crack propagation, and unstable crack propagation in bridges. Fracture mechanics is a method of characterizing fracture in terms of structural parameters familiar to the engineer, namely, stress and flaw size.

Linear-elastic fracture-mechanics (LEFM) technology is based on an analytical procedure that relates the stress field in the

vicinity of a crack tip to the nominal stress applied to the structure, to the size and shape of the crack or crack-like discontinuity, and to the material properties. Figure 2-1 presents the equations that describe the elastic-stress field in the vicinity of a crack tip in a body subjected to tensile stresses normal to the plane of the crack (Mode I deformation).<sup>1)</sup> The stress-field equations show that the distribution of the elastic-stress field in the vicinity of the crack tip is invariant in all structural components subjected to Mode I deformation, and that the magnitude of the elastic-stress field can be described by a single-term parameter,  $K_I$ , designated the stress-intensity factor. Consequently, the applied stress, the crack shape and size, and the structural configuration associated with structural components subjected to Mode I deformation affect the value of the stress-intensity factor but do not alter the stress-field distribution. Relationships between the stress-intensity factor and various body configurations, crack sizes and shapes, and loading conditions have been published.<sup>2)</sup> Three examples of widely used stress-flaw-size relations are presented in Figure 2-2.

One of the underlying principles of fracture mechanics is that unstable fracture occurs when the stress-intensity factor at the crack tip reaches a critical value,  $K_C$ . For Mode I deformation and for small crack-tip plastic deformation (plane-strain conditions), the critical stress-intensity factor for fracture instability is designated  $K_{Ic}$ .  $K_{Ic}$  represents the inherent ability of a material to withstand a given stress-field intensity at the tip



of a crack and to resist progressive tensile crack extension.

Thus,  $K_{Ic}$  represents the fracture toughness of the material and has units of  $\text{ksi}\sqrt{\text{inch}}$  ( $\text{MPa}\sqrt{\text{m}}$ ).

The critical stress-intensity factor,  $K_{Ic}$ , represents the terminal conditions in the life of a structural component. The total useful life of the component is determined by the time necessary to initiate a crack and to propagate the crack from subcritical dimensions to the critical size,  $a_c$ . Crack initiation and subcritical crack propagation may be caused by cyclic stresses in the absence of an aggressive environment (fatigue), by an aggressive environment under sustained load (stress-corrosion cracking), or by the combined effects of cyclic stresses and an aggressive environment (corrosion fatigue). Because all these modes of subcritical crack propagation are localized phenomena that depend on the boundary conditions at the crack tip, it is logical to expect the subcritical crack-propagation rate to depend on the stress-intensity factor,  $K_I$ , which provides a single-term parameter representative of the stress conditions in the vicinity of the crack tip. Sufficient data are available in support of this observation.<sup>3-8)</sup> Recently, fracture-mechanics parameters have been used to study the effect of stress concentration on fatigue-crack initiation.<sup>9,10)</sup>

The safety and reliability of steel structures are governed by many interrelated factors. Fracture of a structural detail can occur as a result of improper material properties, design, fabrication, inspection, erection, and operating conditions. These parameters govern the initiation, subcritical-crack propagation,

and unstable propagation of cracks in structural details under operating conditions. The sum of the elapsed cycles required to initiate a fatigue crack and to propagate the crack from subcritical dimensions to the critical size represent the fatigue life of the structural component. Consequently, an understanding of crack-initiation behavior, subcritical-crack-propagation behavior and unstable-crack propagation behavior is necessary to develop a fracture-control plan to ensure the safety and reliability of structures. A brief discussion of the parameters that govern the behavior for each of these stages in the life of cyclically loaded structural details subjected to constant amplitude cyclic load fluctuations in benign environments is presented in the following sections. The effects of variable-amplitude random-distribution loading and of aggressive environments on the behavior of cyclically loaded structural components is presented elsewhere.<sup>11)</sup>

### 2.3 FATIGUE-CRACK INITIATION

Conventional procedures used to design structural components subjected to fluctuating loads provide (1) a design fatigue curve (S-N curve), which is based on the prediction of cyclic life from data on nominal stress (or strain) versus elapsed cycles, and (2) a design fatigue chart (Goodman chart), which indicates the maximum and minimum stresses that can be applied to specimens at any given stress ratio,  $R(\sigma_{\min}/\sigma_{\max})$ , and at any selected fatigue life. Data used for plotting a curve or chart are usually obtained by testing unnotched specimens and represent the number of cycles required to initiate a crack in the specimen plus the number of cycles required

to propagate the crack from a subcritical small size to a critical larger dimension. The dimension of the critical crack required to cause terminal fracture depends on the magnitude of the applied stress, the specimen geometry, and the specific testing conditions used.

Figure 2-3 is a schematic S-N curve divided into an initiation component and a propagation component. The number of cycles corresponding to the endurance limit represents initiation life primarily, whereas the number of cycles expended in crack initiation at a high value of applied alternating stress is negligible. As the magnitude of the applied alternating stress increases, the total fatigue life decreases and the percent of the fatigue life to initiate a crack decreases. Consequently, S-N type data do not provide complete information regarding safe-life predictions in structural components, particularly in components having surface irregularities different from those of the test specimens and in components containing crack-like discontinuities, because the existence of surface irregularities and crack-like discontinuities reduces and may eliminate the crack-initiation portion of the fatigue life of structural components.

The initiation of cracks in structural details occurs in regions of stress concentrations as a result of stress fluctuations. Consequently, the discussion in this section concerns fatigue-crack initiation from notches.

Notches in structural components cause stress intensification in the vicinity of the notch tip. The material element at the tip of

a notch in a cyclically loaded structural component is subjected to the maximum stress,  $\sigma_{\max}$ , and to the maximum stress fluctuations,  $\Delta\sigma_{\max}$ . Consequently, this material element is most susceptible to fatigue damage and is, in general, the origin of fatigue-crack initiation. It can be shown that the maximum-stress range (or maximum stress) on this material element can be related to the stress-intensity-factor-range,  $\Delta K_I$  (or stress-intensity factor) parameter as follows:<sup>11)</sup>

$$\Delta\sigma_{\max} = \frac{2}{\sqrt{\pi}} \frac{\Delta K_I}{\sqrt{\rho}} = \Delta\sigma(K_{\dagger}) \quad (2.1)$$

where  $\rho$  is the notch-tip radius,  $\Delta\sigma$  is the applied-nominal-stress range, and  $K_{\dagger}$  is the stress-concentration factor. Although Equation 2.1 is considered exact only when  $\rho$  approaches zero, Wilson and Gabrielse<sup>12)</sup> showed that this relationship is accurate to within 10 percent for notch radii up to 0.180 inch (4.6 mm). A typical specimen and the stress distribution near the notch is shown in Figures 2-4 and 2-5 respectively.

The behavior of specimens containing notches that correspond to various stress-concentration factors is shown in Figure 2-6 for zero-to-tension axial loading. The data are presented in terms of the number of cycles for fatigue-crack initiation,  $N_i$ , at the tip of a notch versus the nominal-stress fluctuation,  $\Delta\sigma$ . The same data are presented in Figure 2-7 in terms of  $N_i$  versus the stress-intensity-factor range divided by the square root of the notch radius,  $\Delta K_I/\sqrt{\rho}$ , which corresponds to the maximum-stress range at the tip of the notch. The data in Figure 2-6 show the significant decrease in the fatigue-crack-initiation life for a given nominal-stress range with increased stress-concentration factor. The data in Figure 2-7 show that  $\Delta K_I/\sqrt{\rho}$ , and therefore  $\Delta\sigma_{\max}$ , is the primary para-

meter that governs the fatigue-crack-initiation behavior in regions of stress concentration for a given steel tested in a benign environment.

The fatigue-crack-initiation behavior of various steels is presented in Figure 2-8 for specimens subjected to zero-to-tension bending stress and containing a notch that resulted in a stress concentration of about 2.5. Because the stress-concentration factor was constant for all specimens and for the various steels, the differences in the fatigue-crack-initiation behavior shown in Figure 2-8 are related primarily to inherent differences in the fatigue-crack-initiation characteristics of the steels. The data show that fatigue cracks do not initiate in steel structural components when the body configuration, the notch geometry, and the nominal-stress fluctuations are such that the magnitude of the parameter,  $\Delta K_I/\sqrt{\rho}$ , and therefore  $\Delta\sigma_{\max}$ , at the root of the notch is less than a given value that is characteristic of the steel. The value of this fatigue-crack-initiation threshold,  $\Delta K_I/\sqrt{\rho} \Big|_{\text{th}}$ , increases with increased yield strength or tensile strength of the steel. The data show that the fatigue-crack-initiation life of a detail subjected to a given nominal-stress range increases with increased tensile strength of the steel. However, this difference in fatigue-crack-initiation life for various steels decreases with increased magnitude of the stress-concentration factor.

Finally, fatigue-crack-initiation data for various steels subjected to stress ratios (ratio of nominal minimum-applied stress to nominal maximum-applied stress) ranging from -1.0 to +0.5, Figure 2-9, indicate that the fatigue-crack-initiation life is governed by the total maximum-stress (tension plus compression) range at the tip of the notch. The data

in Figure 2-10 indicate that the fatigue-crack-initiation threshold  $\left( \frac{\Delta K_I}{\sqrt{\rho}} \right)_{th}$ , for various steels subjected to stress ratios ranging from -1.0 to +0.5 can be estimated from

$$\left( \frac{\Delta K_{total}}{\sqrt{\rho}} \right)_{th} = 10\sqrt{\sigma_{ys}} \quad (2.2)$$

where  $\Delta K_{total}$  is the stress-intensity-factor range calculated by using the sum of the tension- and compression-stress range and  $\sigma_{ys}$  is the yield strength of the material.

## 2.4 FATIGUE-CRACK PROPAGATION

General Behavior. Most fatigue-crack-growth tests are conducted by subjecting a fatigue-cracked specimen to constant-amplitude cyclic-load fluctuations. Incremental increase of crack length is measured, and the corresponding number of elapsed load cycles is recorded. The data are presented on a plot of crack length,  $a$ , versus total number of elapsed load cycles,  $N$ , Figure 2-11. An increase in the magnitude of cyclic-load fluctuation results in a decrease of fatigue life of specimens having identical geometry, Figure 2-12. Furthermore, the fatigue life of specimens subjected to a fixed constant-amplitude cyclic-load fluctuation decreases as the length of the initial crack is increased, Figure 2-13. Consequently, under a given constant-amplitude stress fluctuation, most of the useful cyclic life is expended when the crack length is very small. Various  $a$ -versus- $N$  curves can be generated by varying the magnitude of the cyclic-load fluctuation or the size of the initial crack, or both. These curves reduce

to a single curve when the data are represented in terms of crack-growth rate per cycle of loading,  $da/dN$ , and the stress-intensity-factor range,  $\Delta K_I$ , because  $\Delta K_I$  is a single-term parameter that incorporates the effect of changing crack length and cyclic-load magnitude. The parameter  $\Delta K_I$  is representative of the mechanical driving force. The most commonly used presentation of fatigue-crack-growth data is a log-log plot of the rate of fatigue-crack growth per cycle of load fluctuation,  $da/dN$ , and the fluctuation of the stress-intensity factor,  $\Delta K_I$ .

The fatigue-crack-propagation behavior for metals can be divided into three regions, Figure 2-14. The behavior in region I exhibits a fatigue-crack-propagation threshold,  $\Delta K_{th}$ , which corresponds to the stress-intensity-factor range below which cracks do not propagate under cyclic-stress fluctuations. An analysis of experimental results published on nonpropagating fatigue cracks shows that conservative estimates of  $\Delta K_{th}$  for various steels subjected to various stress ratios,  $R$ , can be predicted from<sup>11,13)</sup>

$$\begin{aligned} \Delta K_{th} &= 6.4 (1 - 0.85 R) \text{ for } R \geq +0.1 \\ \Delta K_{th} &= 5.5 \text{ ksi}\sqrt{\text{inch}} \quad \text{for } R < +0.1 \end{aligned} \tag{2.3}$$

where  $\Delta K_{th}$  is in  $\text{ksi}\sqrt{\text{inch}}$ .

Equation 2.3 indicates that the fatigue-crack-propagation threshold for steels is primarily a function of the stress ratio and is essentially independent of chemical composition or mechanical properties.

The behavior in region II, Figure 2-14, represents the fatigue-crack-propagation behavior above  $\Delta K_{th}$ , which can be

represented by

$$\frac{da}{dN} = A (\Delta K)^n \quad (2.4)$$

where  $a$  = crack length,

$N$  = number of cycles,

$\Delta K$  = stress-intensity-factor range

$A$  and  $n$  are constants.

This behavior is discussed further in the following sections.

In region III the fatigue-crack growth per cycle is higher than predicted for region II. The data show that the rate of fatigue-crack growth increases, and that under zero-to-tension loading (that is,  $\Delta K = K_{\max}$ ), this increase occurs at a constant value of crack-tip displacement,  $\delta_T$ , and at a corresponding stress-intensity-factor value,  $K_T$ , given by<sup>4)</sup>

$$\delta_T = \frac{K_T^2}{E\sigma_{ys}} = 1.6 \times 10^{-3} \text{ in. (0.04 mm)} \quad (2.5)$$

where  $K_T$  = stress-intensity-factor-range value corresponding to onset of acceleration in fatigue-crack-growth rates,

$E$  = Young's modulus,

$\sigma_{ys}$  = yield strength (0.2% offset) (the available data indicate that the value of  $K_T$  can be predicted more closely by using a flow stress,  $\sigma_f$ , rather than  $\sigma_{ys}$ , where  $\sigma_f$  is the average of the yield and tensile strengths).

Acceleration of fatigue-crack-growth rates that determines the transition from region II to region III appears to be caused by the superposition of a ductile-tear mechanism onto the mechanism of cyclic subcritical crack extension, which leaves fatigue striations on the fracture surface. Ductile tear occurs when the strain



at the tip of the crack reaches a critical value.<sup>14)</sup> Thus, the fatigue-rate transition from region II to region III depends on  $K_{\max}$  and on the stress ratio,  $R$ .

Equation 2.5 is used to calculate the stress-intensity-factor value corresponding to the onset of fatigue-rate transition,  $K_T$  (or  $\Delta K_T$  for zero-to-tension loading) in materials that have high fracture toughness (steel A in Figure 2-14) — that is, materials for which the critical-stress-intensity factor,  $K_{Ic}$  or  $K_c$ , is higher than the  $K_T$  value calculated by using Equation 2.5. Acceleration in the rate of fatigue-crack growth occurs at a stress-intensity-factor value slightly below the critical-stress-intensity factor,  $K_{Ic}$ , when the  $K_{Ic}$  (or  $K_c$ ) of the material is less than  $K_T$  (steel B in Figure 2-14). Furthermore, acceleration in the rate of fatigue-crack growth in an aggressive environment may occur at the threshold stress-intensity factor,  $K_{Isc}$ , that corresponds to the highest plane-strain stress-intensity factor below which sub-critical crack propagation does not occur under static loading in a given material and environment. The effect of an aggressive environment on the rate of crack growth is discussed elsewhere.<sup>11)</sup>

Steels. Extensive fatigue-crack-growth-rate data for various steels show that the primary parameter affecting growth rate in region II is the range of fluctuation in the stress-intensity factor, and that the mechanical and metallurgical properties of these steels have negligible effects on the fatigue-crack-growth rate in a room-temperature air environment. The data for martensitic steels, including A514 and A517 steels, fall within a

single band, as shown in Figure 2-15, and the upper bound of the scatter of the fatigue-crack-propagation-rate data for these steels in an air environment can be obtained from

$$\frac{da}{dN} = 0.66 \times 10^{-8} (\Delta K_I)^{2.25} \quad (2.6)$$

where  $a$  is in inch, and  $\Delta K_I$  is in  $\text{ksi}\sqrt{\text{inch}}$ . Similarly, data for ferrite-pearlite steels, including A36, A572, and A588 steels, fall within a single band that is different from martensitic steels, Figure 2-16. The upper bound of the scatter of the fatigue-crack-propagation-rate data for these steels in an air environment can be calculated from

$$\frac{da}{dN} = 3.6 \times 10^{-10} (\Delta K_I)^{3.0} \quad (2.7)$$

where  $a = \text{inch}$

$$\Delta K_I = \text{ksi}\sqrt{\text{inch}}.$$

The stress ratio,  $R$ , and mean stress have negligible effect on the rate of crack growth in region II. However, as has been already discussed, they have a significant effect on the behavior in regions I and III.

The frequency of cyclic loading and the wave form (sinusoidal, triangular, square, trapezoidal) do not affect the rate of crack propagation per cycle of load for steels in benign environments.<sup>5,11)</sup>

## 2.5 FRACTURE TOUGHNESS

The stress-intensity-factor value for a given stress increases with increase crack length until it reaches a critical value,  $K_{IC}$ . At this critical stress-intensity-factor value the

crack propagates unstably and the life of the component is terminated. For Mode I deformation and for small crack-tip plastic deformation (plane-strain conditions), the critical stress-intensity factor for fracture instability,  $K_{Ic}$ , represents the inherent ability of a material to resist progressive tensile crack extension. However, this fracture-toughness property varies with constraint, and like other material properties such as yield strength, it varies with temperature and loading rate as follows:

$K_C$  = critical-stress-intensity factor for static loading and plane-stress conditions of variable constraint. Thus, this value depends on specimen thickness and geometry, as well as on crack size.

$K_{Ic}$  = critical-stress-intensity factor for static loading and plane-strain conditions of maximum constraint. Thus, this value is a minimum value for thick plates.

$K_{I_d}$  = Critical-stress-intensity factor for dynamic (impact) loading and plane-strain conditions of maximum constraint,

where  $K_C$ ,  $K_{Ic}$ , or  $K_{I_d} = C\sigma\sqrt{a}$

$C$  = constant, function of specimen and crack geometry,

$\sigma$  = nominal stress, ksi,

$a$  = flaw size, in.

Each of these values is also a function of temperature, particularly for those structural materials exhibiting a transition from brittle to ductile behavior.

By knowing the critical value of  $K_I$  at failure ( $K_C$ ,  $K_{Ic}$ , or  $K_{Id}$ ) for a given material of a particular thickness and at a specific temperature and loading rate, the designer can determine flaw sizes that can be tolerated in structural members for a given design stress level. Conversely, he can determine the design stress level that can be safely used for an existing crack that may be present in a structure.

As an introductory numerical example of the design application of fracture mechanics, consider the equation relating  $K_I$  to the applied stress and flaw size for a through-thickness crack in a wide plate, that is  $K_I = \sigma\sqrt{\pi a}$ .

This general relationship among material toughness ( $K_C$ ), nominal stress ( $\sigma$ ), and crack size ( $a$ ) is shown schematically in Figure 2-17. If a particular combination of stress and crack size in a structure ( $K_I$ ) reaches the  $K_C$  level, fracture can occur. Thus there are many combinations of stress and flaw size (e.g.,  $\sigma_f$  and  $a_f$ ) which may cause fracture in a structure that is fabricated from a steel having a particular value of  $K_C$  at a particular service temperature, loading rate, and plate thickness. Conversely, there are many combinations of stress and flaw size (e.g.,  $\sigma_o$  and  $a_o$ ) that will not cause failure of a particular structural material.

Assume that laboratory test results show that for a particular structural steel with a yield strength of 80 ksi (552 MPa), the  $K_C$  is  $60 \text{ ksi}\sqrt{\text{in}}$ . ( $66 \text{ MPa}\sqrt{\text{m}}$ ) at the service temperature, loading rate, and plate thickness used in service. Also assume that the design stress is 20 ksi (138 MPa). Substituting  $K_I = K_C = 60 \text{ ksi}\sqrt{\text{in}}$ .

(66 MPa $\sqrt{m}$ ) into the equation for a through-thickness flaw in Figure 2-18 results in  $2a = 5.7$  in. (145 mm). Thus for these conditions the tolerable through-thickness flaw size would be about 5.7 in. (145 mm). For a design stress of 45 ksi (310 MPa), the same material could tolerate a flaw size,  $2a$ , of only about 1.1 in. (27.9 mm). If residual stresses such as may be due to welding are present, so that the total stress in the vicinity of a crack is 80 ksi (552 MPa), the tolerable flaw size is reduced considerably. Note from Figure 2-18 that if a tougher steel is used — for example, one with a  $K_{IC}$  of 120 ksi $\sqrt{in.}$  (132 MPa $\sqrt{m}$ ) — the tolerable flaw sizes at all stress levels are significantly increased. If the toughness of a steel is sufficiently high, brittle fractures will not occur, and failures under tensile loading will be ductile in nature, similar to the failure of a tension-test specimen. Fortunately, most structural steels have this high level of toughness at service temperatures and loading rates.

A useful analogy for the designer is the relation among applied load,  $P$ , nominal stress,  $\sigma$ , and yield stress,  $\sigma_{ys}$  (or ultimate stress,  $\sigma_u$ ) in an unflawed structural member, and among applied load,  $P$ , stress intensity,  $K_I$ , and critical stress intensity for fracture ( $K_{IC}$ ,  $K_{IC}$ , or  $K_{ID}$ ) in a structural member with a flaw. In an unflawed structural member, as the load is increased the nominal stress increases until an instability (yielding at  $\sigma_{ys}$  or fracture at ultimate stress,  $\sigma_u$ ) occurs. As the load is increased in a structural member with a flaw (or as the size of the

flaw grows by fatigue or stress-corrosion), the stress intensity,  $K_I$ , increases until an instability (fracture at  $K_{Ic}, K_{Ic}, K_{Id}$ ) occurs. Thus the  $K_I$  level in a structure within its design life should always be kept below the appropriate  $K_{Ic}$  value in the same manner that the nominal design stress ( $\sigma$ ) is kept below the yield strength ( $\sigma_{ys}$ ).

Another analogy that may be useful in understanding the fundamental aspects of fracture mechanics is the comparison with the Euler column instability (Figure 2-19). The stress level required to cause instability in a column (buckling) decreases as the slenderness ratio ( $L/r$ , where  $L$  is the length of the column and  $r$  is the least radius of gyration of column section) increases. Similarly, the stress level required to cause instability (fracture) in a flawed tension member decreases as the flaw size ( $a$ ) increases. As the stress level in either case approaches the yield strength, both the Euler analysis and the  $K_{Ic}$  analysis are invalidated because of yielding. To prevent buckling, the actual stress and ( $L/r$ ) values must be below the Euler curve. To prevent fracture, the actual stress and flaw size,  $a$ , must be below the  $K_{Ic}$  level shown in Figure 2-18. Obviously, using a material with a high level of notch toughness in Figure 2-18 [e.g., a  $K_{Ic}$  level of  $120 \text{ ksi}\sqrt{\text{in.}}$  ( $133 \text{ MPa}\sqrt{\text{m}}$ ) compared with  $60 \text{ ksi}\sqrt{\text{in.}}$  ( $66 \text{ MPa}\sqrt{\text{m}}$ )] will increase the possible combinations of design stress and flaw size that a structure can tolerate without fracturing.

The plane-strain critical fracture-toughness,  $K_{Ic}$ , value for constructional steels usually cannot be obtained for plate

thicknesses, operating temperatures, and rates of loading that are appropriate for bridges because these steels usually exhibit elastic-plastic or plastic behavior under these operating conditions. Thus engineering estimates for  $K_{IC}$  behavior at various temperatures and loading rates have been made by using empirical correlations with data obtained from various specimens<sup>11)</sup> (such as Charpy specimen) that do not satisfy the strict requirement imposed on fracture-mechanics testing.

## 2.6 FRACTURE-CONTROL PLAN

Most engineering structures in existence are performing safely and reliably. The comparatively few service failures in structures indicate that present-day practices governing material properties, design, and fabrication procedures are generally satisfactory. However, the occurrence of infrequent failures indicates that further understanding and possible modifications in present-day practices are needed. The identification of the specific modifications needed requires a thorough study of material properties, design, fabrication, inspection, erection, and service conditions.

Structures are fabricated in various sizes and are subjected to numerous service conditions. Thus, it is very difficult to develop a set of rules that is sufficiently general to ensure the safety and reliability of all structures. The safety and reliability of structures and the correct prediction of their overall resistance to failure by fracture or fatigue can be approximated best by using a fracture-control plan for each of the various types of structures, for example, bridges. A fracture-control plan is

a detailed procedure used

1. To identify all the factors that may contribute to the fracture of a structural detail or to the failure of the entire structure.
2. To assess the contribution of each factor and the synergistic contribution of these factors to the fracture process.
3. To determine the relative efficiency and trade-off of various methods to minimize the probability of fracture.
4. To assign responsibility for each task that must be undertaken to ensure the safety and reliability of the structure.

The development of a fracture-control plan for complex structures requires knowledge of the magnitude and distribution of applied and residual stresses for critical members, of the environmental conditions and their effects on structural integrity, and of the quality of fabrication and inspection. Although such information may have to be developed, the formulation of a fracture-control plan that is based on the available information for a given application should result in a better understanding of the fracture characteristics of the structure under consideration.

A fracture-control plan is a procedure tailored for a given application and cannot be extended indiscriminately to other applications. However, general fracture-control guidelines that pertain to classes of structures (such as bridges, ships, pressure vessels, etc.) can be formulated for consideration in the develop-



ment of a fracture-control plan for a particular structure within any particular class of structures.

The correspondence among fracture-control plans based on crack initiation, crack propagation, and fracture toughness of materials, and a fracture-control plan based on fabrication, inspection, design, and fracture toughness of materials can be readily demonstrated by using fracture-mechanics concepts. The fact that crack initiation, crack propagation, and fracture toughness are functions of the stress-intensity fluctuation,  $\Delta K_I$ , and of the critical-stress-intensity factor  $K_{Ic}$  — which are in turn related to the applied nominal stress (or stress fluctuation) — demonstrates that a fracture-control plan for various structural applications depends on:

1. The fracture toughness,  $K_{Ic}$  (or  $K_c$ ), of the material at the temperature and loading rate representative of the intended application. The fracture toughness can be modified by changing the material used in the structure.
2. The applied stress, stress rate, stress concentration, and the stress fluctuation, which can be altered by design changes and by proper fabrication.
3. The initial size of the discontinuity and the size and shape of the critical crack, which can be controlled by design changes, fabrication, and inspection.

The total useful life of structural components is determined by the time necessary to initiate a crack and to propagate the crack from subcritical dimensions to the critical size. The life

of the component can be prolonged by extending the crack-initiation life and the subcritical-crack-propagation life. Consequently, crack initiation, subcritical crack propagation, and fracture toughness characteristics of structural materials are primary considerations in the formulation of fracture-control guidelines for structures. The discussion presented in the preceding sections showed that the fatigue-crack-initiation life can be increased significantly by proper changes in the design of the structural detail. The fatigue-crack-initiation life for a given detail geometry can be increased significantly by decreasing the magnitude of the applied-stress range and, for a given stress range, by changing the geometry of the detail to decrease the stress (or strain) concentration. The fatigue-crack-initiation life for a structural detail subjected to a given stress range can be increased by selecting a higher strength steel. However, this difference between steel having different tensile strengths decreases significantly as the stress concentration increases.

Another advantage derived from decreasing the magnitude of the stress concentration through proper design is an increase in the fatigue-crack-propagation life of cracks that are in the immediate neighborhood of a stress concentration and are subjected to the high magnitude of the localized stress range. Consequently, significant increase in the fatigue-crack life can be achieved by proper design and careful fabrication of structural details.

The stress-intensity-factor range has been shown to be the primary parameter that affects the rate of fatigue-crack

propagation per cycle of loading. The chemical composition and mechanical properties have a very small effect on the fatigue-crack-propagation life for bridge steels. This observation has been utilized in the development of the AASHTO fatigue-design specifications that are presented in the following chapter. Thus, a significant decrease in the fatigue-crack-propagation rate per cycle of loading and a corresponding increase in the fatigue-crack-propagation life can be achieved only by decreasing the magnitude of the stress-intensity-factor range. For structural details having identical geometries and initial fabrication discontinuities, such as attachments and coverplate details, a decrease in the applied stress range can result in a significant decrease in the fatigue-crack-propagation rate, Figure 2-20, region I. This can be accomplished by changes in the design of a detail. Similarly, for a given stress range, the fatigue-crack-propagation life can be increased significantly by decreasing the size of the initial discontinuities for a given structural detail, Figure 2-20, region II. This can be accomplished by improving the quality of fabrication and by inspection.

The fracture-toughness behavior for bridge steels subjected to a given rate of loading can be divided into three levels of performance. These three levels of performance — namely, plane-strain, elastic-plastic, and plastic, Figure 2-21<sup>11)</sup> — represent increased levels of fracture toughness and, under a given stress condition, correspond to increased tolerable crack sizes prior to fracture. Consequently, increased fracture toughness for a given

material and design should increase the subcritical crack-propagation life for the component. An increase in the level of fracture toughness from plane-strain behavior to elastic-plastic behavior results in a significant increase in the fatigue life of the component, Figure 2-20, region III. The AASHTO material-toughness requirements ensure this level (elastic-plastic) of performance under the intermediate rates of loading and for minimum operating temperatures for bridges. For most structural applications, some moderate level of elastic-plastic behavior at the service temperature and loading rates constitutes a satisfactory performance criterion. An increase in the level of fracture toughness from elastic-plastic behavior to plastic behavior has only a small effect on the fatigue life for bridge components (Figure 2-20, region IV) because the rate of fatigue-crack growth becomes so large that even if the critical crack size is doubled or even tripled, the effect on the remaining fatigue life is small.

The fatigue behavior for bridge components and the AASHTO fatigue-design requirements played a significant role in the development of the AASHTO material-toughness requirements. The basis for current AASHTO fatigue design and of the AASHTO material toughness requirements are presented in the following chapters.

## REFERENCES

1. G. R. Irwin, "Analysis of Stresses and Strains Near the End of a Crack Traversing a Plate," Journal of Applied Mechanics, Vol. 24, 1975, p. 361.
2. H. Tada, P. C. Paris, and G. R. Irwin, editors, Stress Analysis of Cracks Handbook, Del Research Corporation, Hellertown, Pa., 1973.
3. P. C. Paris and F. Erdogan, "A Critical Analysis of Crack Propagation Laws," Transactions of the ASME, Journal of Basic Engineering, Series D, Vol. 85, No. 3, 1963, p. 528.
4. J. M. Barsom, "Fatigue-Crack Propagation in Steels of Various Yield Strengths," Transactions of the ASME, Journal of Engineering for Industry, Series B, Vol. 93, No. 4, November 1971, p. 1190.
5. J. M. Barsom, "Effect of Cyclic-Stress Form on Corrosion-Fatigue Crack Propagation Below  $K_{I,SCC}$  in a High-Yield-Strength Steel," Corrosion Fatigue: Chemistry, Mechanics, and Microstructure, International Corrosion Conference Series, Volume NACE-2, National Association of Corrosion Engineers, 1972.
6. W. G. Clark, Jr., and H. E. Trout, Jr., "Influence of Temperature and Section Size on Fatigue Crack Growth Behavior in Ni-Mo-V Alloy Steel," Journal of Engineering Fracture Mechanics, Vol. 2, No. 2, November 1970, p. 107.
7. H. H. Johnson and P. C. Paris, "Sub-Critical Flaw Growth," Journal of Engineering Fracture Mechanics, Vol. 1, No. 3, June 1968, p. 3.
8. R. P. Wei, "Some Aspects of Environment-Enhanced Fatigue-Crack Growth," Journal of Engineering Fracture Mechanics, Vol. 1, No. 4, April 1970, p. 633.
9. J. M. Barsom and R. C. McNicol, "Effect of Stress Concentration on Fatigue-Crack Initiation in HY-130 Steel," Fracture Toughness and Slow Stable Cracking, ASTM STP 559, American Society for Testing and Materials, 1974.
10. W. G. Clark, Jr., "An Evaluation of the Fatigue Crack Initiation Properties of Type 403 Stainless Steel in Air and Steam Environments," Westinghouse Research Laboratory Report 72-1E7-FAILT-PI, August 25, 1972.
11. S. T. Rolfe and J. M. Barsom, Fracture and Fatigue Control in Structures: Application of Fracture Mechanics, Prentice-Hall, Inc., New York, 1977.
12. W. K. Wilson and S. E. Gabrielse, "Elasticity Analysis of Blunt Notched Compact Tension Specimens," Research Report 71-1E7-LOWFA-RI, Westinghouse Research Laboratory, February 5, 1971.

13. J. M. Barsom, "Fatigue Behavior of Pressure Vessel Steels," Welding Research Council Bulletin No. 194, May 1974.
14. J. M. Barsom, "Investigation of Subcritical Crack Propagation," Doctor of Philosophy Dissertation, University of Pittsburgh, 1969.

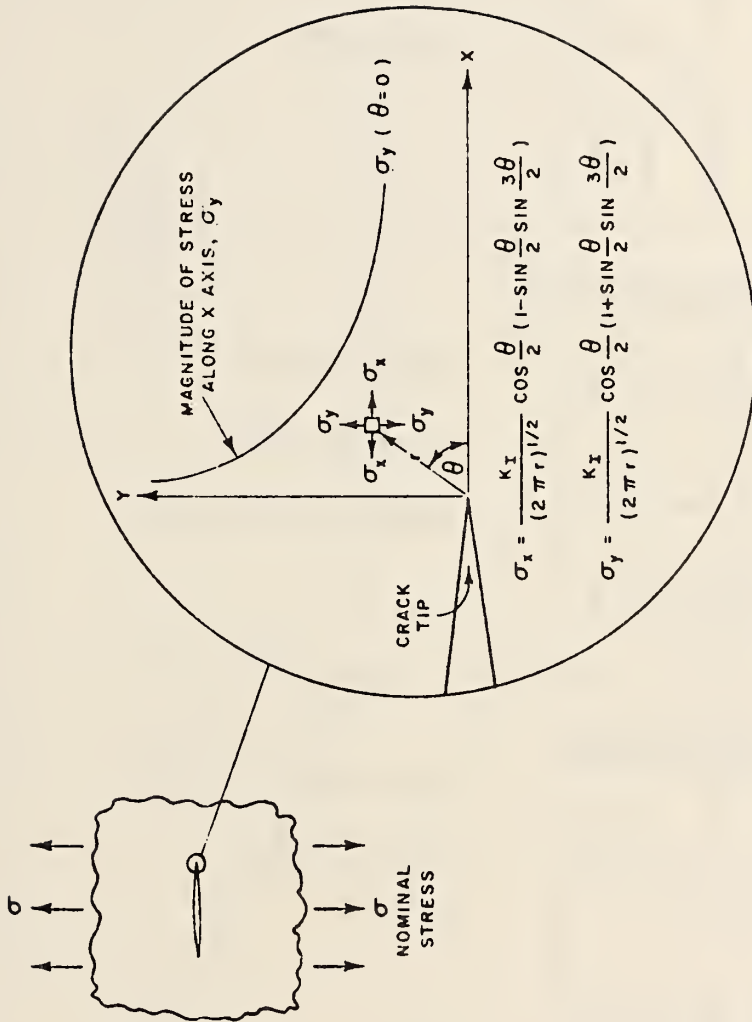
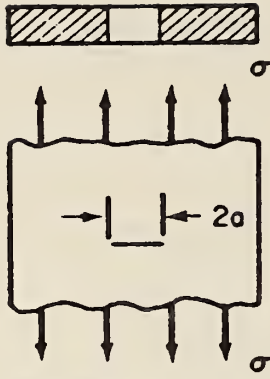
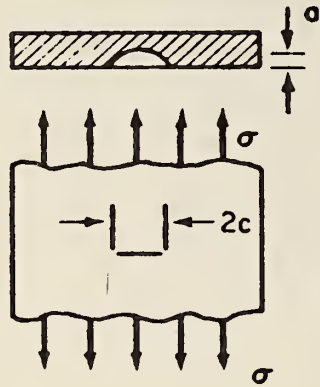


Figure 2-1 Schematic illustration of the elastic-stress-field distribution near the tip of a fatigue crack (Mode I deformation).



THROUGH THICKNESS CRACK

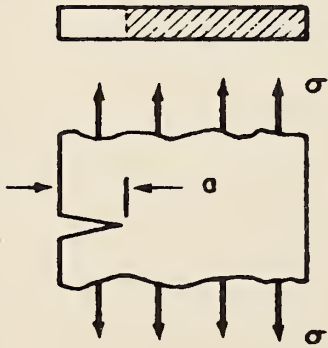
$$K_I = \sigma \sqrt{\pi a}$$



SURFACE CRACK

$$K_I = 1.12 \sigma \sqrt{\pi a / Q}$$

WHERE  $Q = f(a/2c, \sigma)$



EDGE CRACK

$$K_I = 1.12 \sigma \sqrt{\pi a}$$

Figure 2-2  $K_I$  values for various crack geometries.



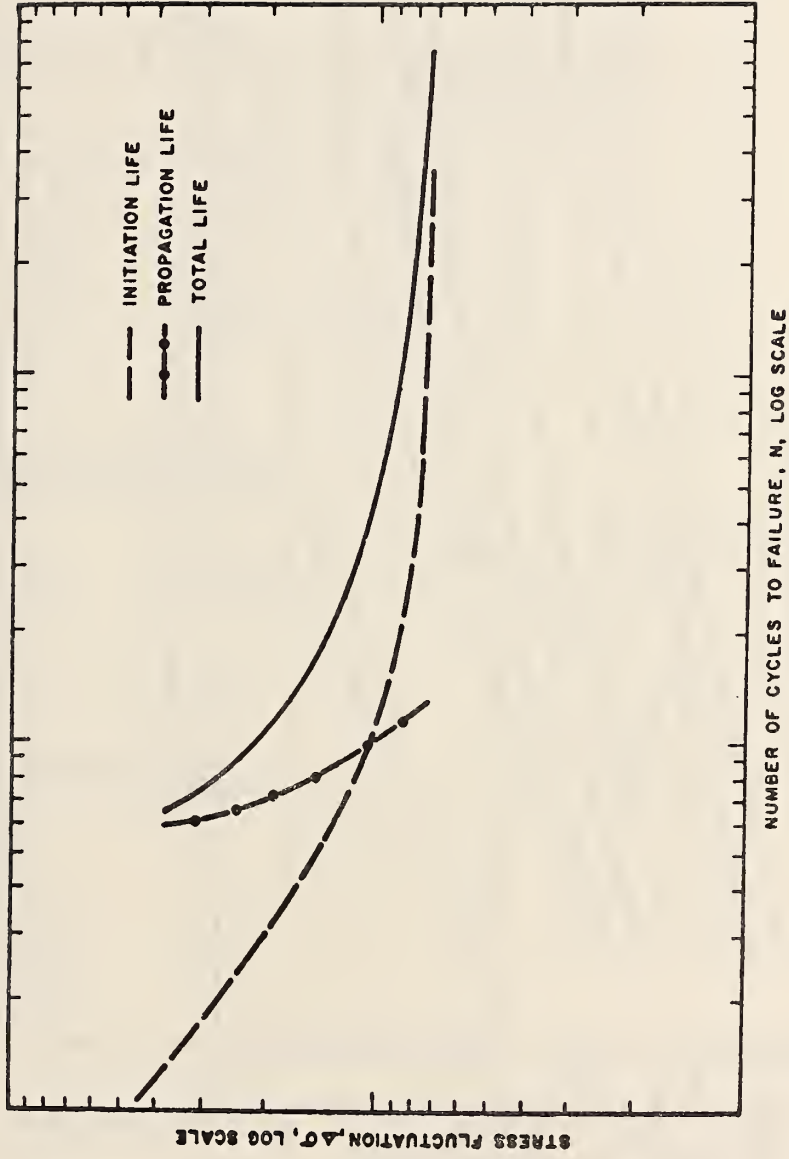


Figure 2-3 Schematic S-N curve divided into initiation and propagation components.

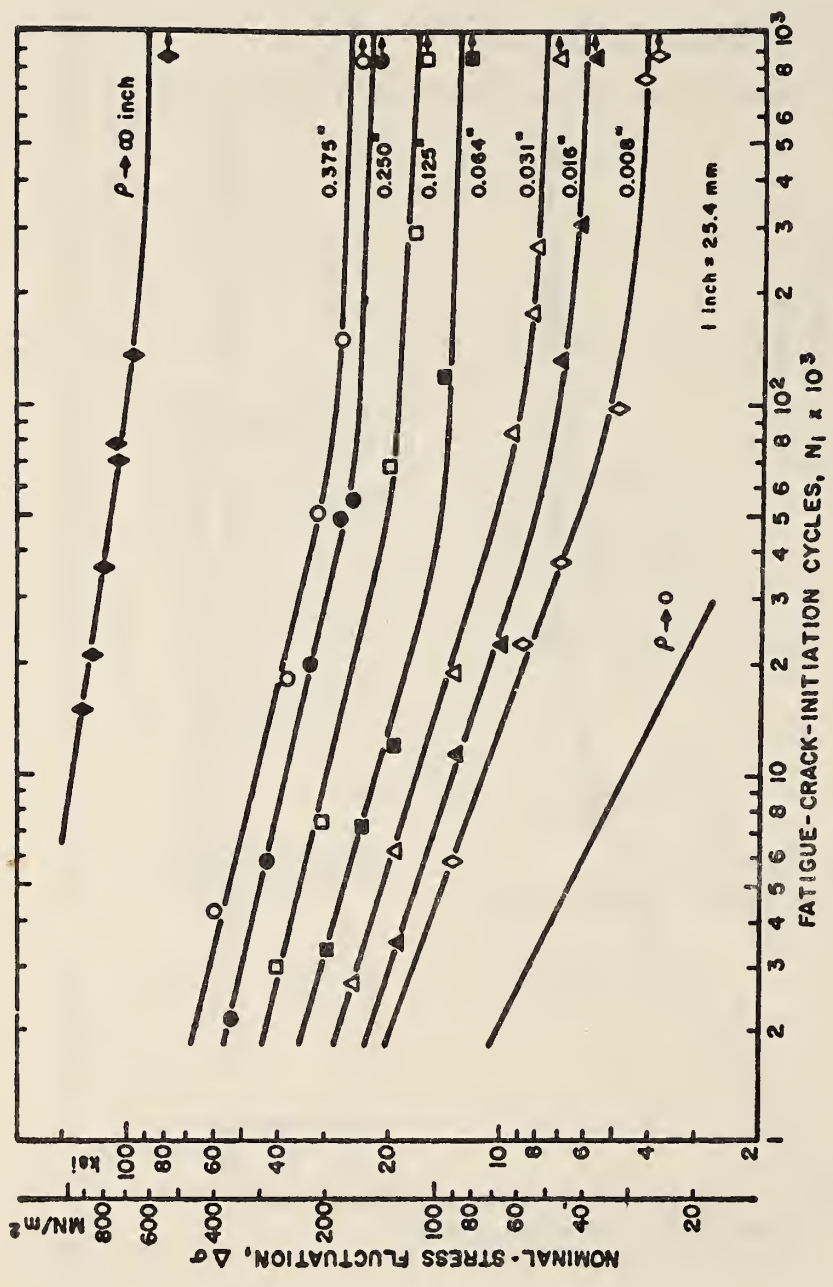


Figure 2-6 Dependence of fatigue-crack initiation of HY-130 steel on nominal-stress fluctuations for various notch geometries.

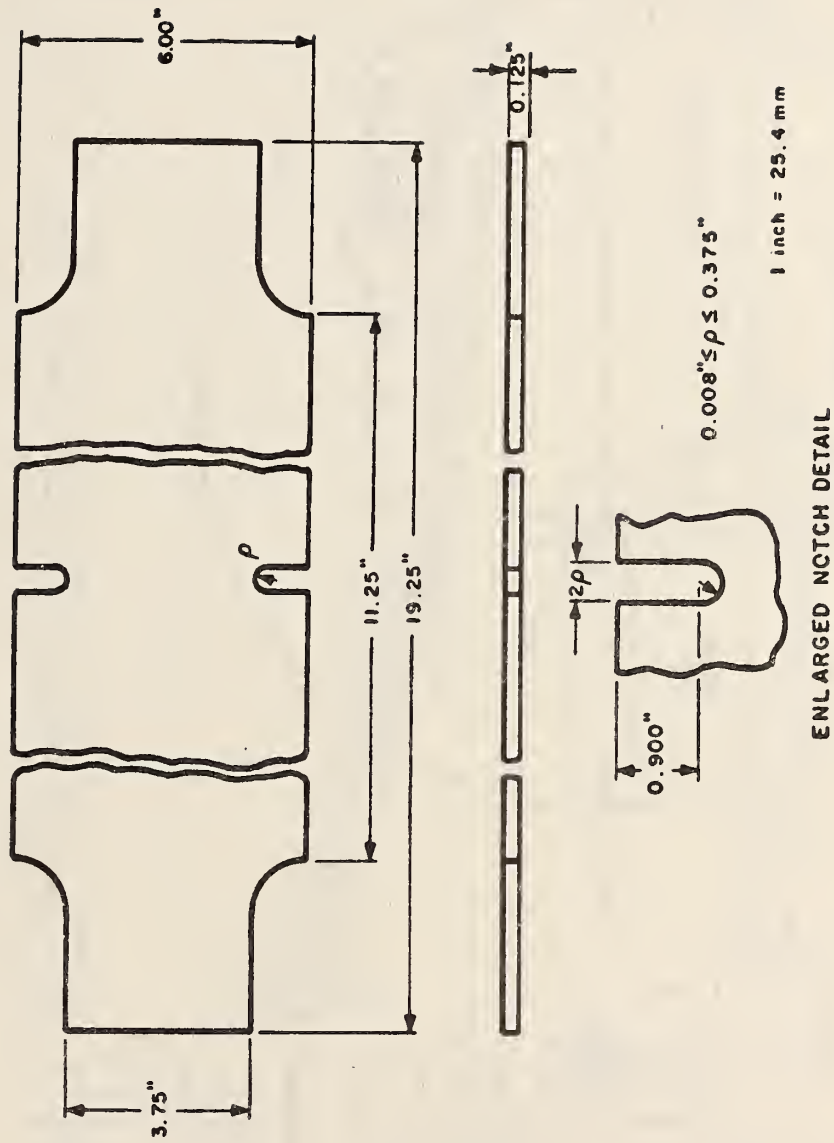


Figure 2-4 Double-edge-notched specimens.

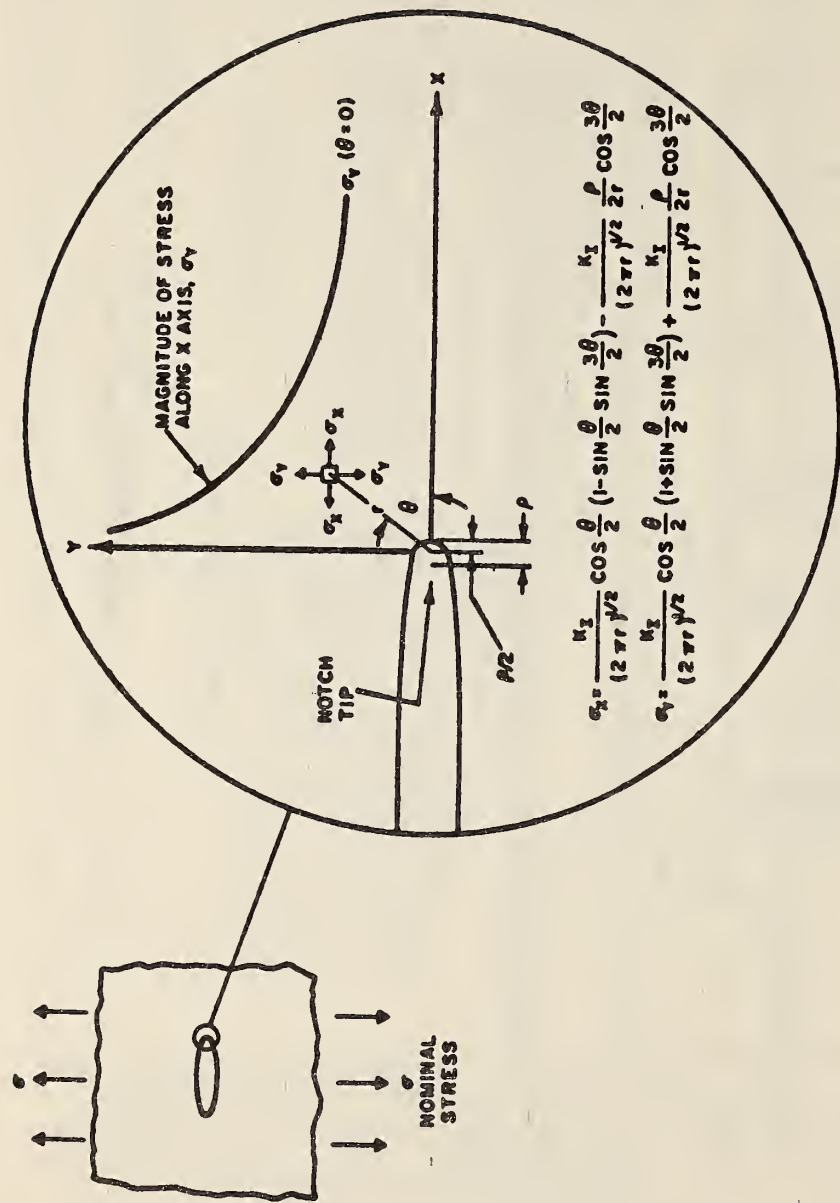


Figure 2-5 Schematic illustration of the elastic-stress-field distribution near the tip of an elliptical notch (Mode I deformation).

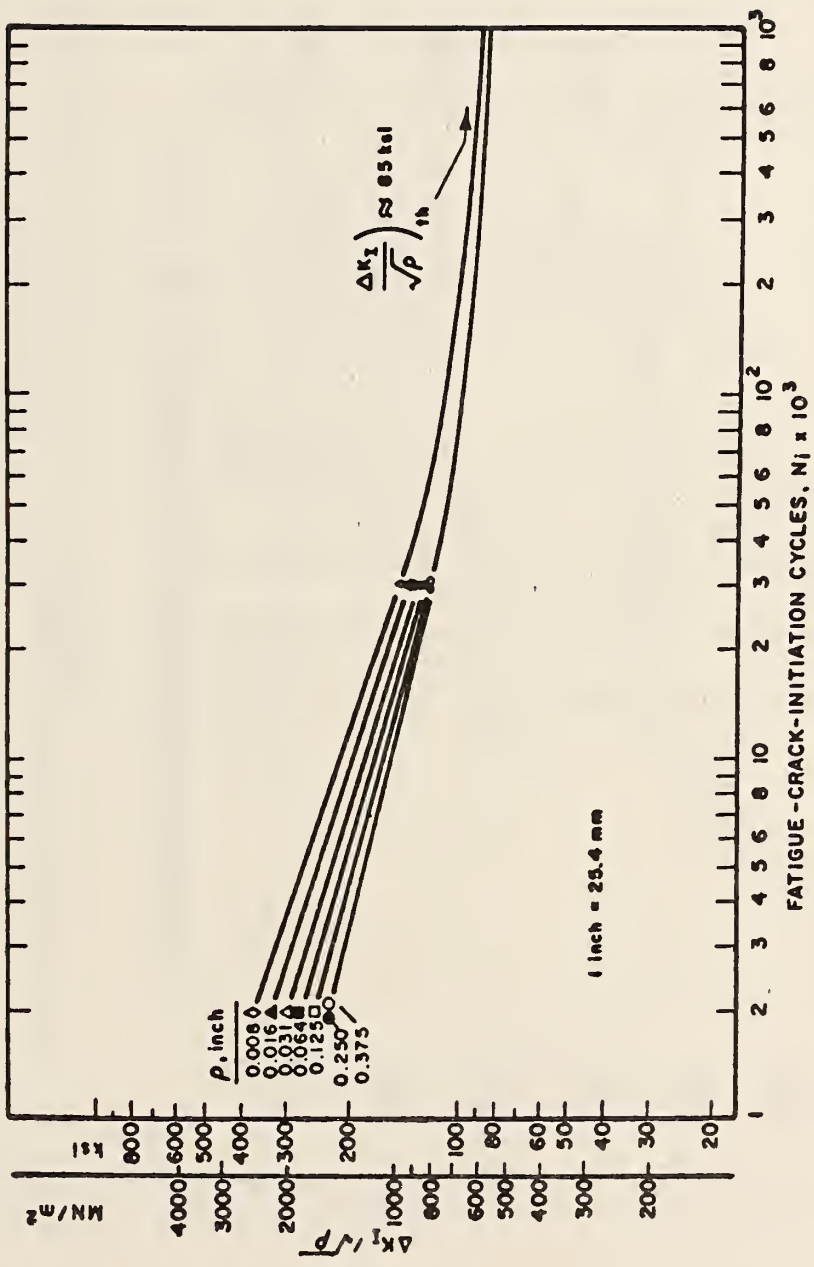
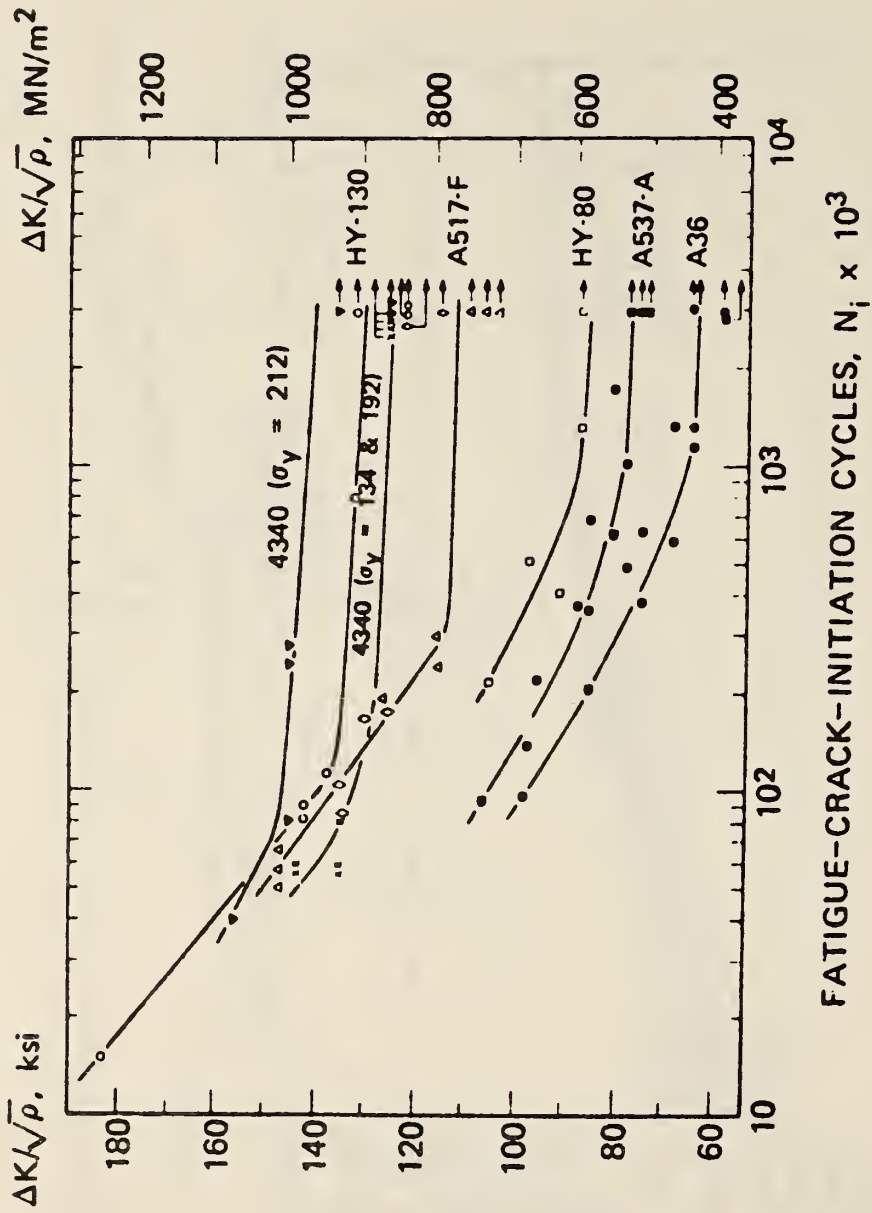


Figure 2-7 Correlation of fatigue-crack-initiation life with the parameter  $K_I/\sqrt{\rho}$  for HY-130 steel.



FATIGUE-CRACK-INITIATION CYCLES,  $N_i \times 10^3$

Figure 2-8 Fatigue-crack-initiation behavior of various steels at stress ratio of  $\pm 0.1$ .

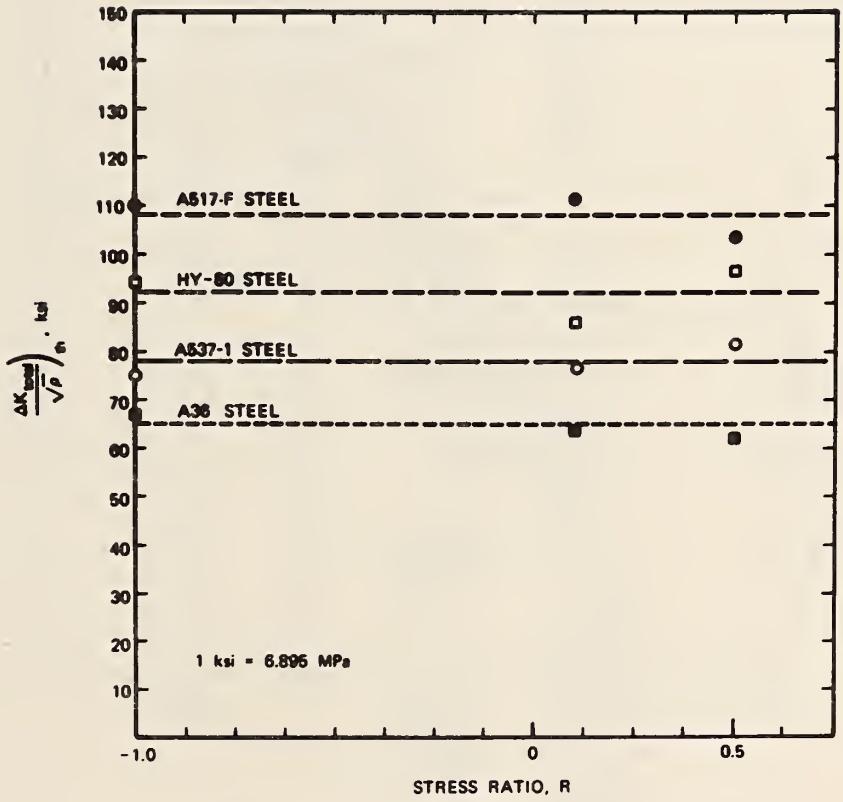


Figure 2-9 Independence of fatigue-crack-initiation threshold on stress ratio.

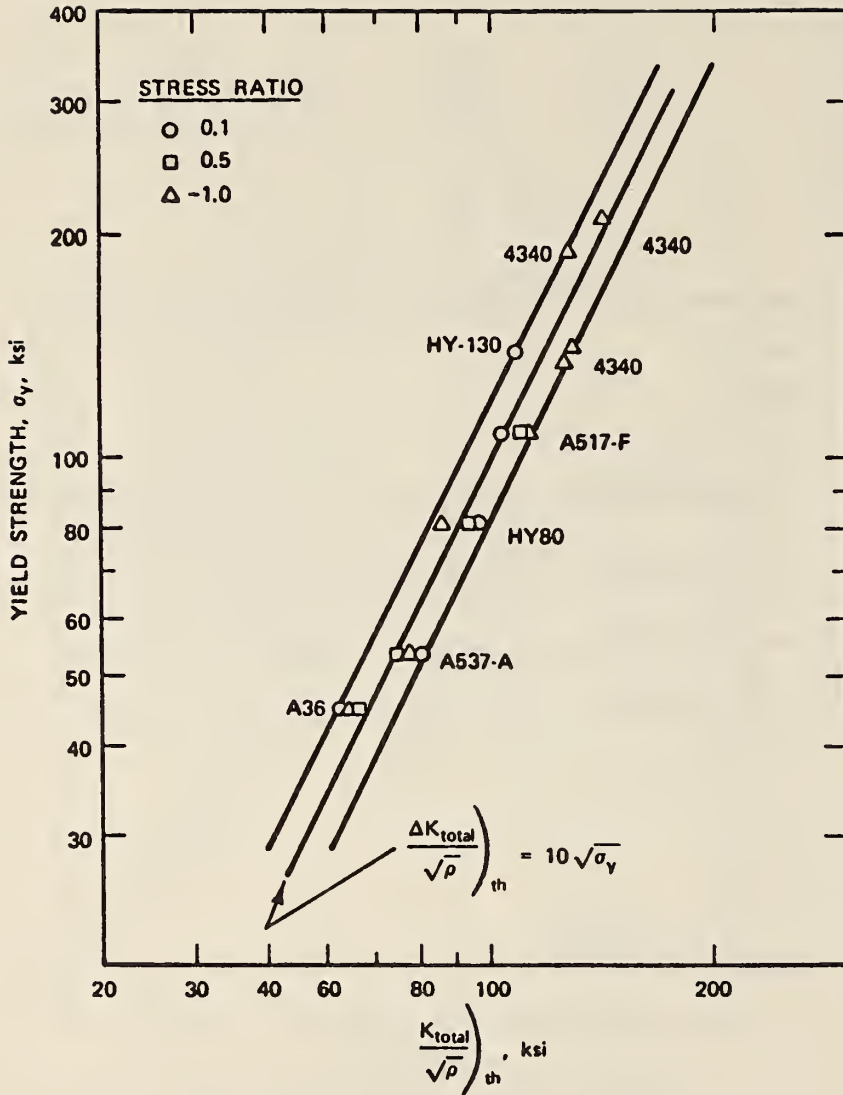


Figure 2-10 Dependence of fatigue-crack-initiation threshold on yield strength.



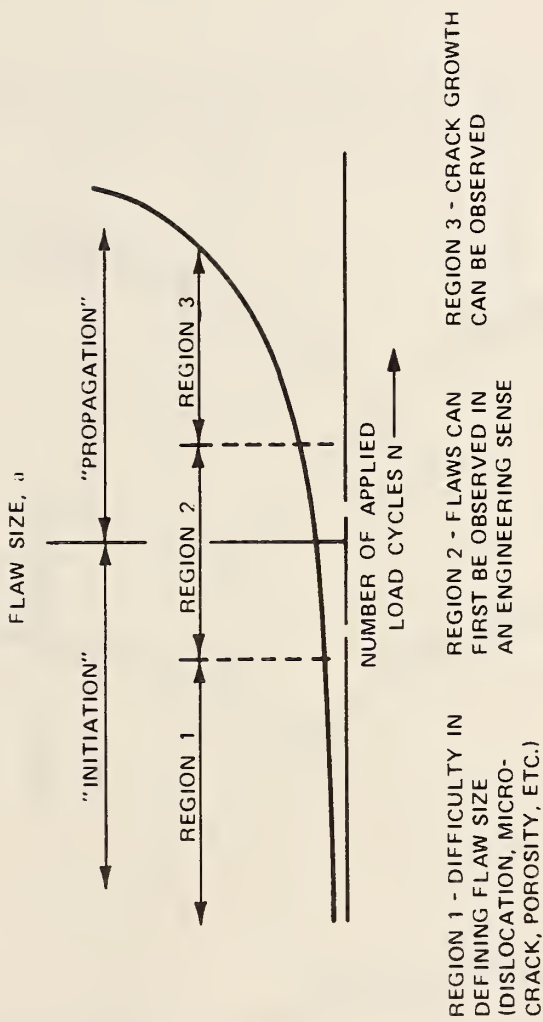


Figure 2-11 Schematic showing relation between "initiation" life and "propagation" life.

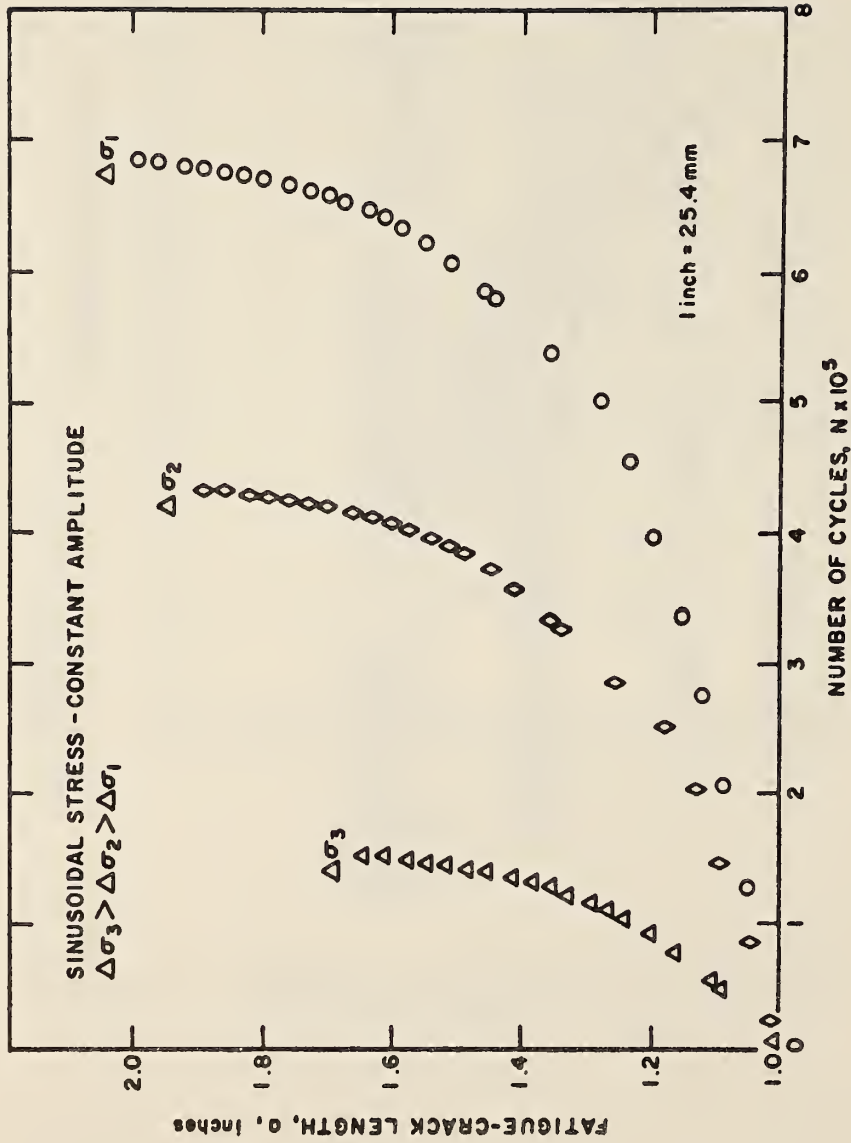


Figure 2-12 Effect of cyclic-stress range on crack growth.

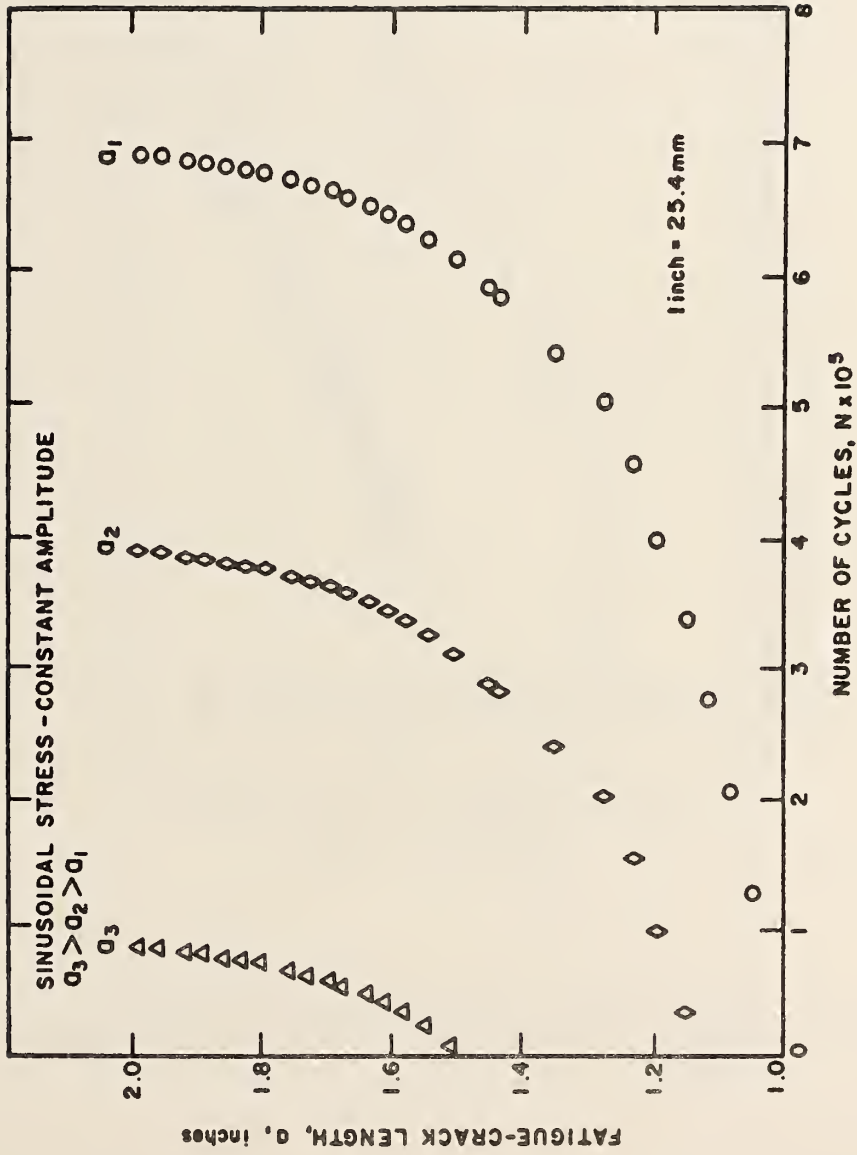


Figure 2-13 Effect of initial crack length on crack growth.

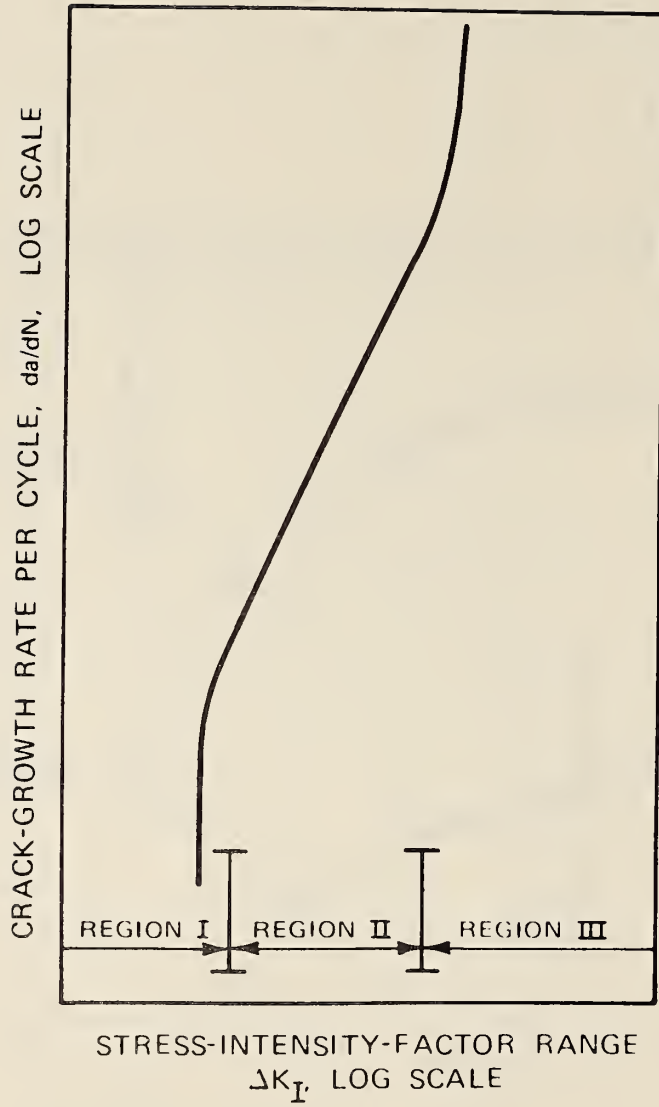


Figure 2-14 Schematic representation of fatigue-crack growth in steel.

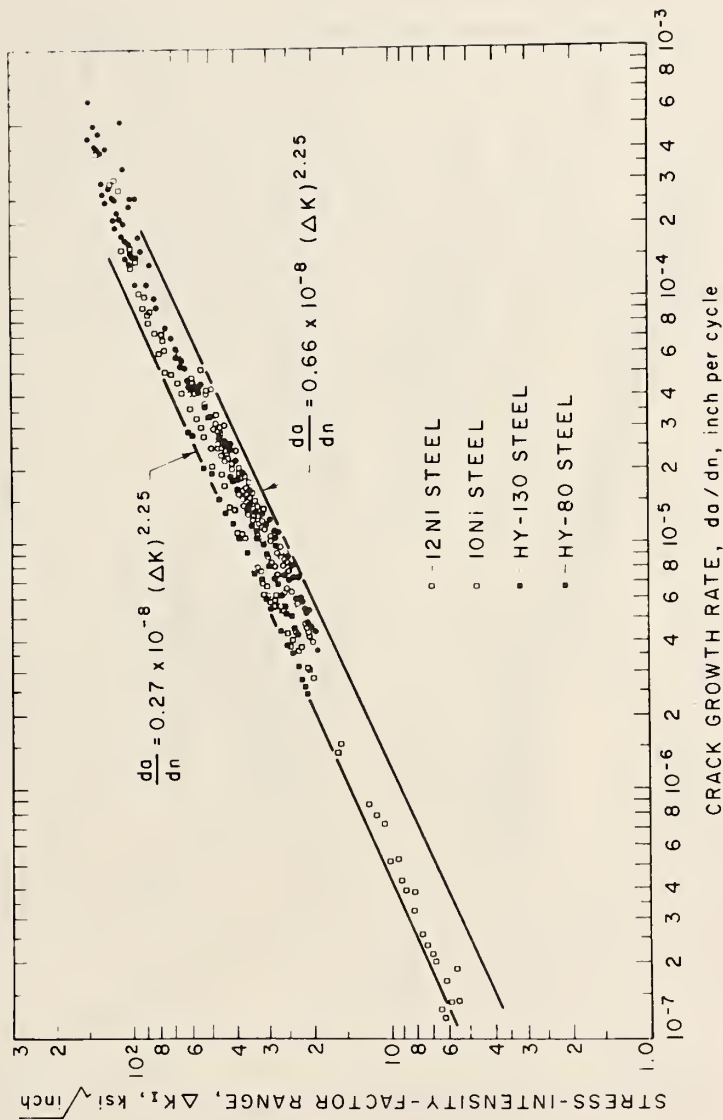


Figure 2-15 Summary of fatigue-crack-propagation data for martensitic steels.

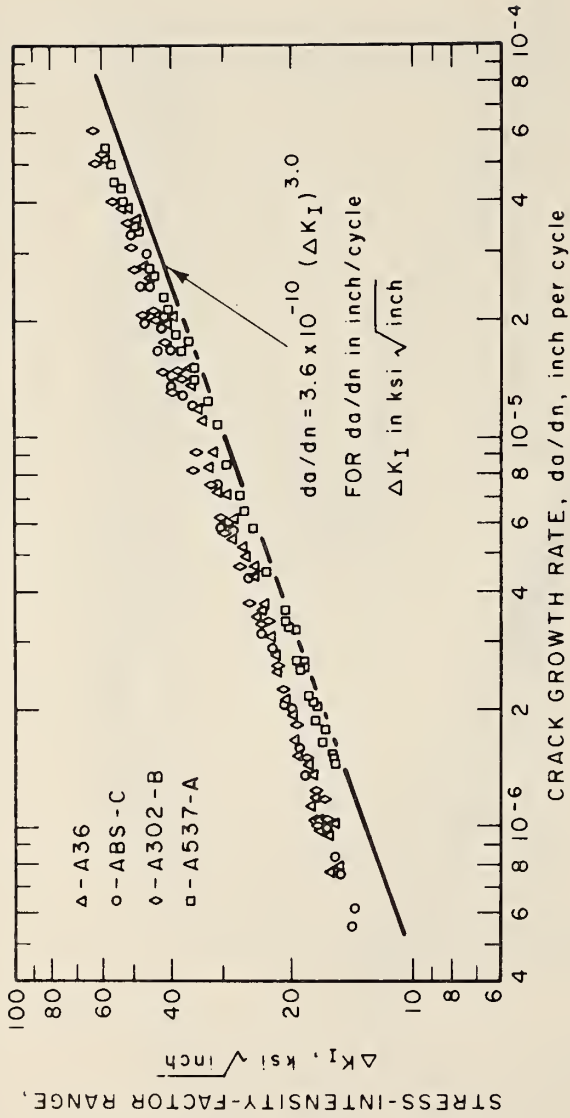


Figure 2-16 Summary of fatigue-crack-growth data for ferrite-pearlite steels.

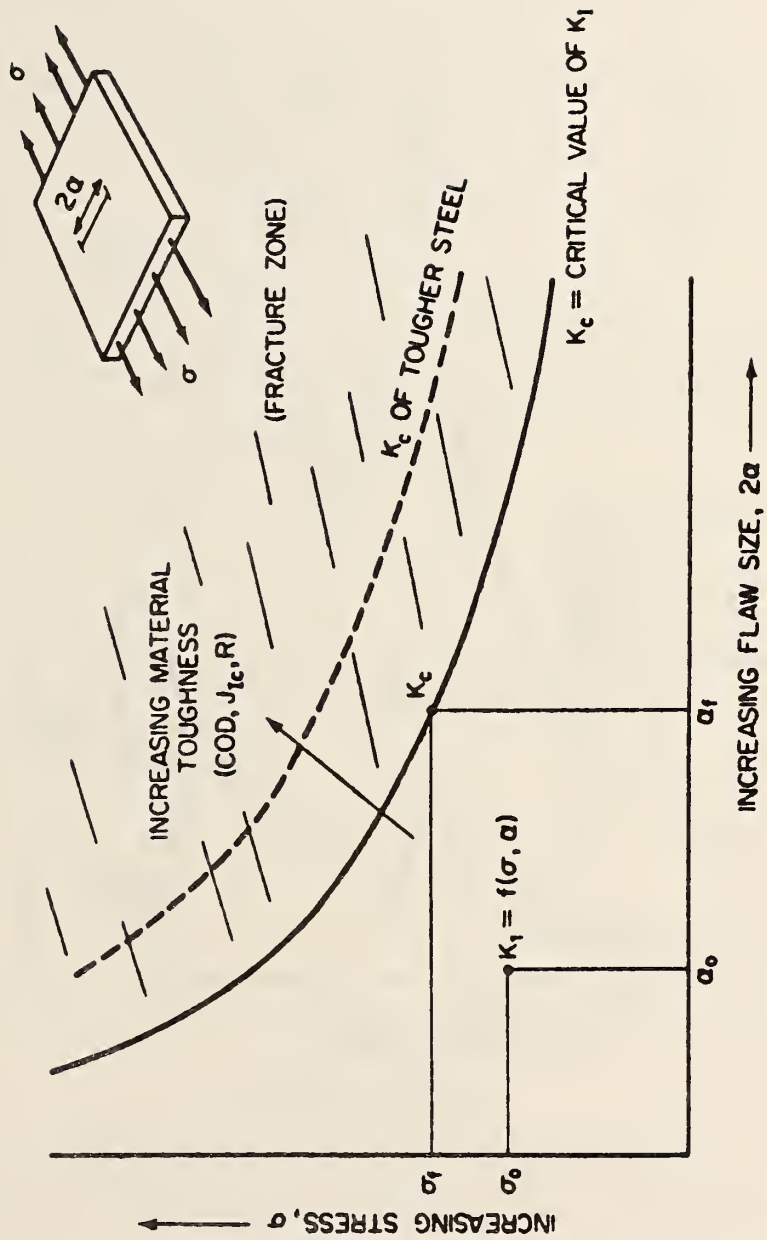


Figure 2-17 Schematic showing relation between stress, flaw size, and material toughness.

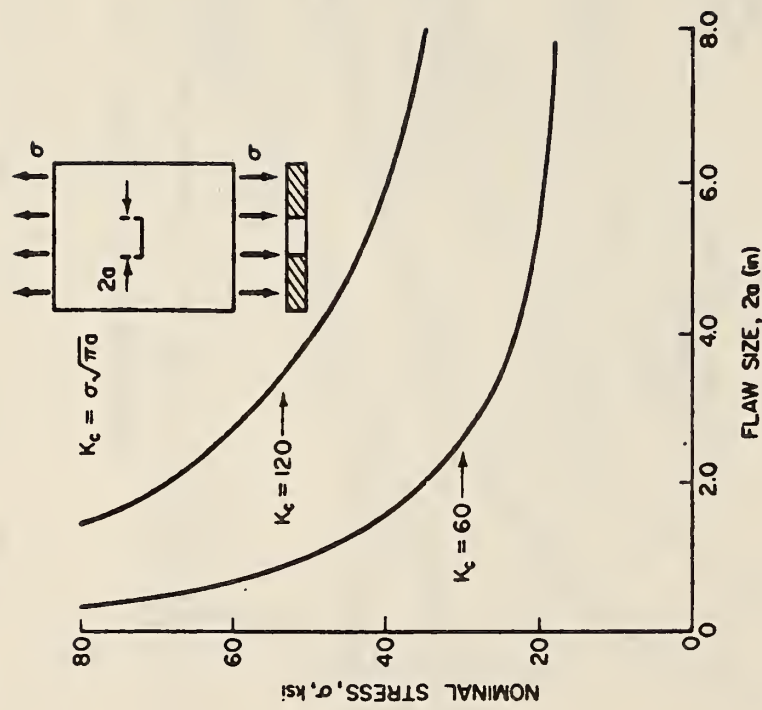
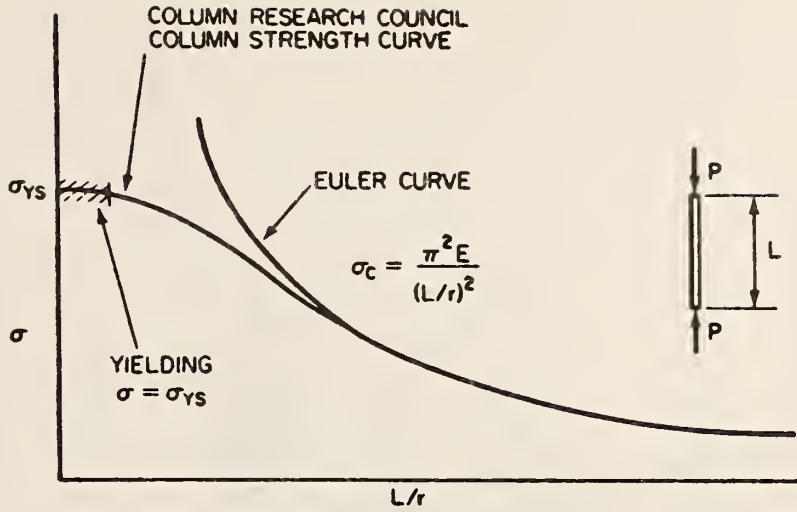
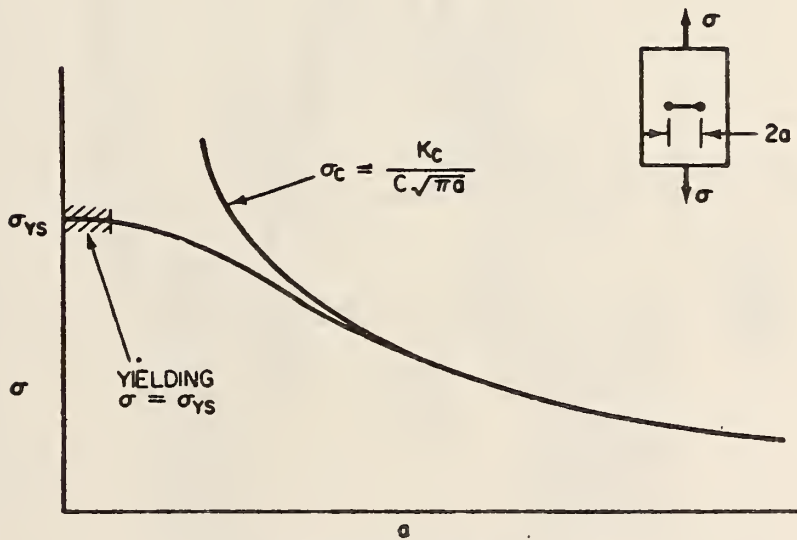


Figure 2-18 Stress-flaw size relation for through-thickness crack.





(a) COLUMN INSTABILITY



(b) CRACK INSTABILITY

Figure 2-19 Column instability and crack instability (after Madison and Irwin).

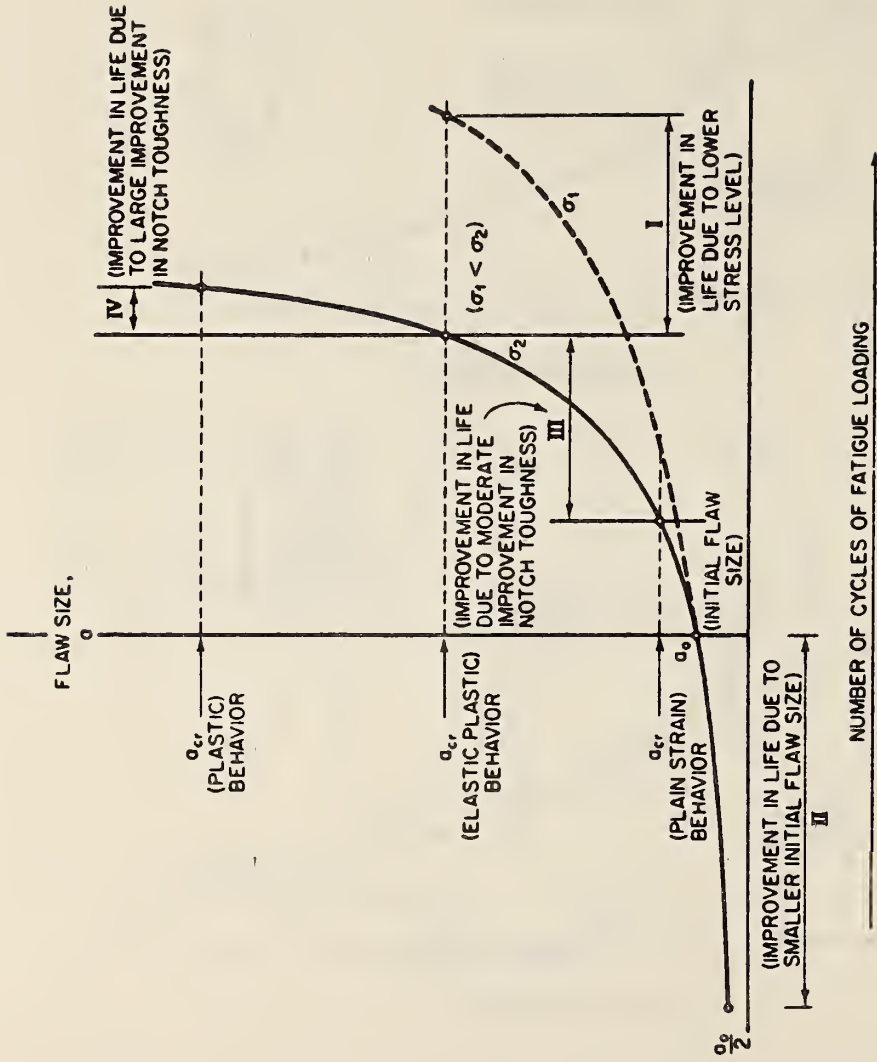


Figure 2-20 Schematic showing effect of notch toughness, stress, and flaw size on improvement of life of a structure subjected to fatigue loading.

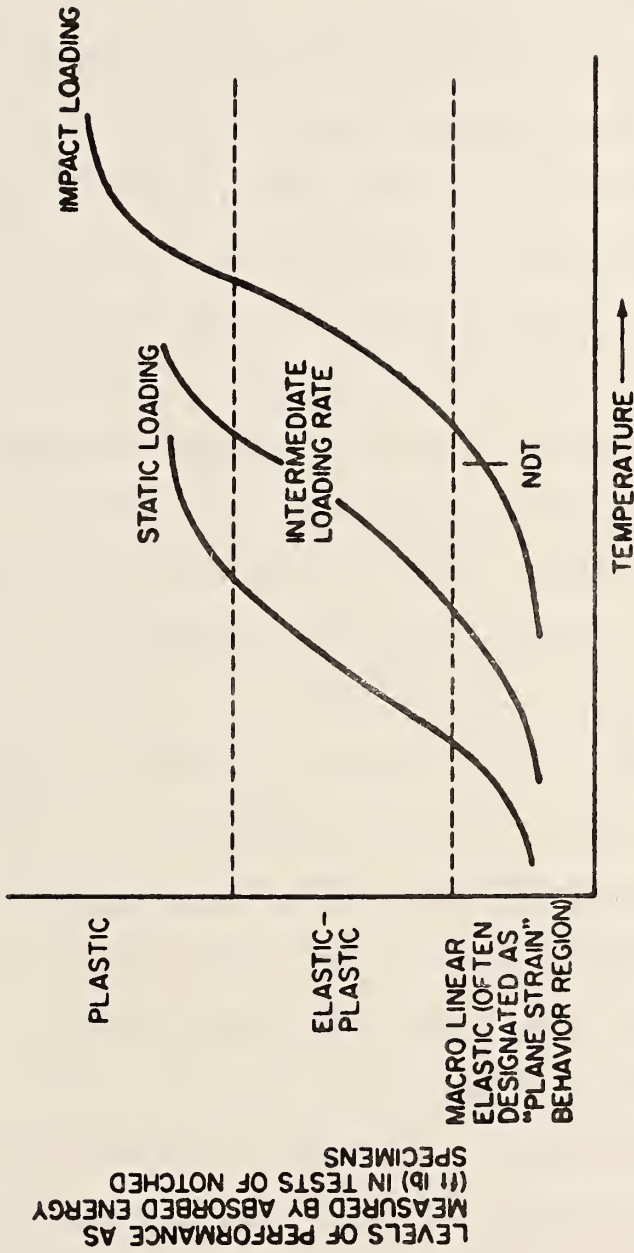


Figure 2-21 Schematic showing relation between notch-toughness test results and levels of structural performance for various loading rates.

## CHAPTER 3. FATIGUE BEHAVIOR OF WELDMENTS AND THE AASHTO REQUIREMENTS

### 3.1 INTRODUCTION

Experience with actual bridge structures has indicated that most cracks have developed because of fatigue. Fatigue cracks may eventually result in unstable brittle fracture. However, this is invariably preceded by the growth of the fatigue cracks from either internal flaws or surface discontinuities that reside near geometrical changes in the cross section. Concern with fatigue cracking has grown during the last ten years. A number of studies in the United States and abroad have attempted to define the basic fatigue strength of a large variety of commonly used welded structural details.<sup>1,2,3)</sup> A review of the literature that was available in 1965 indicated that it was desirable to undertake tests on specimens that simulated prototype connections. Many of the early studies were only able to provide approximate design relationships because of limitations in the test data. Often many variables were introduced in an experiment that involved a limited number of specimens. This made it impossible to clearly establish the significance of many variables. To overcome the shortcomings of these earlier tests, more recent studies<sup>1,2)</sup> have used beam tests in order that the test detail more closely resembles the prototype connection. This permitted shortcomings with specimen type to be overcome, (i.e., problems with residual stresses and other uncontrolled variables). The cover-plate shown in Figure 3-1 is typical of the type of beam detail that was used to establish the fatigue behavior of typical bridge connections.<sup>1)</sup>

### 3.2 FATIGUE OF WELDED DETAILS

Experience with fatigue crack growth in structural details has indicated that two primary types of fatigue cracks occur. One is the crack that grows from internal discontinuities. These discontinuities occur in a number of welded details. In welded plate girders without attachments, most laboratory fatigue cracks were observed to originate in the web-flange-fillet welds at internal discontinuities such as porosity, lack of fusion or trapped slag. As Figure 3-2 demonstrates, these cracks may occur on either the tension or compression flanges of welded built-up girders. The reason that the cracks form in both tension and compression flanges can be understood by examining the residual stresses that exist in welded beams. The welding process results in tensile residual stresses along the weld. This means that the internal discontinuities that exist in the weld reside in a residual tension stress field that is at or near the yield point. Hence the crack doesn't know whether or not the stress cycle is compression or tension.

Typical of the internal discontinuities that have resulted in fatigue cracks in welded built-up details is the small fatigue crack shown in Figure 3-3. You will note that the crack has assumed a penny shape and originated at an internal discontinuity which appears as a porosity or gas pocket.<sup>1,2)</sup> As this type of fatigue crack grows it maintains its penny shape even though the crack penetrates one of the free surfaces of the welded built-up component. Also, note that the longitudinal discontinuity which is parallel to the stress field because of the lack of fusion from the two parallel

web-to-flange fillet welds had no effect upon the shape or fatigue crack growth behavior. Further crack growth showed that the penny shaped crack was maintained until the crack tip had penetrated the bottom flange. Final fracture is at a higher rate of growth and usually results in complete failure of the tension flange as shown in Figure 3-4.

If we examine the fatigue test data for the welded plate girder without attachments, we obtain the relationship shown in Figure 3-5 where stress range is plotted as a function of the number of cycles to failure. Three levels of minimum stress were examined and are indicated by the three different symbols. A mean line and its lower tolerance line are also shown. Figure 3-5 demonstrates that there is no significant effect of minimum stress. In other words, the stress ratio,  $R$ , did not have a pronounced effect upon the fatigue behavior and stress range alone provided for the fatigue behavior.

It is also of interest to examine the effect of the type of steel. It is apparent in Figure 3-6 that all grades of structural steel with yield stress ranging from 36 ksi to 100 ksi provide the same basic fatigue strength. This test data is in general agreement with the basic studies on fatigue crack growth discussed in Chapter 2.

The studies that were plotted in Figures 3-5 and 3-6 were from a single program sponsored by the National Cooperative Highway Research Program (NCHRP) and carried out at Lehigh University since 1967<sup>1,2)</sup>. It is also beneficial to compare the results that

were acquired with earlier test data. This is done in Figure 3-7 and shows that there is good agreement with the earlier test data. Some manually made welds that were tested in 1940 fall below the lower confidence limit and indicate that above average discontinuities existed for these early welded processes. The type of behavior described for plain welded beams is also typical of the behavior experienced at groove welded flanges.

Another major class of detail studied is the beam with welded attachments that experiences fatigue crack growth from a terminating weld toe. Let us first examine cover-plated beams with longitudinal fillet welds attaching the cover-plate to the beam flange. For this detail the fatigue crack starts at the weld periphery where small discontinuities exist at the terminating weld toes which are perpendicular to the applied stress field. As Figure 3-8 demonstrates, the crack grows through the flange thickness as a semielliptical surface crack. Nearly all of its fatigue life is exhausted during this stage of growth. The percentage of life that remains after the crack has penetrated the flange thickness is only 2 to 5 percent. When transverse end welds are also used to attach the cover-plate to the beam flange, the crack also forms at the weld toe that is perpendicular to the applied stress as shown in Figure 3-9. However, as the fracture surface indicates, the semielliptical surface crack that penetrates the flange thickness has a different geometry because the discontinuities exist all along the weld toe. This results in a crack shape that is more severe than the cover-plated beam with longitudinal welds alone.

When the test data for the cover-plated beam is plotted with stress range as a function of cycle life (see Figure 3-10), it is again apparent that the minimum stress did not have a significant influence on fatigue behavior. Stress range is seen in Figure 3-10 to account for the fatigue strength of the cover plate structural detail. Hence dead load stresses are not a factor in fatigue design.

The test results are plotted for three grades of structural steel with yield stress ranging from 36 to 100 ksi in Figure 3-11. These yield strengths generally represent the bounds of material used in bridge construction. It is apparent that the type of steel did not significantly affect the fatigue strength.

Other types of cover-plated beams were examined to ascertain whether or not changes in cover-plate geometry had a significant influence upon their fatigue strength. This included wide cover-plates, thick cover-plates, cover-plates attached to rolled or welded beams, and multiple cover-plates. The test results confirmed that crack growth in a multiple cover-plated beam is not much different than that experienced in the other types of cover-plated beams. It is apparent that the crack has initiated at the terminating weld toe of the partial length cover-plate, penetrated the primary cover-plate, and then entered into the beam flange via the continuous longitudinal welds connecting the primary cover-plate to the beam flange. The results of these different types of welded cover-plate details are summarized in Figure 3-12. This shows that large variations in cover-plate geometry have only minor



influences on the basic fatigue strength. All coverplated beams can be reasonably treated by the same design classification.

We have examined two welded details; one in which crack growth was experienced from an internal discontinuity in the longitudinal web-to-flange welds of the welded beams and one in which crack growth was experienced from the weld toe termination of coverplates. Both of these details have demonstrated that the major factor influencing fatigue strength is the stress range. Neither the minimum stress, that is the dead load stress in the structure nor the type of steel were found to significantly affect fatigue strength. A number of other structural details have been examined, however not as extensively as the welded beam and cover-plated beam. Because these two extremes in welded steel details indicated that neither type of steel or minimum stress were very significant, subsequent studies have focussed more on defining the basic fatigue strength in terms of stress range using fewer grades of steel and not as many levels of minimum stress.

Full scale tests on girders having a variety of types of stiffeners were also made. The stiffeners were either attached to the web alone or welded to the web and flange. These details were examined in regions of bending stress alone and in regions of bending and shear as shown in Figure 3-13. Other tests were undertaken on the smaller scale beams with a variety of welded attachments as illustrated in Figure 3-14. Among the major variables studied were the attachment length and the type of weld configuration attaching the component to the beam flange.

The tests on these girders and beams indicated that the crack formation was very similar to the cover-plated beam in that all of the details involved crack growth from a terminating weld toe. The crack has been observed to penetrate through the plate thickness at the weld toe termination as a semielliptical surface crack as shown in Figure 3-15. The cracks were observed to initiate at micro discontinuities that were perpendicular to the stress field. A number of small semielliptical surface cracks can be seen along the weld toe. As the cracks continue to grow they appear to coalesce forming a longer semielliptical surface crack.

If we examine the results of these tests on beams with stiffeners attached to the web or web and flange (see Figure 3-16), we observe again that stress range as a function of cycle life is the dominant variable defining fatigue strength. We have also found that the bending stress range alone provides an adequate definition of the fatigue strength. This results because the direction of principal stress is continuously changing as moving loads cross the span. Hence, the bending component becomes more predominant in structures with moving loads.

If we examine the phases of crack growth for the different stiffener types we can see that when the stiffener is attached to the web alone that somewhere between 80 and 90% of the fatigue strength is exhausted propagating the crack through the web alone (see Figure 3-17). Thereafter the crack grows up the web and down into the flange before the remaining life is exhausted. When the stiffener is welded to both the web and flange, the cracks are

simultaneously propagating into the web and flange. When the crack has penetrated the flange thickness, nearly all of its fatigue strength is exhausted. Hence, even though the crack that grows into the web might have some effect due to shear, this is more than off-set by other factors.

Hence, all stiffeners can be treated as the same type of welded detail. When we examine the behavior of other attachments we also observe that crack growth initiates from the termination of a weld toe perpendicular to the stress field. This is illustrated in Figure 3-18 for an eight inch long attachment that was welded to a tension flange.

In this case the attachment was welded to the flange by longitudinal welds alone. Crack growth has initiated from the longitudinal weld toes and penetrated into the flange at the interior welds as semielliptical surface cracks. The longitudinal welds that were attached to the flange tips permitted the crack to grow as an edge crack. The results of studies on beams with four-inch attachments are summarized in Figure 3-19. Again, stress range is seen to be the dominant variable affecting fatigue strength. A four-inch length attachment is seen to provide a fatigue strength that is rapidly approaching the lower bound provided by the cover-plated beam. The test data fall between the lower confidence limit provided by the plain welded beam and the mean fatigue strength of the cover-plated beam. Because stress range is the major variable influencing fatigue strength, it is now possible to take the various welded beam details that

had been examined and group them in convenient categories of fatigue strength. Figure 3-20 shows the stress range-cycle life relationship, with the upper bound the plain welded beam and progressing successively lower to the cover-plated beam at the lower limit. These lines represent the lower confidence limits of fatigue data for the various details and were used to derive design stress ranges for various numbers of design stress cycles.

### 3.3 AASHTO FATIGUE REQUIREMENTS

Four different cycle lines and their corresponding stress ranges are tabulated in Table 3-1. These range from 100,000 cycles which represents a minimum number of design stress cycles to over 2,000,000 cycles which is an approximation of the fatigue limit. Category A is applicable to the rolled beam and plate without attachments. Category B is applicable to the plain welded beam and various groove welds that have been non-destructively inspected. Categories C, D and E are applicable to the various groove and fillet welded connections that have their weld toe terminating perpendicular to the stress field so that crack growth initiates from a weld toe. The basic stress range concept can be demonstrated to be directly related to the crack growth- $\Delta K$  relationship from fracture mechanics. In plain welded beams, cracks initiate from discontinuities in the web-to-flange weld and grow as a penny shaped crack<sup>4)</sup>. The stress intensity factor for this crack is mathematically well defined. When the crack growth rate is measured in a welded beam, the rate of crack propagation is very compatible with the  $\Delta K$ -crack growth rate relationship observed for ferrite-pearlite steels (see Figure 3-21).

When a satisfactory mathematical expression is available to describe the stress intensity at complex welded details it is possible to estimate their fatigue strength in terms of basic crack growth data discussed in Chapter 2.

If the penny-shaped model is examined carefully as shown in Figure 3-22, we observe that most of the fatigue strength is exhausted at crack growth rates that are below most of the experimental crack growth data that have been acquired. Figures 3-21 and 3-22 show that the fatigue strength has been exhausted for crack growth occurring below  $10^{-6}$  and  $10^{-4}$  in/cycles into the low crack growth rate region. When crack growth studies have been undertaken at or near the crack growth threshold, they have indicated that the crack growth threshold is about  $3 \text{ ksi}\sqrt{\text{in}}$  ( $3.3\text{MPa}\sqrt{\text{m}}$ ).

Experience with small test beams has confirmed the crack growth threshold. This can be seen in Figure 3-23 where cover plated beams are plotted as a function of cycle life. A number of beams have been tested to an extreme life of 100,000,000 cycles without cracking. This fatigue limit was observed to be compatible with the crack growth threshold of  $3 \text{ ksi}\sqrt{\text{in}}$  ( $3.3\text{MPa}\sqrt{\text{m}}$ ). More recent studies have indicated that the fatigue limit may be even lower on larger beams which more closely approximate the sizes found in actual bridges. Additional work is currently underway in this area.

We have examined the basic fatigue strength under constant cycle loading. Actual structures are subjected to loads that produce a variable stress cycle in both time and magnitude. Hence, it is of interest to examine the relationship between constant

cycle and variable cycle loading. For more than thirty years, Miner's Rule has been used to provide the link between constant cycle and variable cycle loading. Several years ago a major project conducted at the Applied Research Laboratories of the U.S. Steel Corporation under the sponsorship of NCHRP<sup>5)</sup> was initiated to examine the fatigue behavior of bridge weldments for non-uniform loadings. In this study plain welded beams and beams with cover plates were examined. These beams had the same configuration of the earlier studies that were undertaken at Lehigh University. A Rayleigh probability density curve was selected to describe the variable stress spectrum to which the beams were subject as shown in Figures 3-24 and 3-25. Relatively large variations in the variable cycle stress range were imposed. This was undertaken by varying the ratio of the parameter  $S_{rd}/S_{rm}$  as is demonstrated in this illustration. When this ratio is zero it corresponds to constant cycle stresses. As the ratio is increased a very large variation in the stress range results.

Both A36 and A514 beams were tested under variable cycle loading. The stress ranges corresponding to the probability density curve were completely randomized so that a random cyclic loading was applied at a given level of minimum stress corresponding to the variable stress spectrum. These stresses were randomized and increments of 500, 1,000, or 1,500 cycles were continuously applied to the test beams until failure. The results of these studies on cover plated beams were correlated with the constant cycle fatigue data by transforming the variable stress range spectrum

into an equivalent stress range. This was accomplished using the root-mean-square (RMS) of the randomly applied stress range spectrum which was observed to provide a good fit to the test data as shown in Figures 3-24 and 3-25.

A comparable result was obtained when Miner's Law was used to derive an equivalent stress range. Figure 3-25 shows that good correlation can be achieved using either the Miner's Rule or the root-mean-square of the variable stress range spectrum. Both methods provide a satisfactory method of relating the variable stress range cycles that are experienced in structures to the constant cycle loading that has been used in the laboratory to derive the basic fatigue strength relationships.

Fatigue specifications in the United States have always used a design reference load and its corresponding number of equivalent stress cycles for fatigue design. This merely reflects the fact that the actual variable stress cycles which occur at a greater frequency and lower magnitude of stress have been transformed to the design reference loading. The behavior of the AASHTO Road Test bridges suggested there was a need to acquire stress history measurements on bridges in service. These measurements have been acquired since the early 1960's<sup>6,7)</sup>.

Measurements of gross vehicle weight have also been acquired yearly by the various states. Figure 3-26 shows the frequency of occurrence of the gross vehicle weight distribution that resulted from the 1970 FHWA nationwide loadometer survey<sup>8)</sup>. Subsequent surveys have indicated a comparable distribution exists today.

Measurements on highway bridges have demonstrated that the measured stresses provide the same general trend as the gross vehicle weight distribution. The measurements have also indicated that the actual stresses in a bridge are always less than the stresses one would calculate from the applied loads. This means that the actual measured stress ranges are a factor  $\alpha$  less than the stresses that would be predicted.

A number of experimental studies have been undertaken since the early 1960's to determine the value of  $\alpha$ . These indicate that  $\alpha$  is between 0.5 and 0.8 depending upon the bridge and member<sup>8)</sup>. For longitudinal members the average factor is about 0.7, assuming that the loads crossing the structure correspond to a single vehicle on the bridge. The reason that there are reductions in stress are such factors as impact, the load distribution in the structure, and the design idealization versus the actual three dimensional behavior. For example, the lateral bracing system is often beneficial in reducing the stresses in the main member because it works with the structure much more than assumed in the design process.

Design lives were derived for the 1974 AASHTO Interim Specifications using observed behavior. Miner's Law was used to derive the design stress cycle tables that appear in the specification for longitudinal and transverse members. This was done using a stress spectrum compatible with the gross vehicle weight distribution that was described by the 1970 FHWA nationwide survey. This resulted in an equivalent number of design stress cycles which is a



function of the design life, the factor  $\alpha$  and the average daily truck traffic (ADTT) that will use the structure throughout its life. The factor  $\alpha$  was chosen conservatively to assure that adequate fatigue provisions would result. For specification purposes, traffic that corresponded to an extremely heavily traveled road was defined as 2500 trucks per day. The actual calculations resulted in about 4000 trucks per day. However, in view of the uncertainties in projecting future traffic and other unknown factors, a 2500 average daily truck traffic volume was used. A minimum service life of 70 years was also utilized to arrive at the AASHTO Specification. The specification provides a means of assuring that fatigue crack growth is unlikely to occur throughout the design life of the structure. Design limits appearing in the 1974 AASHTO Specification are given in Table 3-1 while Figures 3-27 and 3-28 show typical welded details and the fatigue design curves respectively.

## REFERENCES

1. J. W. Fisher, K. H. Frank, M. A. Hirt, and B. M. McNamee, "Effect of Weldments on the Fatigue Strength of Steel Beams," NCHRP Report 102, 1970 Highway Research Board.
2. J. W. Fisher, P. A. Albrecht, B. T. Yen, D. J. Klingerman, and B. M. McNamee, "Fatigue Strength of Steel Beams with Transverse Stiffeners and Attachments," NCHRP Report 147, 1974, Transportation Research Board.
3. T. R. Gurney, Fatigue of Welded Structures, Cambridge University Press, 1968.
4. M. A. Hirt and J. W. Fisher, "Fatigue Crack Growth in Welded Beams," Engineering Fracture Mechanics, Vol. 5, 1973.
5. C. G. Schilling, K. H. Klippstein, J. M. Barsom, and G. T. Blake, "Fatigue of Welded Steel Bridge Members Under Variable Amplitude Loading," NCHRP Research Result Digest 60, TRB, 1974.
6. G. R. Cudney, "The Effects of Loading on Bridge Life," Highway Research Record No. 263, HRB, 1968.
7. C. F. Galambos and C. P. Heins, "Loading History of Highway Bridges, Comparison of Stress Range Histograms," Highway Research Record No. 354, HRB, 1971.
8. J. W. Fisher, Guide to 1974 AASHTO Fatigue Specifications, AISC, 1974.

TABLE 3.1

CATEGORY	STRESS RANGE (KSI)			
	100,000 CYCLES	500,000 CYCLES	2,000,000 CYCLES	OVER 2,000,000 CYCLES
A	60	36	24	24
B	45	27.5	18	16
C	32	19	13	10
D	27	16	10	7
E	21	12.5	8	5

TYPE OF DETAIL  
PARTIAL LENGTH COVER PLATES

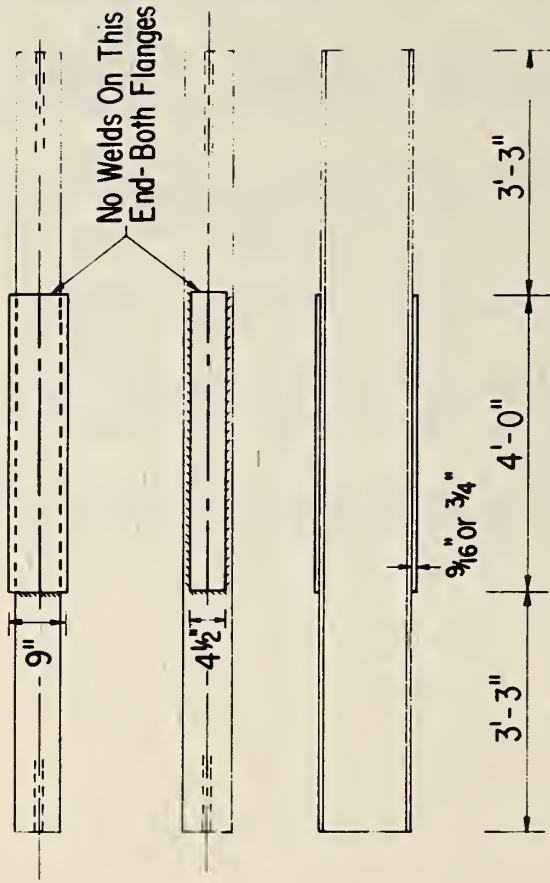


Figure 3-1 Schematic showing details of cover-plated beams.

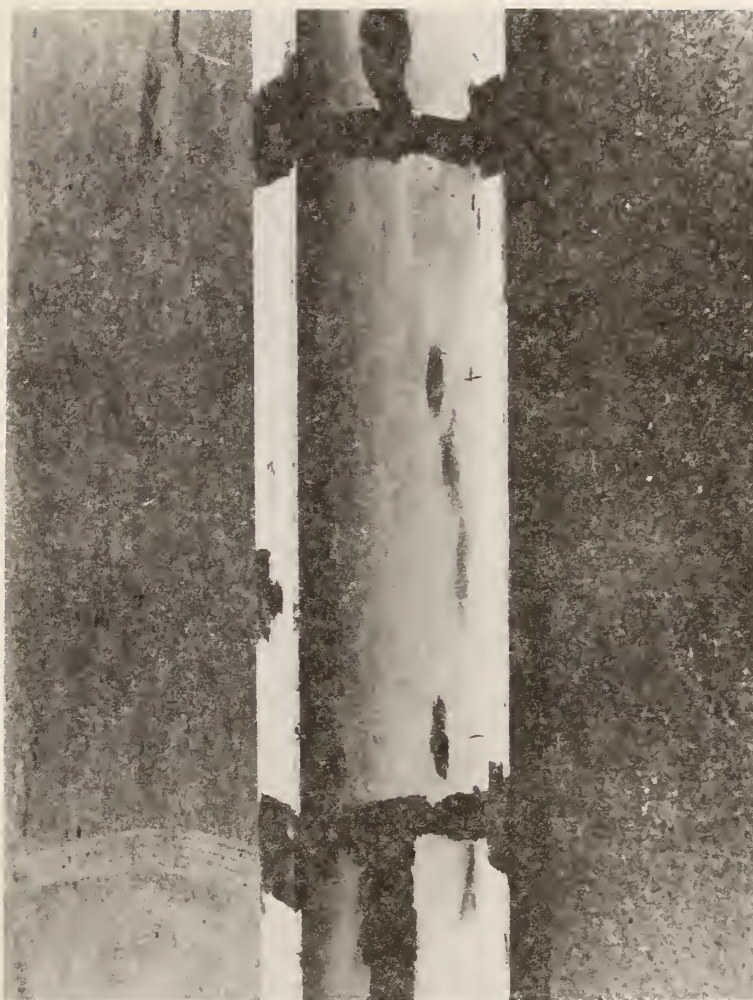


Figure 3-2 Fatigue cracks in compression flange (top) and tension flange (bottom) for A514 steel welded beam.

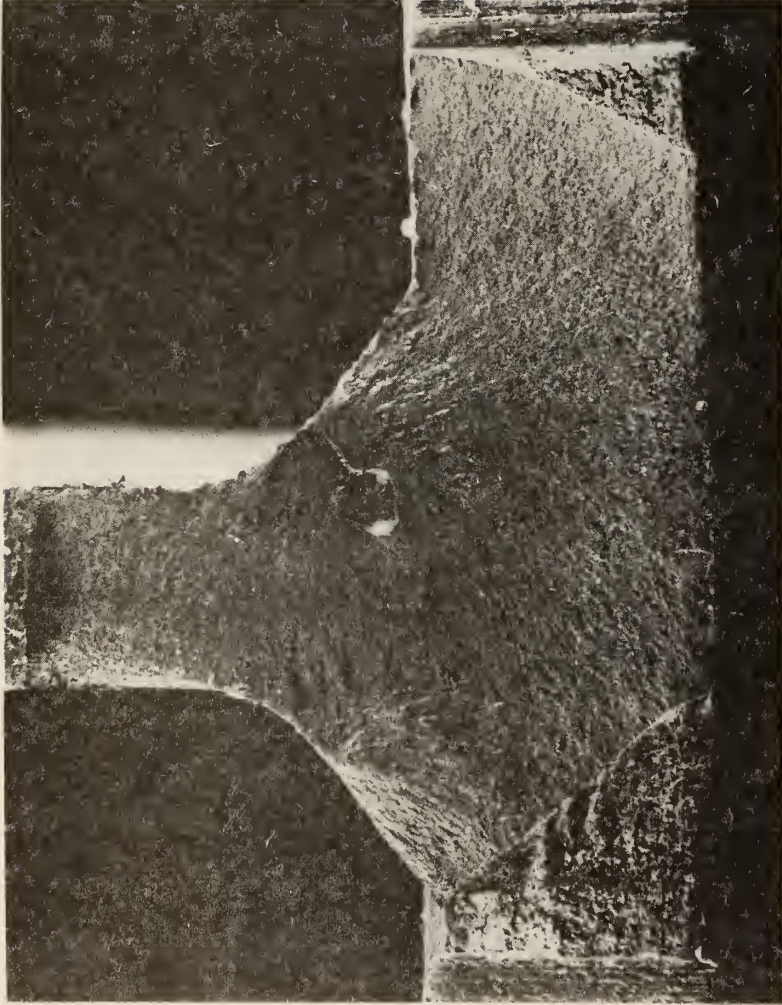


Figure 3-3 Fatigue crack originating from gas pocket in fillet weld of welded beam.

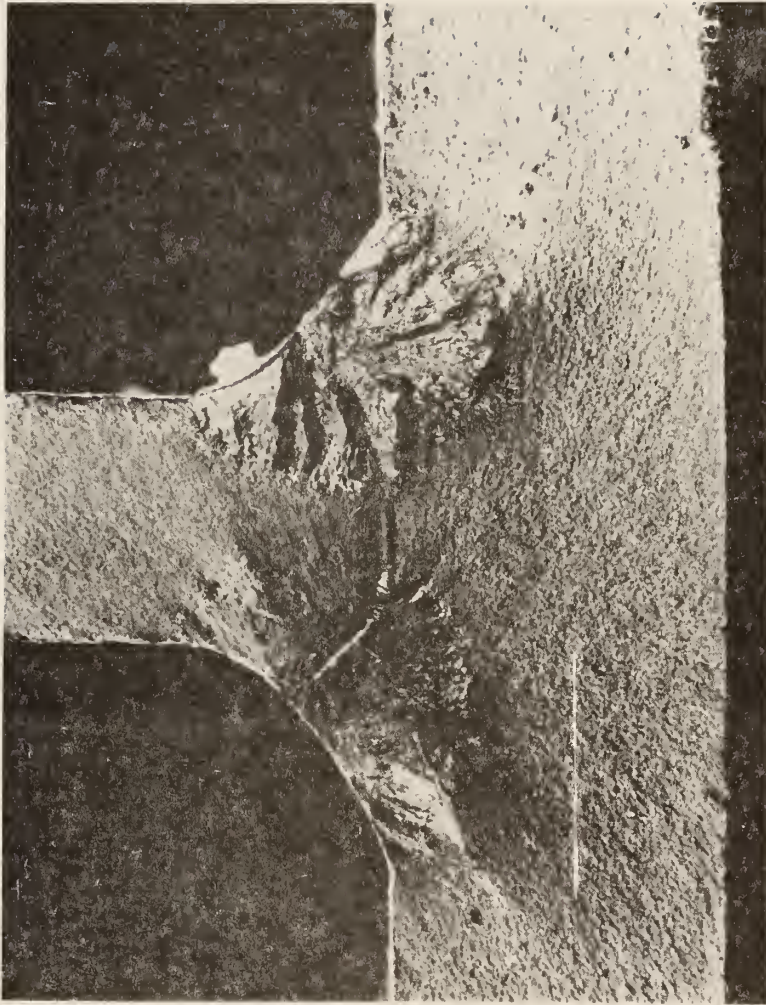


Figure 3-4 Fatigue crack after destroying flange of welded beam.

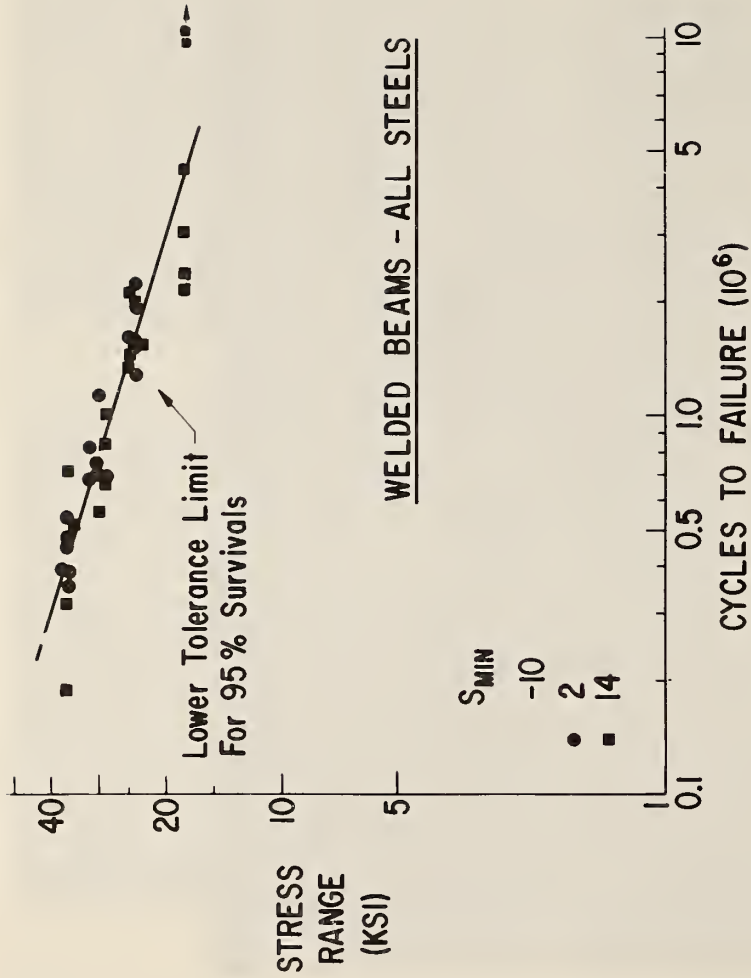


Figure 3-5 Effect of stress range and minimum stress on the fatigue strength of welded beams.



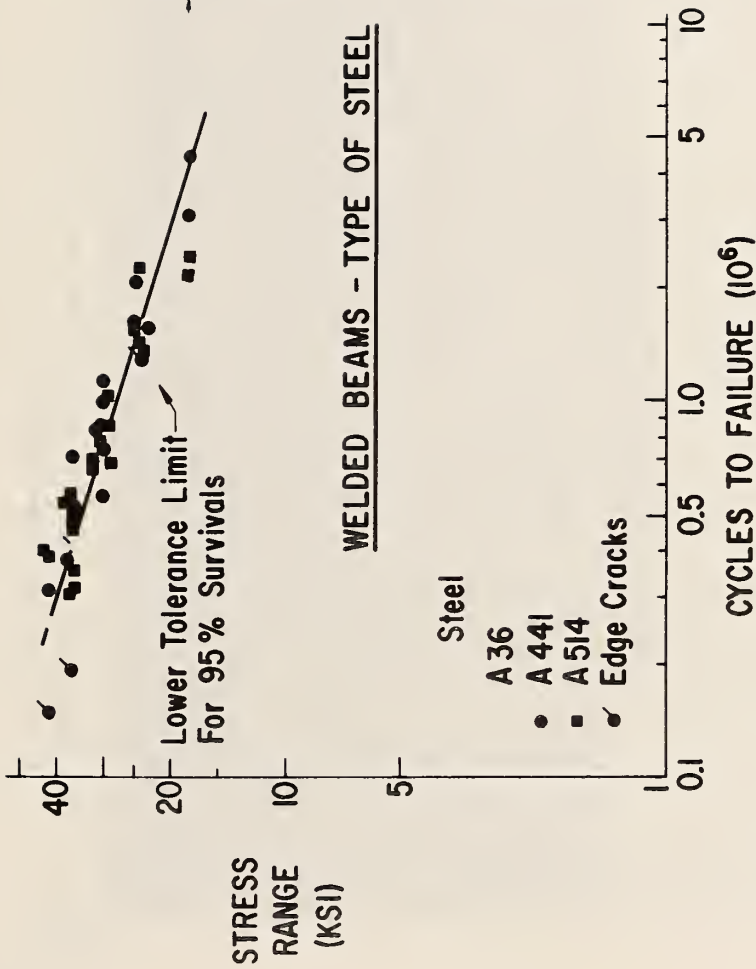


Figure 3-6 Effect of grade of steel on fatigue strength of welded beams.

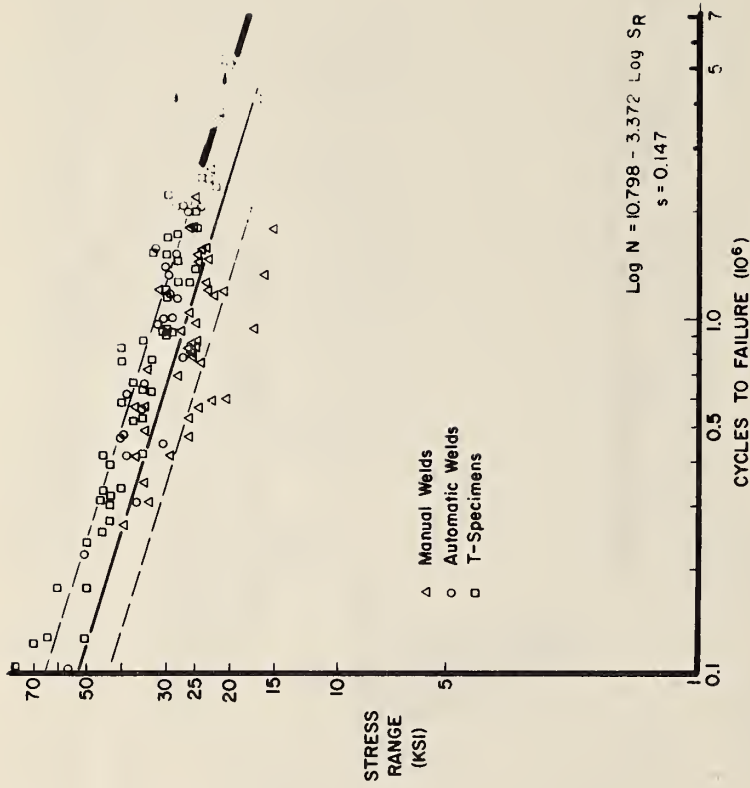


Figure 3-7 Comparison of all previous work on longitudinal fillet weldments with results from beam tests.

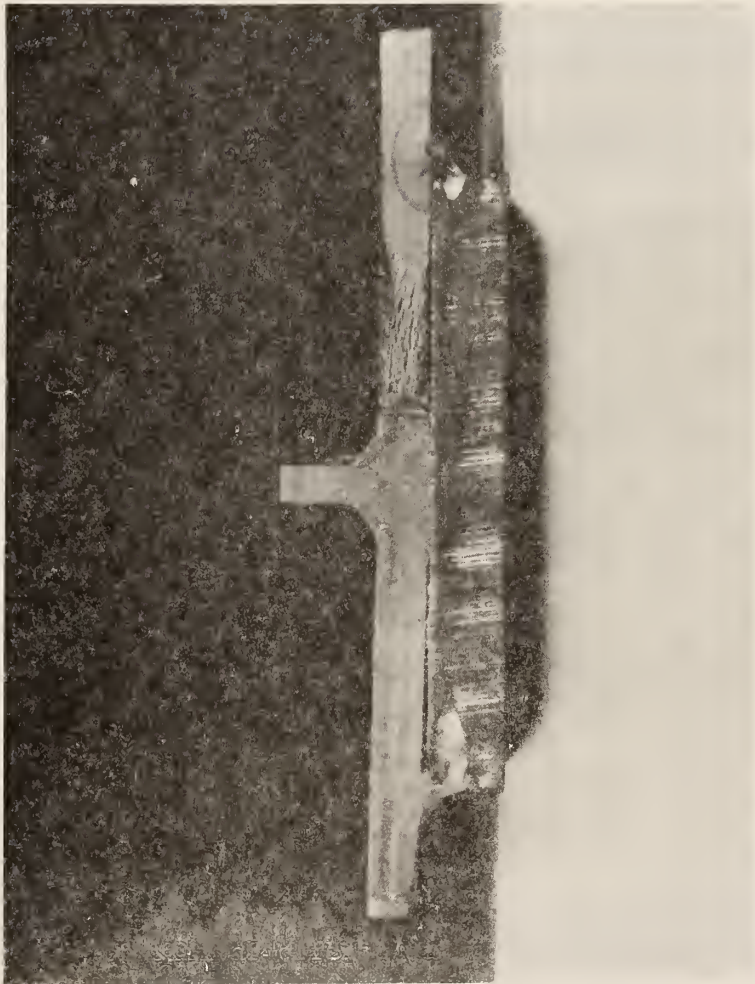


Figure 3-8 Stages of crack growth at unwelded end of cover plates.

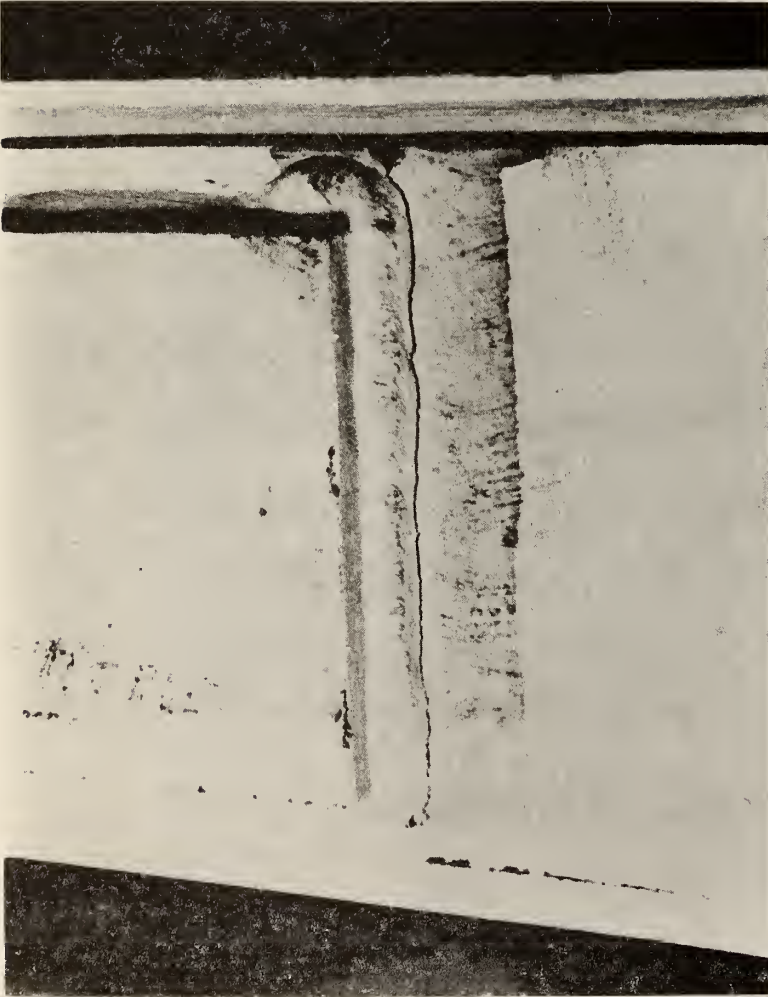


Figure 3-9 Crack formation at toe of transverse fillet weld connecting cover plate to beam flange.

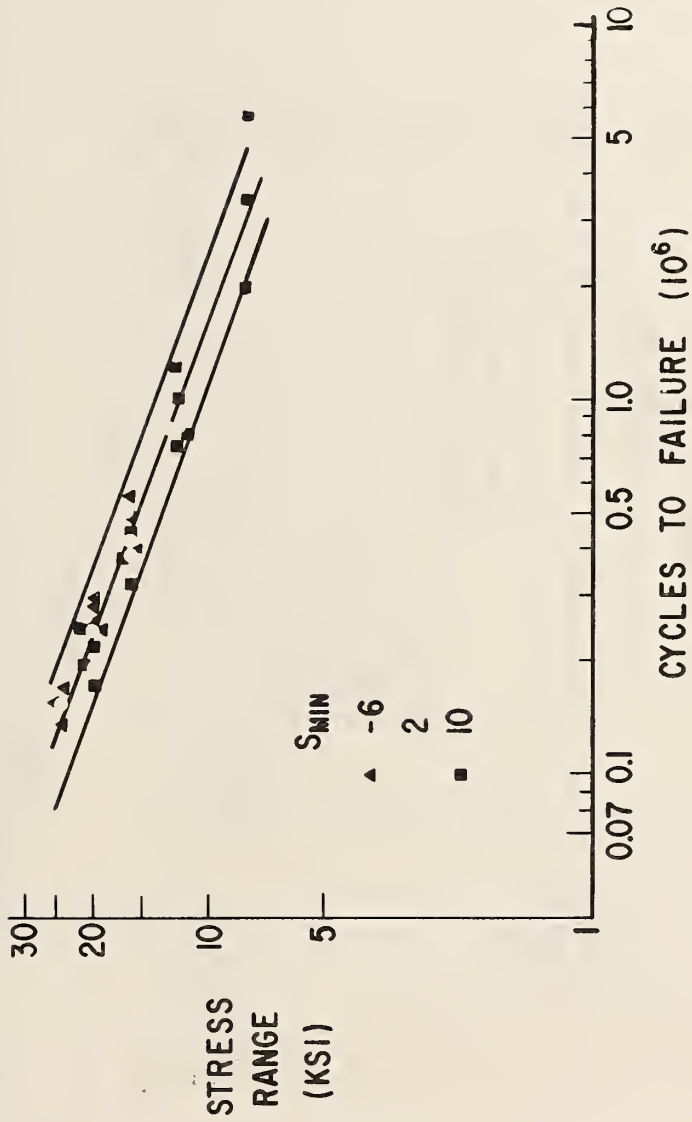


Figure 3-10 Effect of stress range and minimum stress on the cycle life for the welded end of cover-plated beams.

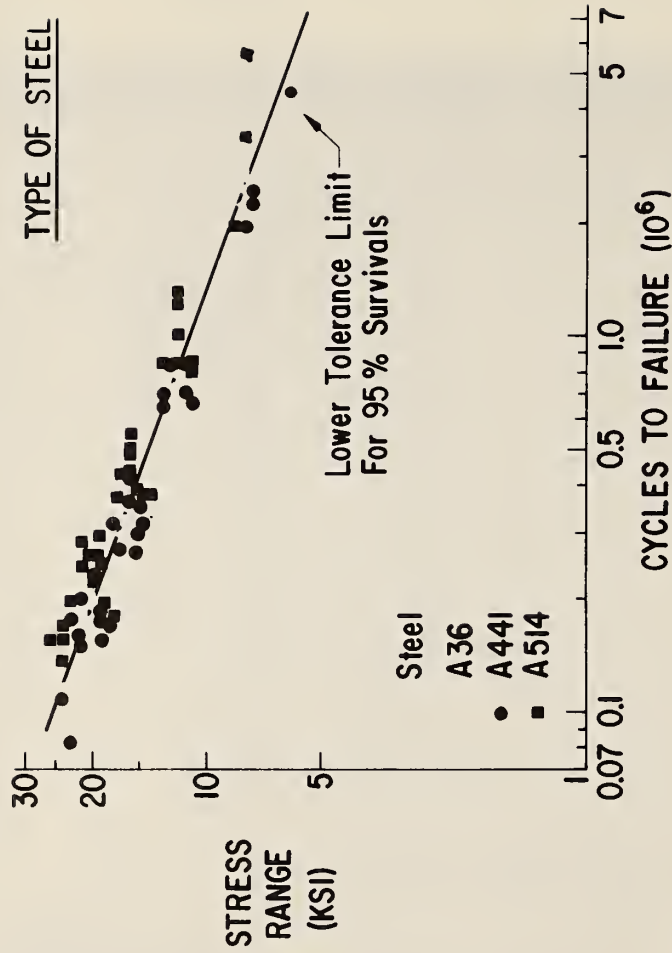


Figure 3-11 Effect of grade of steel on the fatigue strength of beams with transverse end-welded cover plates.

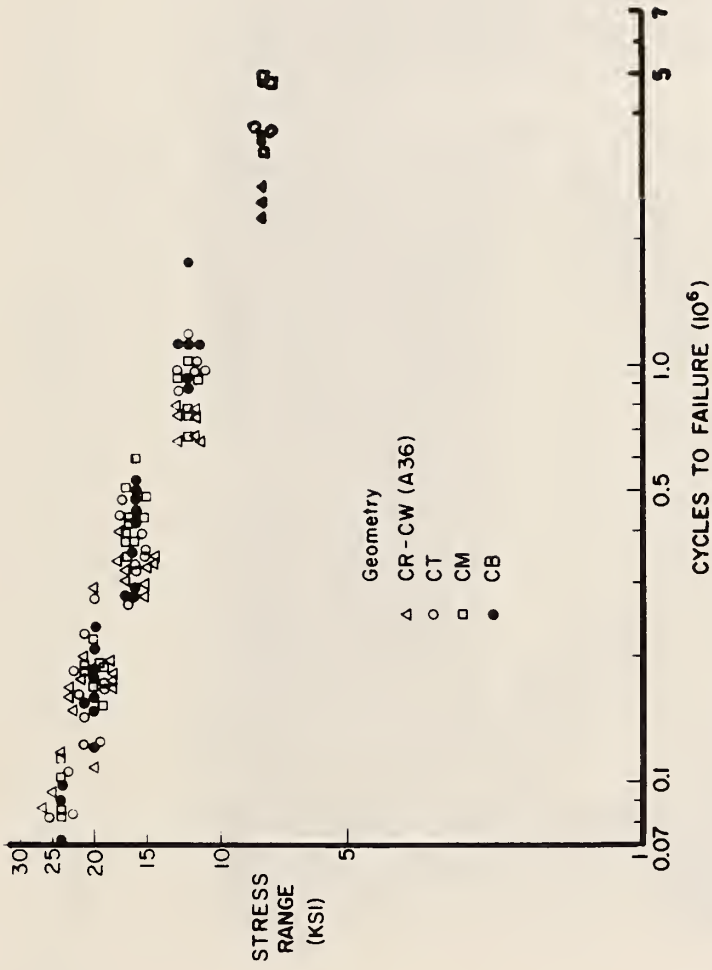


Figure 3-12 Effect of cover-plate geometry on the fatigue strength of beams with end-welded cover plates.

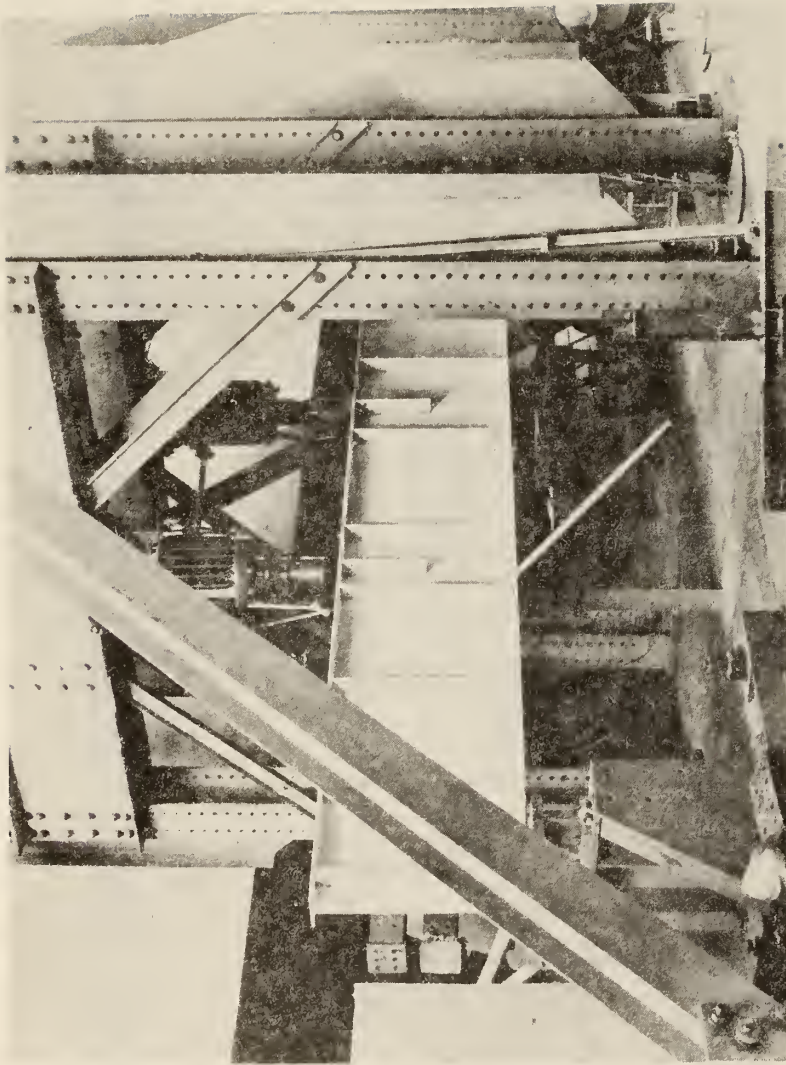


Figure 3-13 Test setup for "full scale" girders with transverse stiffeners.



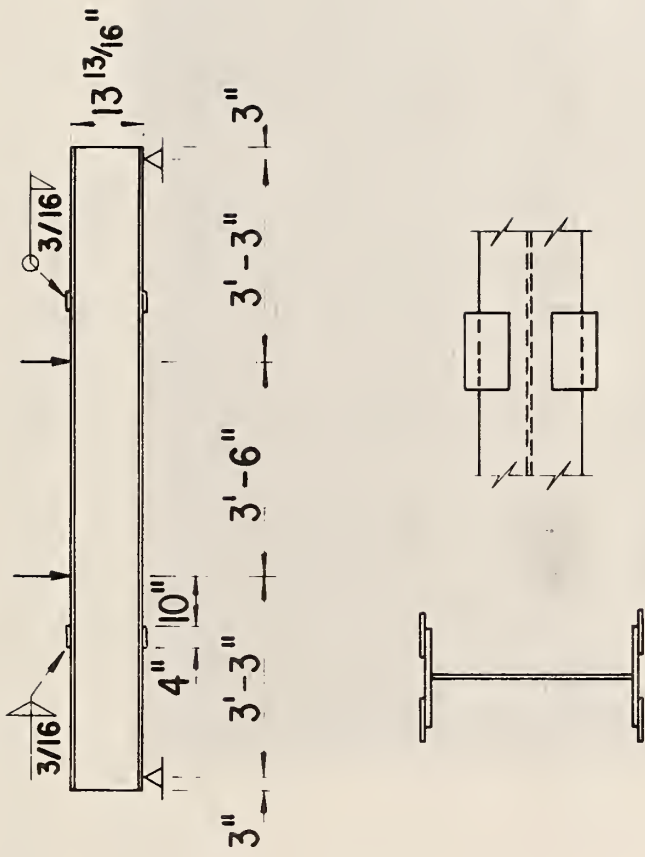


Figure 3-14 Details of beams with welded flange attachments.

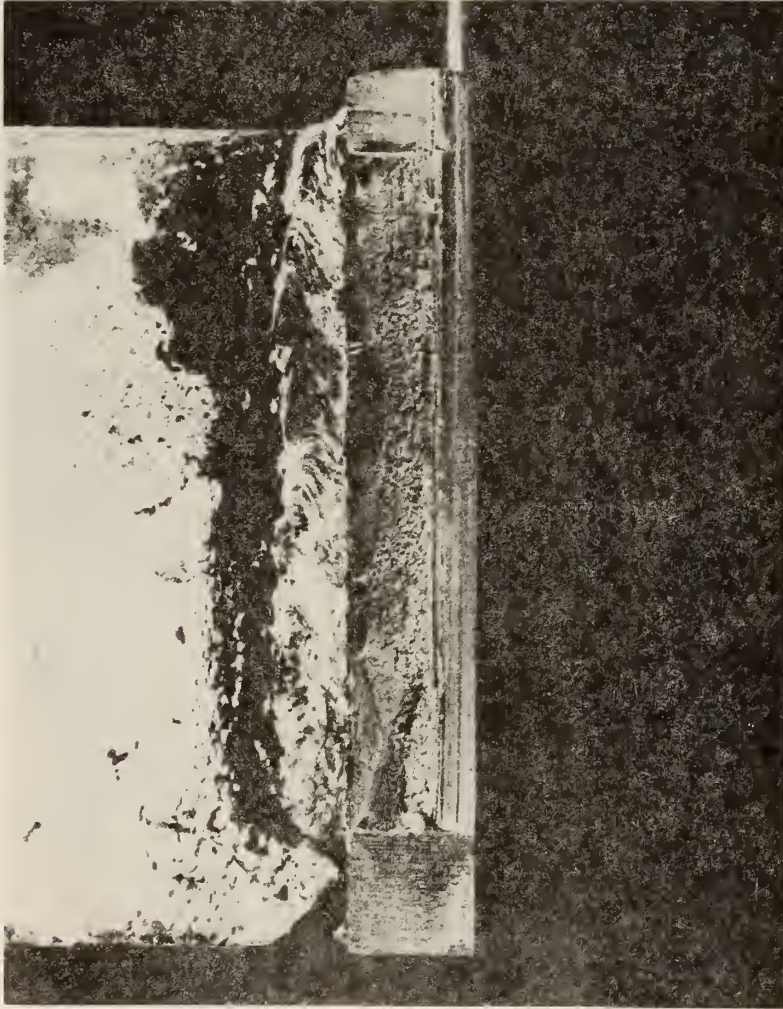


Figure 3-15 Multiple fatigue crack growth at the toe of a stiffener-to-tension flange weld.

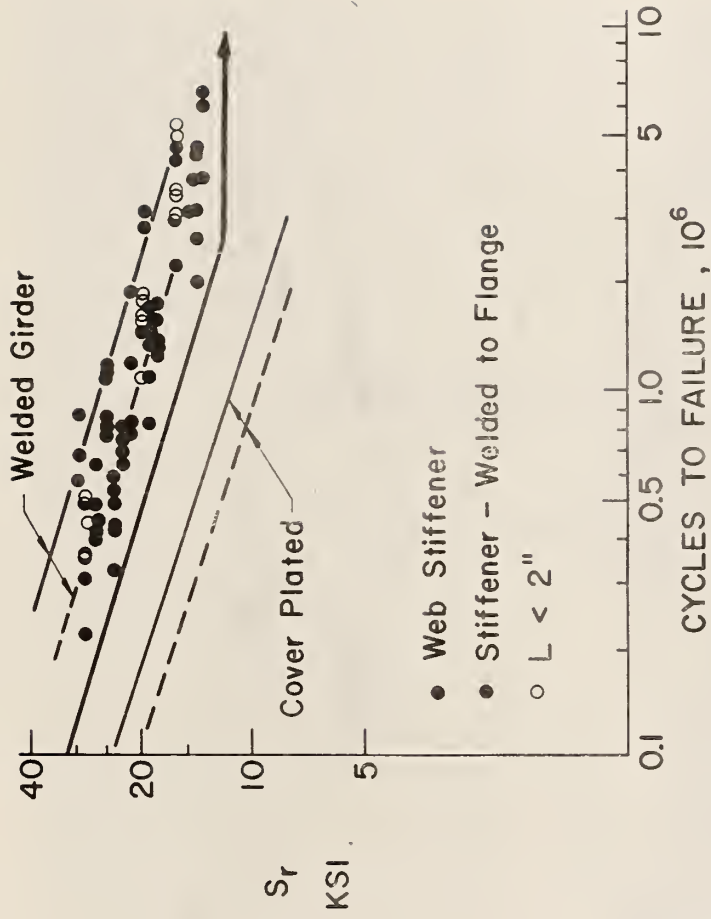
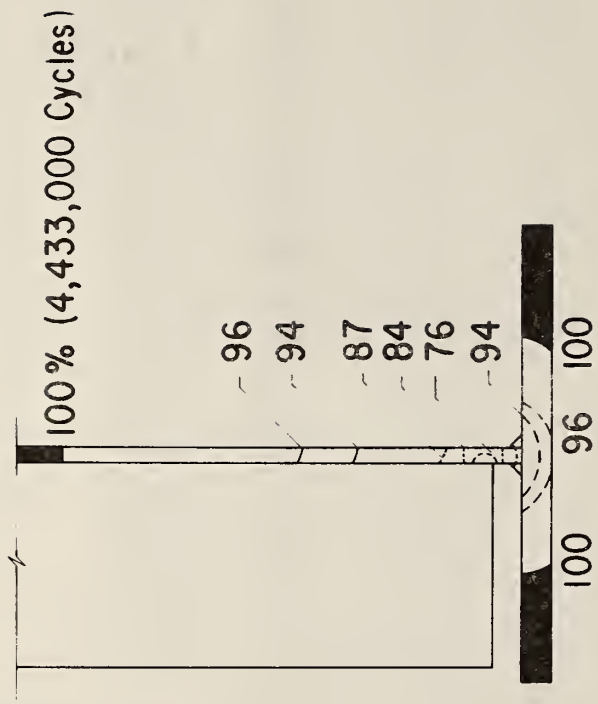


Figure 3-16 Summary plot for various types of transverse stiffeners. Types 1 and 2 welded to web alone, Type 3 welded to web and flange.



**PHASES OF CRACK GROWTH AT STIFFENER TYPE I**

Figure 3-17 Stages of crack growth at stiffener welded to web alone.



Figure 3-18 Typical failure at flange attachment with no transverse weld.

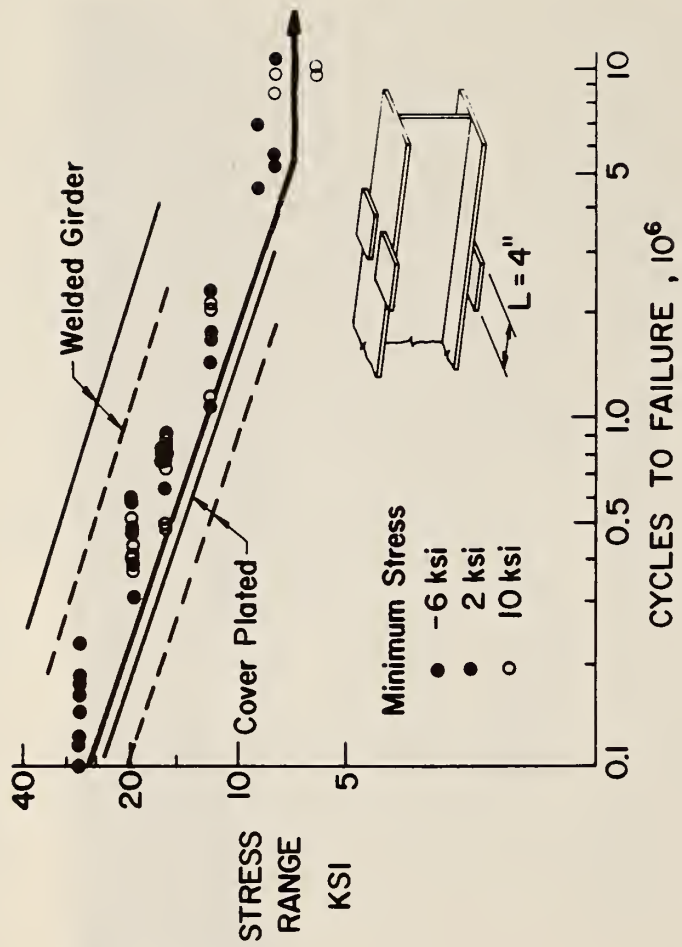


Figure 3-19 Effect of stress flange and minimum stress on fatigue strength of 4 in. long attachments.

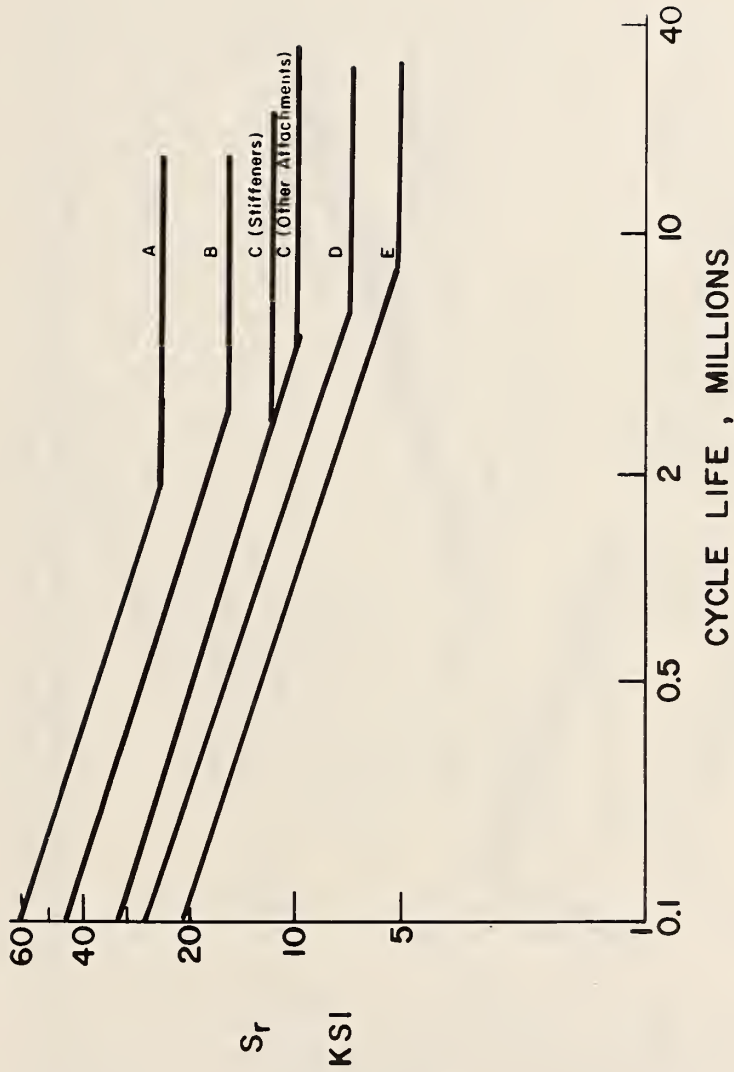


Figure 3-20 Summary of welded details showing welded beam, 2 in., 4 in. and cover-plated beams.

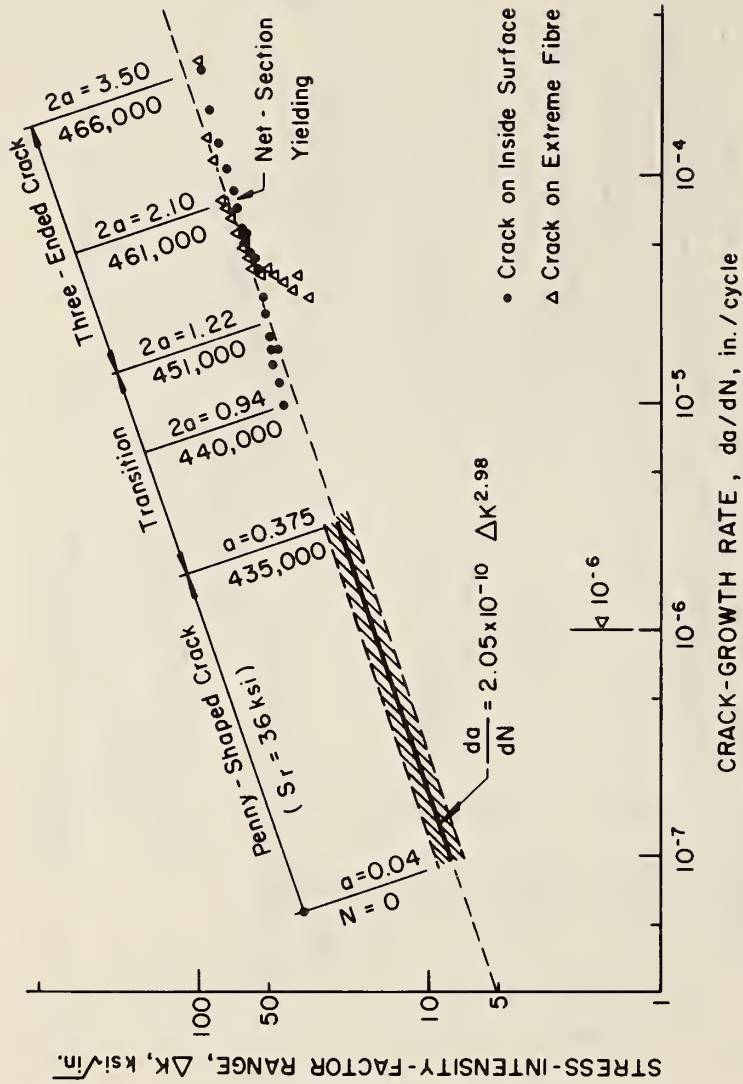


Figure 3-21 Various stages of crack growth and their comparison with measured rates in a welded beam.



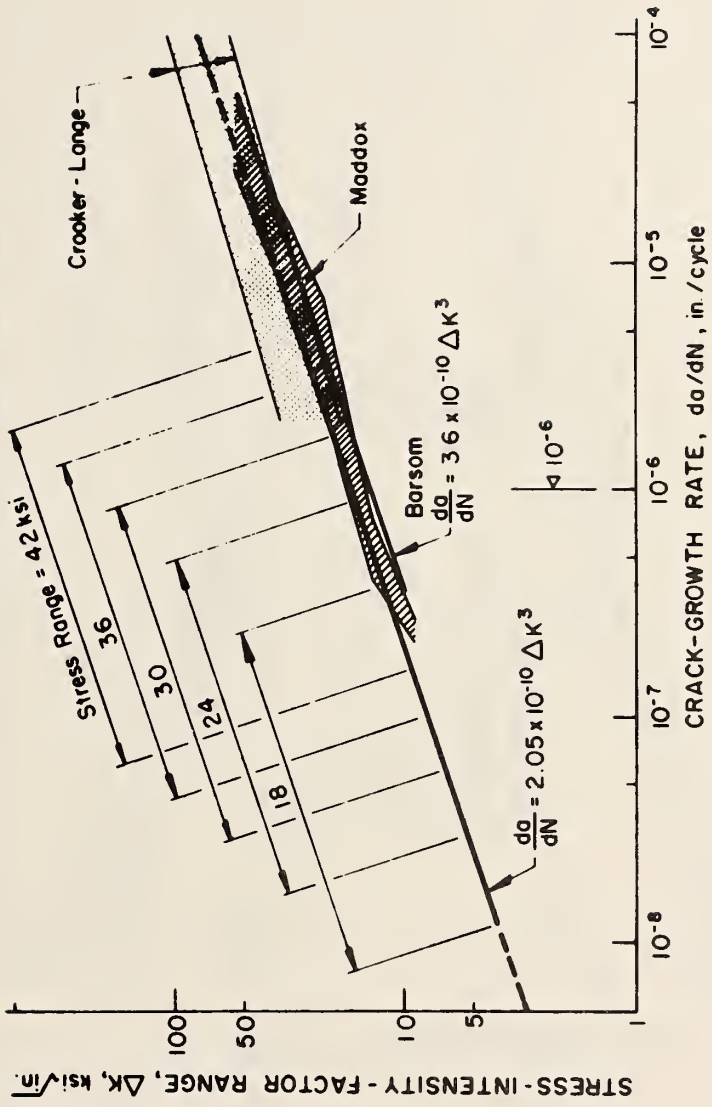


Figure 3-22 Ranges of stress for crack growth from a penny-shaped crack and comparison of crack growth rate with available measurements.

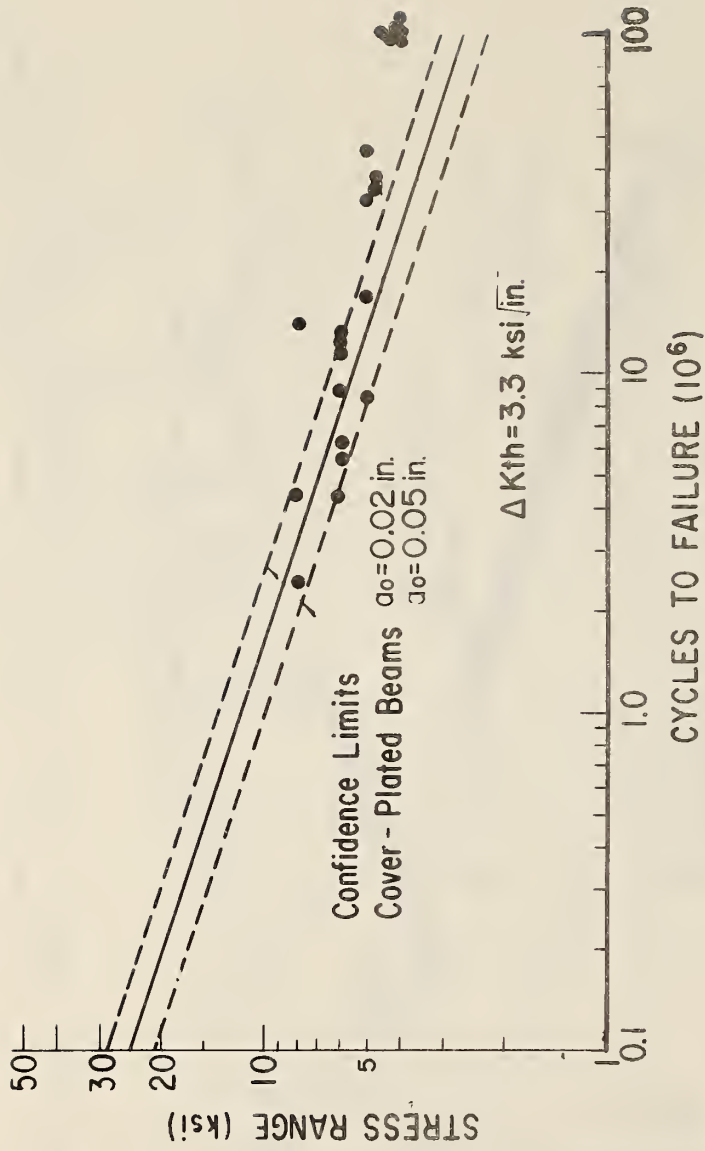


Figure 3-23 Stress Range-Cycle Life behavior near crack growth threshold with estimated initial crack size.

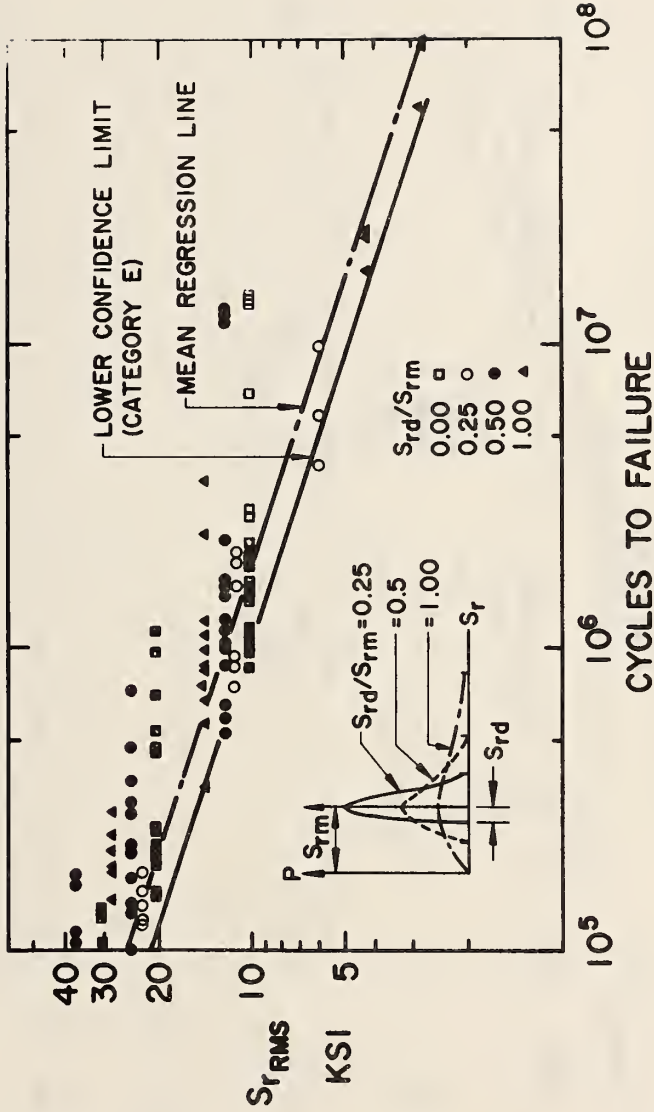


Figure 3-24 Comparison of beams with random variable stress cycles with constant cycle fatigue strength using root-mean-square stress range.

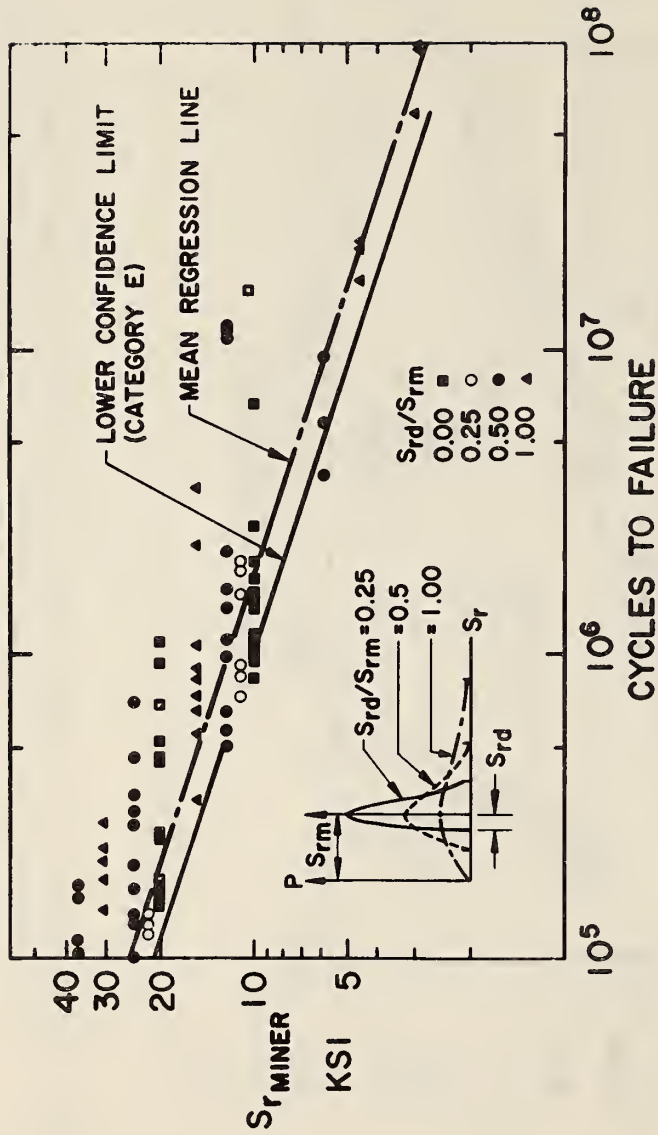


Figure 3-25 Comparison of beams with random variable stress cycles with constant cycle fatigue strength using Miner's effective stress range.

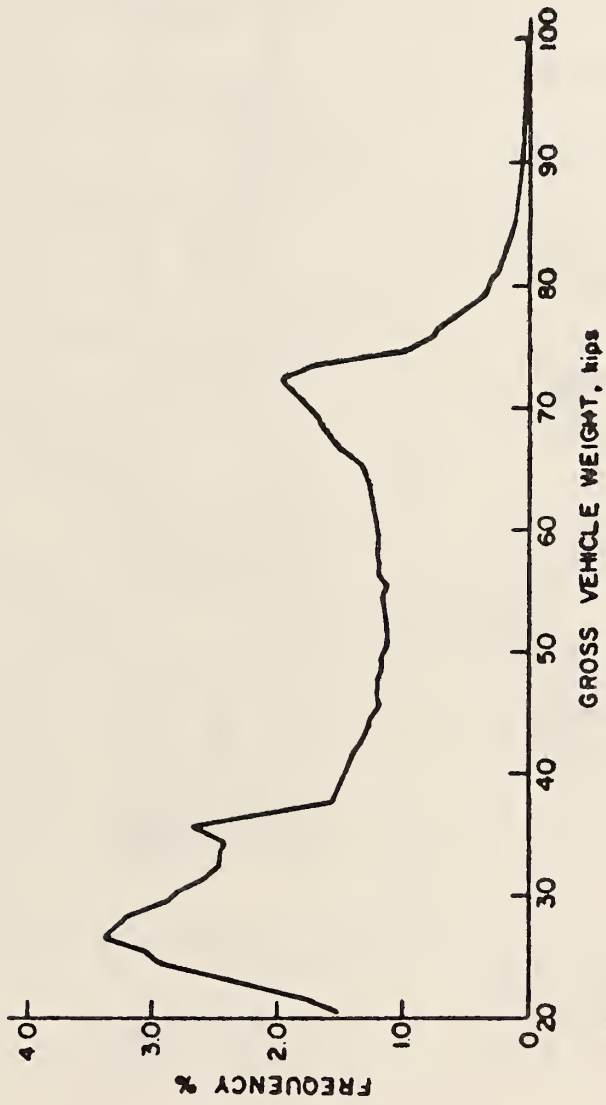
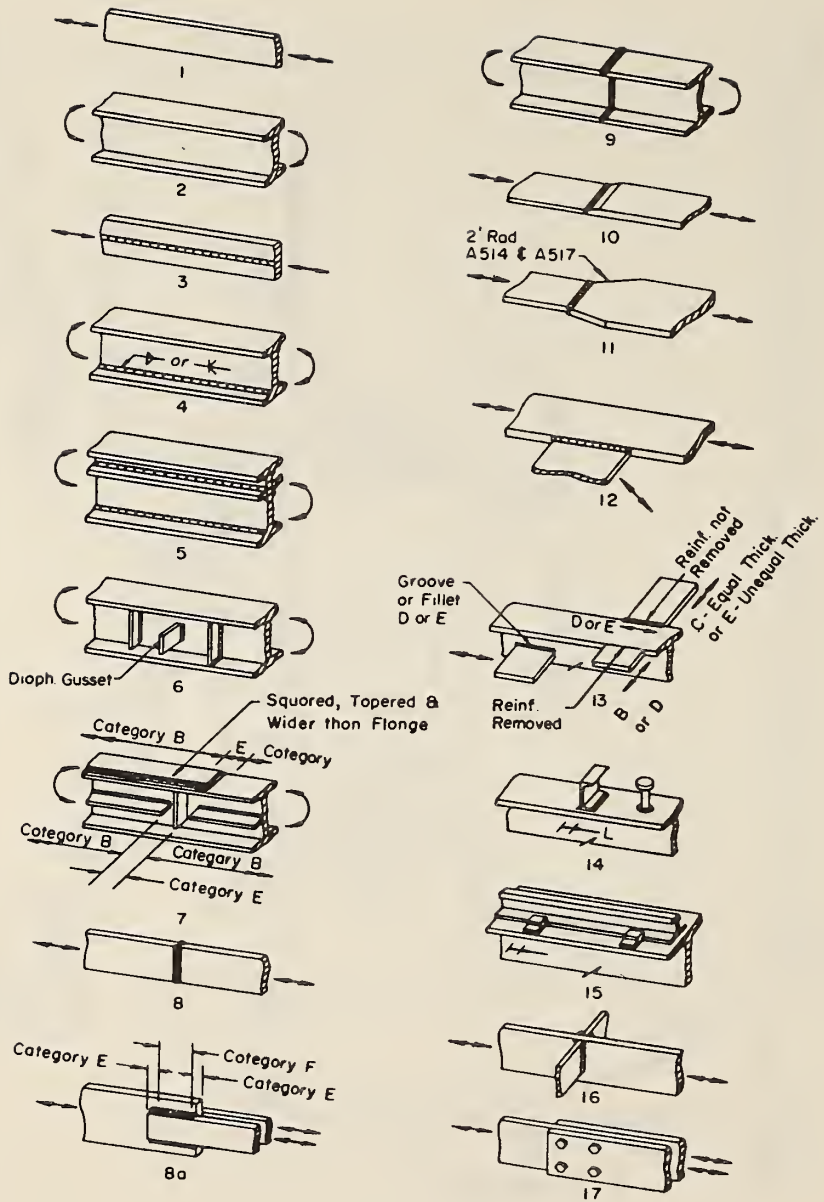
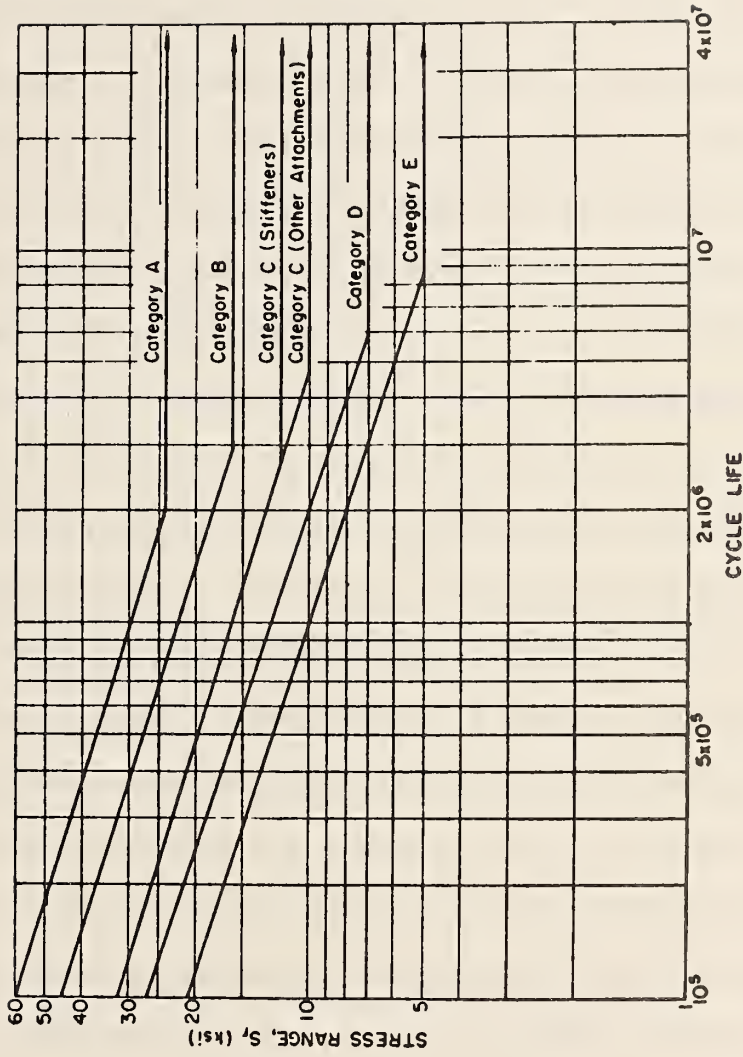


Figure 3-26 Gross vehicle weight distribution from 1970 FHWA Nationwide Loadometer Survey.



3-27 Examples of AASHTO Categories A to E.



3-28 Design stress range curves for Categories A to E.

## CHAPTER 4. FRACTURE BEHAVIOR AND THE AASHTO FRACTURE REQUIREMENTS

### 4.1 INTRODUCTION

Fracture Mechanics has evolved over the last twenty years as a result of the technical community's attempt to measure and quantify the ability of a material to withstand fracture. During this twenty year period, great progress has been made in terms of both theory and experiment. A major portion of this work has been guided by ASTM Committee E24 on Fracture Testing of Metals which has developed a number of standard methods for measuring fracture toughness.

It is quite obvious that the characterization of a material's fracture resistance is a very difficult task. If one considers a generalized structure as shown in Figure 4-1, it is possible to obtain all of the load deflection curves shown for a given material by only varying the relative size of the crack to the size of the structure. These load deflection curves range from very linear up to the point of fracture to highly nonlinear at the point of fracture. Thus a complete characterization of a material's resistance must allow for this widely different response. Also, the measured resistance to fracture of a material generally depends on the test temperature and testing speed. Furthermore, fracture resistance depends to some degree on the manufacturing process used to produce the material. No material is isotropic. There are always some variations in structure from one location to another. These variations can have a great effect on a measured property and as such must



be accounted for.

Faced with the difficult and complex task of assessing a material's fracture resistance, three very distinct approaches to the quantification or measurement of fracture resistance evolved. These are most easily described as fracture appearance tests<sup>1,2,3)</sup>, fracture energy measurements<sup>3,4)</sup>, and fracture mechanics type measurements<sup>5,6)</sup>. The tests described in references 1 through 6 are representative of only some of the existing tests.

In the case of the fracture appearance tests or the energy measurement tests, generally a curve of fracture appearance or energy versus temperature is obtained from tests of three point notched bend bars such as shown in Figure 4-2. These results are then used to rank various materials or lots of a given material in terms of relative fracture resistance. For the most part, these tests cannot be used to predict a failure load or critical crack or defect size in a structure. However, they do find use in the design process in that they can be used for specification purposes and in quality assurance programs.

Fracture mechanics type tests have usually evolved from a more theoretical basis than fracture appearance or fracture energy tests and are generally related to a stress analysis of the test sample. These tests are usually more difficult and expensive to perform. Also, they tend to be restricted to very definite forms of material response. In the particular case of ASTM Standard E399<sup>5)</sup>, the actual test procedure is very restrictive. However, the results obtained from such test methods can be used to predict critical crack

sizes or failure loads if the response of the structure falls within the framework of the test procedure. This is a great benefit which has produced a wide use of methods such as E399<sup>5)</sup> even though the test procedures are restrictive, complex, and somewhat expensive.

As of this time there is no universally accepted characterization of a material's fracture resistance. Along with ASTM Standard E399<sup>5)</sup>, which has already been pointed out to be of limited use, a large number of other fracture resistance measurements have been developed. Some of these tests have reached the stage of being standards<sup>1,2,3,5,6)</sup> while others are used by a single researcher or laboratory for a specific purpose. It is the purpose of this chapter to briefly discuss some of the standard and some of the non-standard measures of fracture resistance, to place these measures in a single framework, and to discuss the current AASHTO toughness requirements.

## 4.2 FRACTURE APPEARANCE TESTS

Three tests which can be placed in the category of fracture appearance tests are the ASTM tests E23<sup>3)</sup>, E208<sup>2)</sup>, and E436<sup>1)</sup>. The ASTM test E23<sup>3)</sup> is the familiar Charpy test procedure. The more common specimen employed with this standard is the Charpy V-notch (CVN) specimen which is a notched bar 55 mm long by 10x10 mm square as shown in Figure 4-3. The results of the CVN tests are usually presented in the form of curves of energy absorbed during fracture versus temperature and per cent shear, a measure of surface appearance, versus temperature. The usefulness of CVN tests is normally limited to ranking the fracture resistance of a material in relative terms.

The CVN test is also of limited usefulness in the sense that it represents a very small specimen or volume of material. The fracture response of a large bulk of material can be quite different. There have been recent attempts to tie CVN testing to fracture mechanics type concepts<sup>7,8)</sup>. These proposed concepts are still the subject of much research.

ASTM standard method E208<sup>2)</sup> is used to determine the nil-ductility transition (NDT) temperature of a material. In this procedure a small weld bead is deposited on the surface of a bar type specimen as shown in Figure 4-3. The purpose of the weld is to provide a brittle material for initiation of a cleavage crack in the base metal during the test. The specimens are struck at various temperatures by a falling weight. By observing the subsequent fracture appearance the NDT temperature is determined. The NDT temperature is useful in ranking the relative fracture performance of materials and can be used for design purposes<sup>9)</sup>. Although the NDT test is primarily a fracture appearance test it has been related to fracture mechanics concepts by Irwin<sup>10)</sup>.

ASTM test method E436<sup>1)</sup> for Drop-Weight Tear Tests of Ferritic Steels is very similar to CVN testing. The major difference is that the notched specimen is approximately 250 mm long by 75 mm deep by full plate thickness as shown in Figure 4-3. This test reports fracture appearance as a function of test temperature. The primary use of E436 is for ranking the fracture resistance of pipe line steels.

### 4.3 FRACTURE ENERGY MEASUREMENTS

Two test methods representative of fracture energy measurements are ASTM Standard E23<sup>3)</sup> and the Dynamic Tear (DT) test<sup>4)</sup> developed at the Naval Research Laboratory, both of which utilize impact testing of notched bend bars. E23 and CVN testing has already been discussed as part of the fracture appearance tests. The DT test consists of testing 3 point notched bend bars at impact loading rates. The DT specimen is shown in Figure 4-3. In the DT test procedure, the fracture energy is measured as a function of temperature. The actual measurement of the fracture energy can be done in one of two ways. One technique measures the residual energy left in the impact hammer or falling weight while the other uses an instrumented loading tup to measure the impulse during fracture<sup>11)</sup>. This impulse can be used to calculate fracture energy. DT testing has also been correlated with fracture mechanics concepts<sup>9)</sup>. As was the case for CVN-fracture mechanics correlations this is still the subject of various research efforts.

### 4.4 FRACTURE MECHANICS MEASUREMENTS

A major difference between fracture mechanics tests for measuring fracture resistance and the fracture appearance and fracture energy tests is that the fracture mechanics tests are normally based on a detailed stress analysis of the test specimen. Furthermore, these measurement procedures are designed to assess fracture resistance in a manner which produces a relationship among flaw size, applied load and measurable material properties. Such a relationship can be functionally expressed as

$$f(\sigma, a, A, B, \dots) = 0 \quad (4.1)$$

where

$f(\dots)$  is a functional relationship among the quantities in parentheses.

$\sigma$  is a measure of the applied load.

$a$  is a measure of the crack size.

$A, B, \dots$  are appropriate material constants.

The usefulness of a relationship such as equation 4.1 should be clear. Once the material constants are known, the inter-relationship between applied load and defect size can be determined. Given a crack size, a critical failure load can be calculated and vice versa.

Fracture mechanics measurements can be classified as linear or nonlinear depending upon the load displacement behavior of the structure or specimen. The load displacement curves shown in Figure 4-1 are examples of this. The initial attempts at a meaningful fracture mechanics measure of fracture resistance were limited to materials and situations in which the load displacement curves were basically linear up to the point of fracture. This is quite reasonable when the complexities of nonlinear behavior are considered. Also, the initial problems facing fracture mechanics during its early development were fracture of high yield strength materials which had low fracture resistance. This combination clearly fell into the linear class.

ASTM Standard E399 for Plane Strain Fracture Toughness of Metallic Materials<sup>5)</sup> was developed by ASTM Committee E24 for the measurement of fracture toughness of very high strength materials.

The standard E399 measures the plane strain fracture toughness,  $K_{IC}$ .  $K_{IC}$  is the critical stress intensity factor at failure, where the stress intensity factor  $K$ , is a single term parameter which represents the severity of the influence of a crack on the stress distribution. The stress intensity factor reflects the applied load, crack geometry and specimen geometry<sup>12)</sup>. As indicated in Chapters 1 and 2, the relationship between  $K$  and  $K_{IC}$  is most easily understood in terms of a tensile test. In a tensile test stress is calculated as load over area or  $P/A$ . From the actual tensile test the yield stress is then calculated. In a fracture test the stress intensity  $K$  is a mathematical function of applied load and defect size. At the point of failure a critical  $K$  called  $K_{IC}$  is calculated from the failure load and failure crack size.

In order for a test to be valid according to E399 various highly restrictive conditions must be met. One of these is that the loading rate must be very slow. Also, the crack size and specimen width for typical test specimens as shown in Figure 4-4 must meet the conditions

$$a \geq 2.5 \left( \frac{K_{IC}}{\sigma_{ys}} \right)^2 \quad (4.2)$$

and

$$B \geq 2.5 \left( \frac{K_{IC}}{\sigma_{ys}} \right)^2 \quad (4.3)$$

where  $\sigma_{ys}$  is the 0.2% offset yield stress of the material. In effect when a  $K_{IC}$  level is measured, which meets the requirements of equations 4.2 and 4.3, then the bulk of the specimen is responding linearly.

For a material which is temperature and strain rate sensitive<sup>13)</sup> a typical plot of  $K$  versus temperature in Figure 4-5 might represent its behavior.  $K_{ID}$  as plotted in Figure 4-6 is a measure of a material's dynamic fracture toughness, and meets the size requirements of E399. The major departure of  $K_{ID}$  testing from E399 is that the loading rate is high.

Along with ASTM Standard E399 other fracture mechanics measures exist. More recently work has been directed to characterizing the nonlinear fracture response of materials. Examples of this are the British Crack Opening Displacement method<sup>6)</sup>, the J integral<sup>14)</sup>, and others<sup>15,16)</sup>. These nonlinear methods will not be considered here.

#### 4.5 BRIDGE STEEL BEHAVIOR

The fracture behavior of bridge steels is affected by temperature, strain rate, and plate thickness<sup>13,17)</sup>. Figures 4-5 through 4-7 show the basic effect of these three variables on fracture toughness. Figure 4-5 shows that as temperature increases the measured fracture toughness herein designated as  $K_C$  slowly rises from a plateau value until a transition temperature is reached at which point  $K_C$  rises very rapidly. Figure 4-6 shows that the variation of  $K_C$  with temperature is similar for static loads and very fast rates of loading. Generally the dynamic curve is shifted to the right so that the transition region where  $K_C$  is increasing rapidly occurs at a higher temperature. Barsom and Rolfe<sup>7)</sup> have shown that this shift in transition temperature with loading rate can be predicted on the basis of yield strength and Barsom<sup>18)</sup>

currently uses the formula

$$T_{\text{SHIFT}} = 215 - 1.5\sigma_y \quad (4.4)$$

for  $36 \text{ ksi} < \sigma_y < 140 \text{ ksi}$  (248 to 965 MPa)

$$T_{\text{SHIFT}} = 0.0$$

for  $\sigma_y > 140 \text{ ksi}$  (965 MPa)

The basic behavior shown in Figures 4-5 and 4-6 is due to both a metallurgical transition in the micro fracture processes with temperature and changes of mechanical constraint at the crack tip<sup>18)</sup> (i.e., the ability of the material to flow or plastically deform). As constraint increases, toughness will decrease. Constraint is a function of yield strength such that as yield strength increases constraint decreases. Yield strength is a function of both temperature and strain rate. For bridge steels<sup>13,17)</sup>, yield strength increases as temperature decreases and strain rate increases. Thus, as yield strength increases constraint increases, so toughness will decrease.

The behavior shown in Figure 4-7 is due primarily to changes in constraint<sup>13,17)</sup> due to the differences in thickness. The thicker plates exhibit more constraint at a given temperature and therefore lower toughness. Typical bridge steel behavior as found in reference 13 is shown in Figures 4-8 through 4-17 and was determined using specimens similar to those found in ASTM E399<sup>5)</sup>.



Barsom and Rolfe<sup>7)</sup> noted for dynamic loading or very high strain rates that the transition temperature of the dynamic  $K_{IC}$  curves corresponded to the transition temperature in a standard Charpy V-notch (CVN) test. They also noted that the transition in CVN energy levels for standard CVN specimens tested at very slow loading rates corresponded to the transition temperature for static  $K_{IC}$  measurements. This is schematically shown in Figure 4-18. This led Barsom and Rolfe to attempt a correlation between  $K_{IC}$  and CVN values. This correlation is now given by Barsom<sup>18)</sup> as

$$K_{IC}^2 = 5E (\text{CVN}) \quad (4.5)$$

where

$K_{IC}$  = the plane strain fracture toughness in  $\text{psi}\sqrt{\text{in}}$ .

$E$  = Young's Modulus in psi

CVN = Charpy V-notch energy in foot pounds

To estimate a dynamic  $K_{ID}$  value from equations 4.5 at a specific temperature, one uses the dynamic CVN value at that temperature. Similarly, to estimate a static  $K_{IC}$  value, one would use a CVN energy level obtained from slow loading tests of CVN specimens. Barsom's<sup>18)</sup> equation has been generally substantiated by the work of Roberts<sup>13)</sup>.

#### 4.6 AASHTO FRACTURE TOUGHNESS REQUIREMENTS

The basic American Association of State Highway and Transportation Officials fracture toughness requirements are an outgrowth of a proposal by Frank and Galambos<sup>19)</sup>. These requirements are not imposed in terms of a fracture control plan, but as a quality

assurance check on the material. Table 4.1 gives the current requirements for primary tension members. As can be seen in Table 4.1, the requirements take the form of CVN requirement on the steels based on the expected operating temperature of the bridge. This type of requirement is similar to the Nil Ductility Temperature, NDT, requirements for ship steel<sup>20)</sup> and Fracture Appearance Transition Temperature, FATT, requirement for line pipe<sup>21)</sup>.

The basis for the current AASHTO requirement can be found in the work of Barsom<sup>17)</sup> and Roberts<sup>13)</sup>. The basic concept as developed by Barsom<sup>18)</sup> was to make sure that the material had a temperature transition behavior such that at the particular operating temperature and loading rate the  $K_{Ic}$  level of the steel was rapidly rising. This will assure that the steel will not fracture in a plane strain mode. To more fully understand this, consider Figure 4-19 after Barsom<sup>18)</sup> which shows the CVN behavior of a hypothetical 36 ksi (248 MN/m<sup>2</sup>) steel. Three CVN curves are shown for slow, intermediate and dynamic rates of loading. In the particular case of bridges the normal rate of loading is best represented by intermediate loading rates<sup>22)</sup>. Based on Barsom's work<sup>17)</sup>, the temperature shift for slow to dynamic will be  $\sim 170^{\circ}\text{F}$  ( $81^{\circ}\text{C}$ ) as shown and the shift between intermediate and dynamic  $120^{\circ}\text{F}$  ( $57^{\circ}\text{C}$ ). Now Barsom<sup>18)</sup> argues that if non plane strain behavior is desired, this occurs at about a temperature level equal to the transition temperature plus  $50^{\circ}\text{F}$  ( $24^{\circ}\text{C}$ ). Roughly this is the 15 ft-lb. (20J) CVN temperature plus  $50^{\circ}\text{F}$  ( $24^{\circ}\text{C}$ ). Thus non plane strain behavior is

guaranteed at the minimum service temperature of the bridge if the 15 ft-lb. (20J) CVN level falls 50°F (24°C) below the service temperature.

Since it is difficult to run slow or intermediate strain rate CVN tests, it is more appropriate to make any specification in terms of standard CVN tests. This can be done by utilizing the temperature shift between the intermediate and dynamic CVN curves. Barsom states that this is about 0.75 of  $T_{SHIFT}$  given by equation 4.5. In the case of the 36 ksi (248 MPa) yield strength steel this is 120°F (57°C). Thus, to specify a CVN and testing temperature to guarantee non plane strain behavior one takes the service temperature and subtracts 50°F (24°C) and then adds 120°F (57°C) to this. This then gives the standard dynamic CVN 15 ft-lb. (20J) temperature requirement for the steel in question. Slight modifications of the above arguments were made for steels with  $\sigma_y > 50$  ksi (345 MPa). Barsom gives complete detail of this in reference 18.

It should be evident at this point, as already mentioned, that the current AASHTO toughness requirements are essentially a quality assurance program for material rather than a fracture control plan or system. All that the requirement does is guarantee some minimum level of toughness. It is important to note that the actual level of toughness is not known since in the region of the specification the intermediate loading rate produces a toughness level which was beyond the measurement capabilities of both the work of Roberts<sup>13)</sup> and Barsom<sup>17)</sup>. It is also important to note that this specification is designed for situations where intermediate

loading rates exist. If dynamic loading rates occur then this specification can prove to be inadequate.

## REFERENCES

1. ASTM Standard Method for Drop-Weight Tear Test of Ferritic Steels, E436-74.
2. ASTM Standard Method for Conducting Drop-Weight Test to Determine Nil-Ductility Transition Temperature of Ferritic Steels, E208-69.
3. ASTM Standard Methods for Notched Bar Impact Testing of Metallic Materials, E23-72.
4. Proposed Method for 5/8 in. (16-mm) Dynamic Tear Test of Metallic Materials, ASTM Standards, Part 10, 1976.
5. ASTM Standard Method of Test for Plane-Strain Fracture Toughness of Metallic Materials, E299-72.
6. F. M. Burdekim, Crack Opening Displacement - A Review of Principles and Methods, Practical Fracture Mechanics for Structural Steels, Chapman and Hall, Ltd., 1969.
7. J. M. Barsom, and S. T. Rolfe, "Correlation between  $K_{IC}$  and Charpy V-Notch Test Results in the Transition-Temperature Range," Impact Testing of Metals, ASTM STP 466, 1970, pp. 281-302.
8. R. H. Sailors, and H. T. Corten, "Relationship Between Material Fracture Toughness Using Fracture Mechanics and Transition Temperature Tests," Fracture Toughness ASTM STP 514, 1972, pp. 164-191.
9. W. S. Pellini, "Adventures in Fracture Toughness Characterization Procedures and in Qualitative Interpretation to Fracture-Safe Design for Structural Steels," Naval Research Laboratory Paper 6713, April 3, 1968.
10. G. R. Irwin, J. M. Kraft, P. C. Paris, and A. A. Wells, "Basic Aspects of Crack Growth and Fracture," Naval Research Laboratory Report 6598, Nov. 21, 1967.
11. E. A. Lange and F. J. Loss, "Dynamic Tear Energy - A Practical Performance Criterion for Fracture Resistance," Impact Testing of Metals, ASTM STP 466, 1970 pp. 241-258.
12. P. C. Paris and G. M. Sih, "Stress Analysis of Cracks," Fracture Toughness Testing and Its Applications, ASTM STP 381, 1965, pp. 30-83.
13. R. Roberts, G. R. Irwin, G. V. Krishna, and B. T. Yen, "Fracture Toughness of Bridge Steels - Phase II Report," U. S. Dept. of Transportation Federal Highway Administration Report No. FHWA-RD-74-59, September, 1974.

14. J. D. Landes and J. A. Begley, "Test Results for J-Integral Studies: An Attempt to Establish a  $J_{IC}$  Testing Procedure," Fracture Analysis, ASTM STP 560, 1974, pp. 170-186.
15. F. J. Witt, "The Equivalent Energy Method for Calculating Elastic-Plastic Fracture," presented 4th National Symposium on Fracture Mechanics, Pittsburgh, Pa., August, 1970.
16. Fracture Toughness Evaluations by R-Curve Methods, ASTM STP 527, 1973.
17. J. M. Barsom, "Toughness Criteria for Bridge Steels," Technical Report No. 5 for AISI Project 168, February 8, 1973.
18. J. M. Barsom, "The Development of AASHTO Fracture-Toughness Requirements for Bridge Steels," presented U. S.-Japan Cooperative Science Seminar, Tohoku University, Sendia, Japan, Aug., 1974, available from AISI.
19. K. H. Frank and C. F. Galambos, "Application of Fracture Mechanics to Analysis of Bridge Failures," Proceedings of Specialty Conference on Safety and Reliability of Metal Structures, ASCE, Nov. 2-4, 1972, pp. 279-306.
20. S. T. Rolfe, "Fracture-Control Guidelines for Welded Steel Ship Hulls," Significance of Defects in Welded Structures, Proceedings of the Japan-U.S. Seminar, 1973, Tokyo, ed. by F. Kanazawa and A. S. Kobayashi, University of Tokyo Press, 1974, pp. 218-339.
21. R. J. Eiber, A. R. Duffy, and G. M. McClure, "Fracture Control on Gas Transmission Pipelines," ASM Conference on Fracture Control, January 26-28, 1970, Philadelphia, Pa.
22. Highway Research Board of the NAS-NRC Division of Engineering and Industrial Research, the AASHTO Road Test, Report 4, Bridge Research, Special Report CID, Publication No. 953, NAS-NRC.

TABLE 4-1  
AASHTO FRACTURE-TOUGHNESS SPECIFICATIONS FOR  
BRIDGE STEELS

ASTM DESIGNATION	THICKNESS	ENERGY ABSORBED, (FT.-LB.)		
		ZONE 1*	ZONE 2*	ZONE 3*
A36		15@70F	15@40F	15@10F
A572†	Up to 4" mechanically fastened	"	"	"
	Up to 2" welded	"	"	"
A440		"	"	"
A441		"	"	"
A442		"	"	"
A588†	Up to 4" mechanically fastened	"	"	"
	Up to 2" welded	"	"	"
	Over 2" welded	20@70F	20@40F	20@10F
A514	Up to 4" mechanically fastened	25@30F	25@0F	25@-30F
	Up to 2-1/2" welded	25@30F	25@0F	25@-30F
	Over 2-1/2 to 4" welded	35@30F	35@0F	35@-30F

\*Zone 1: Minimum service temperature 0F and above.

Zone 2: Minimum service temperature from -1 to -30F.

Zone 3: Minimum service temperature from -31 to -60F.

†If the yield point of the material exceeds 65 ksi, the temperature for the CVN value for acceptability shall be reduced by 15F for each increment of 10 ksi above 65 ksi.

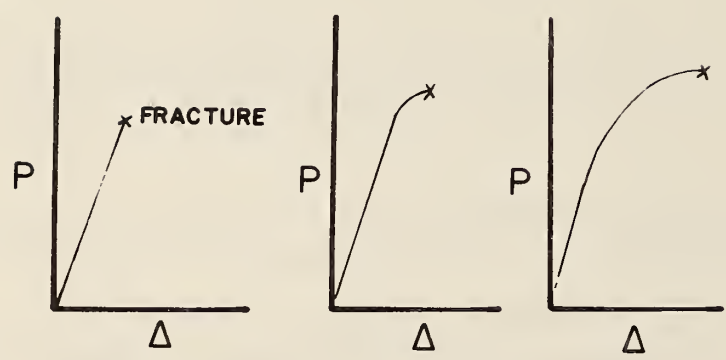
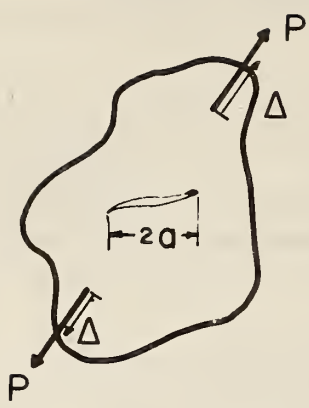


Figure 4-1 Possible load deflection curves up to the point of fracture.



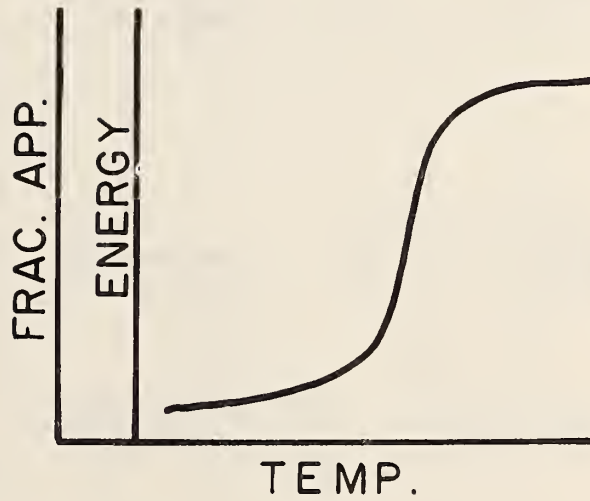
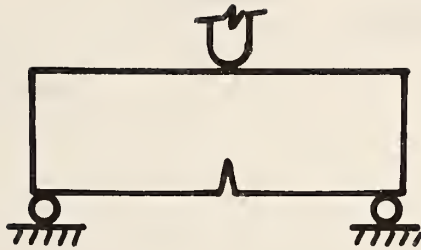


Figure 4-2 Response of a three point bend impact test.

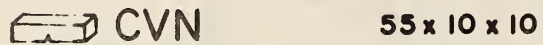
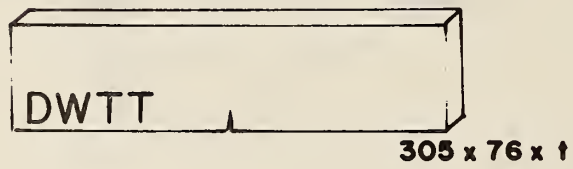
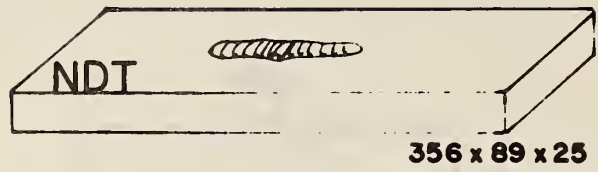


Figure 4-3 Comparison of various fracture test specimens,  
1 in. = 25.4 mm.

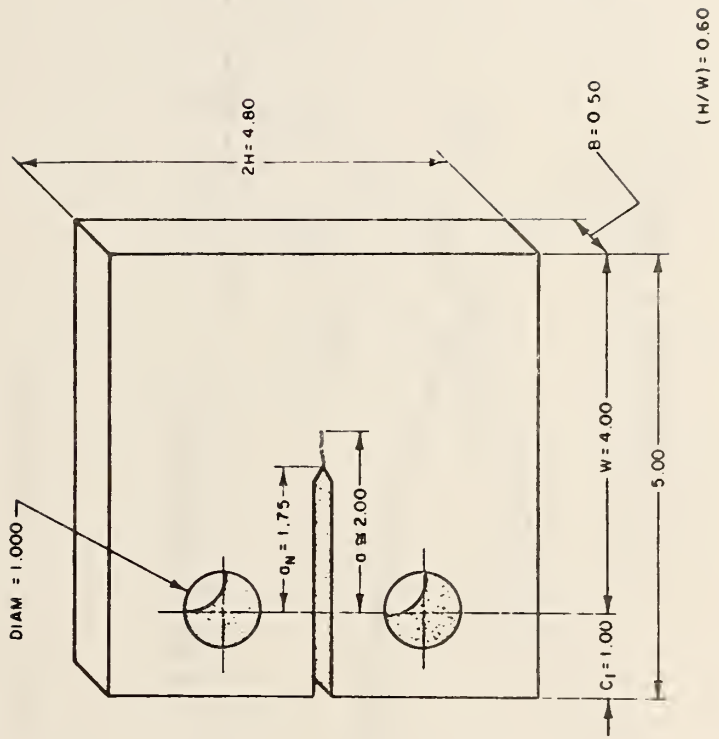


Figure 4-4 ASTM E399 compact tension specimen.

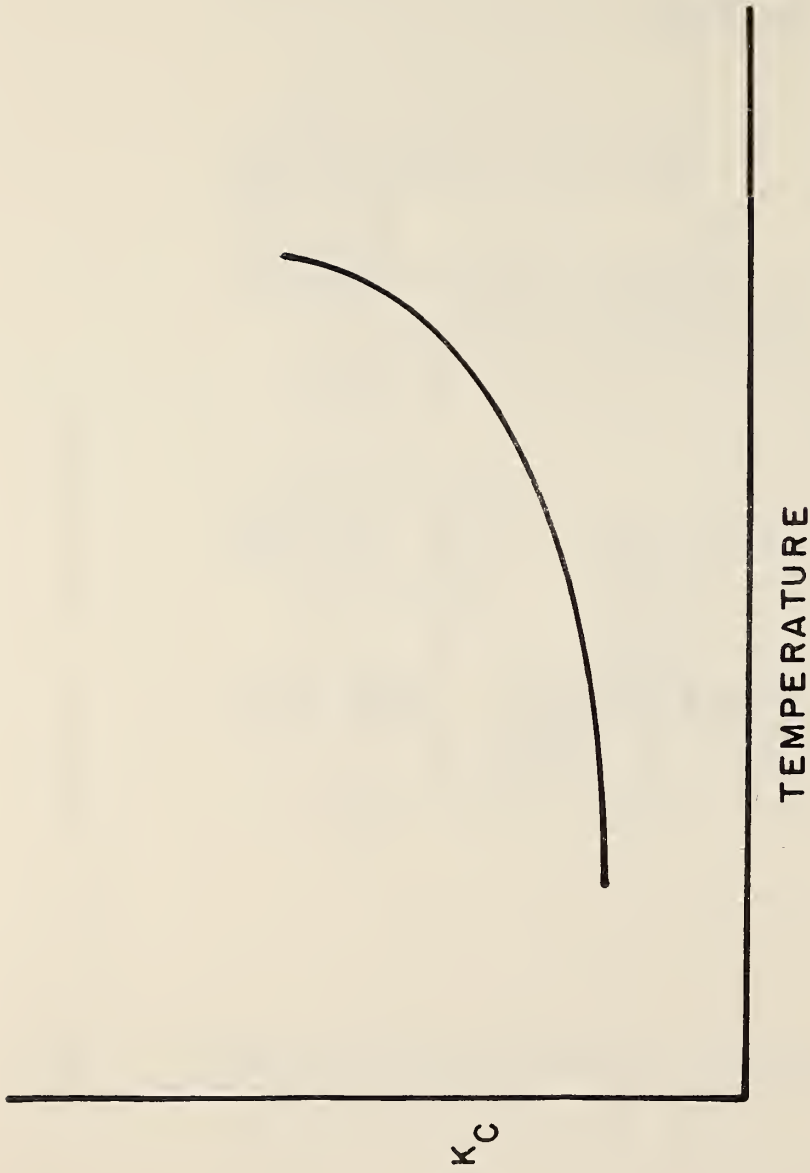


Figure 4-5  $K_C$  response of bridge steels.

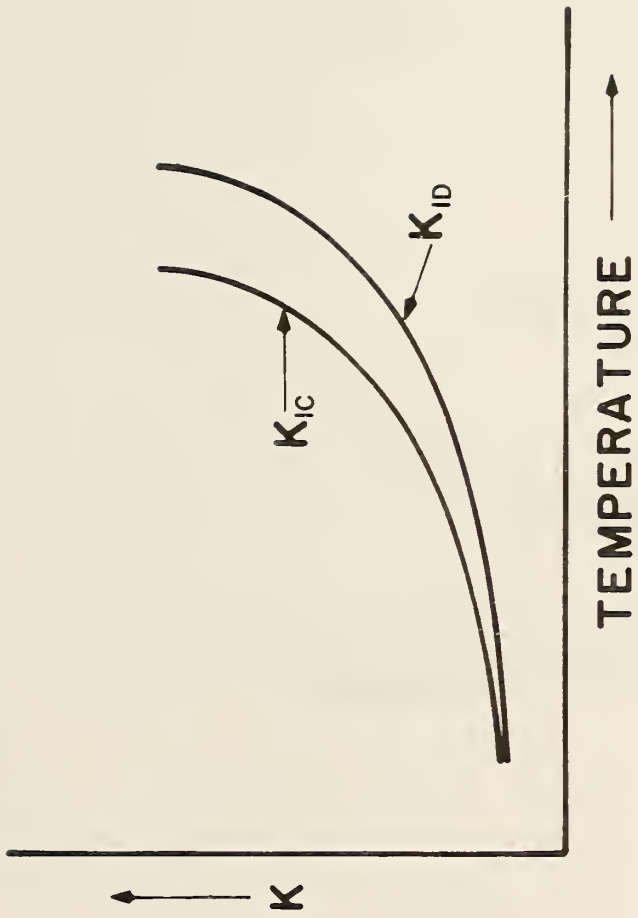


Figure 4-6 Dynamic,  $K_{ID}$ , and static,  $K_{IC}$ ,  $K$  response of typical bridge steels.

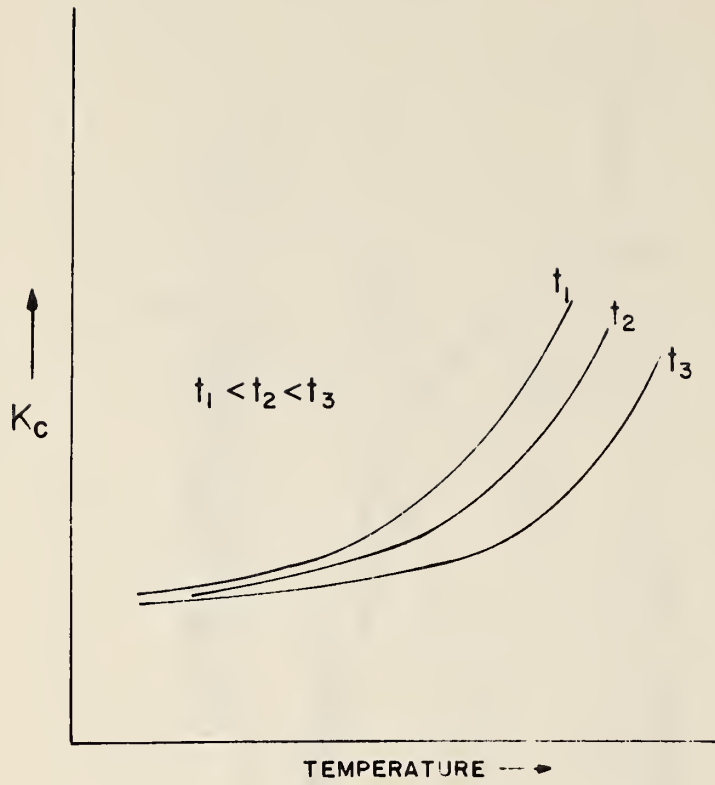


Figure 4-7 Effect of thickness on K response.

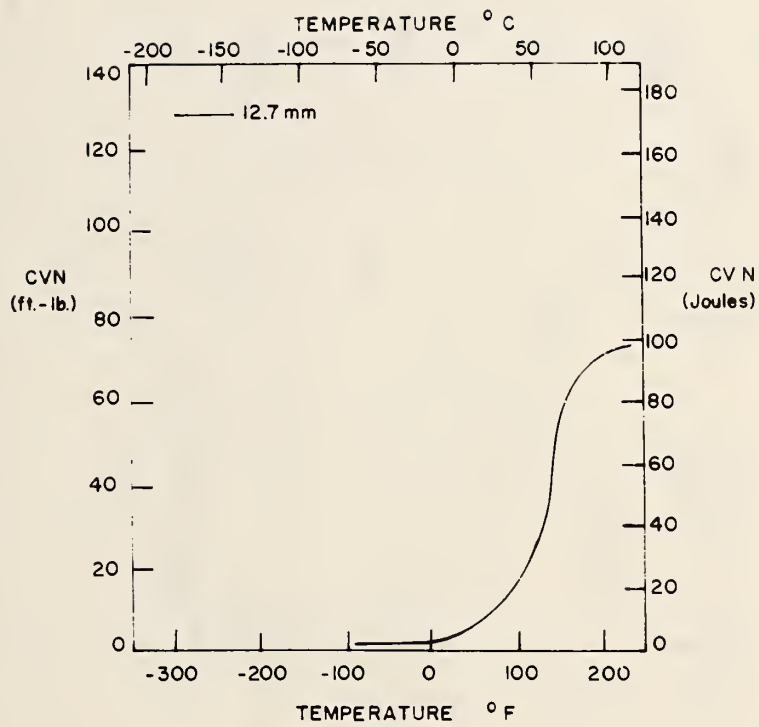


Figure 4-8 CVN results A7 steel.

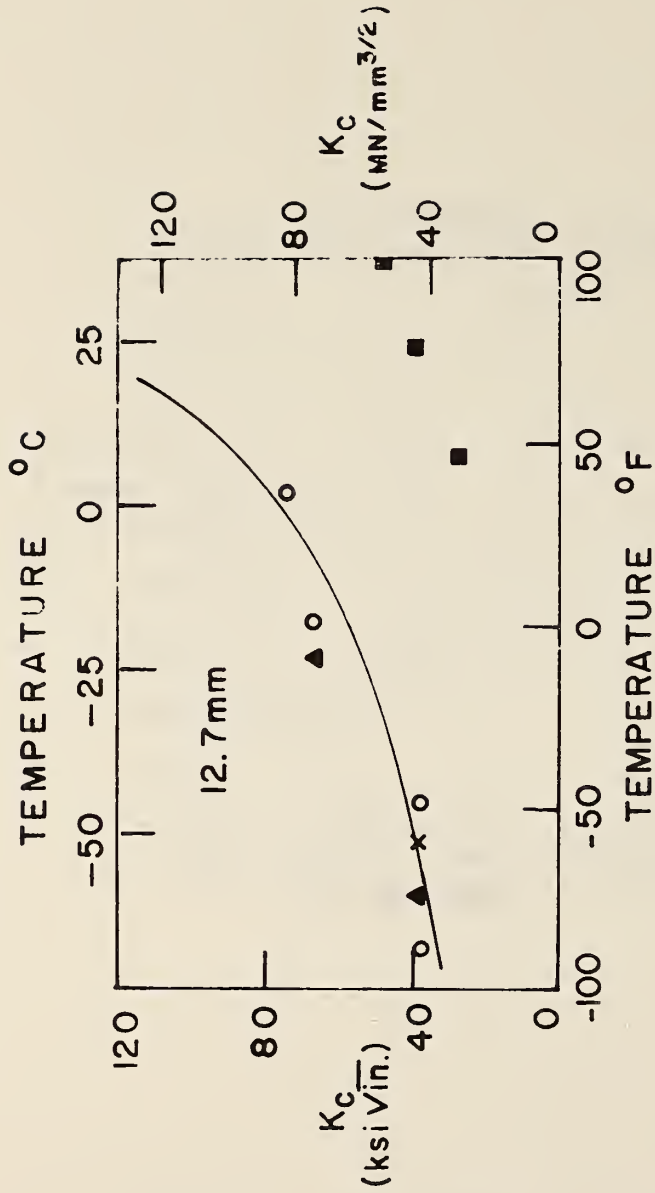


Figure 4-9 K data A7 steel -- Δ = R values, ○ = dynamic K values, ● = static K values, and ■ = estimate from Equation 4.5, x point of maximum valid K.



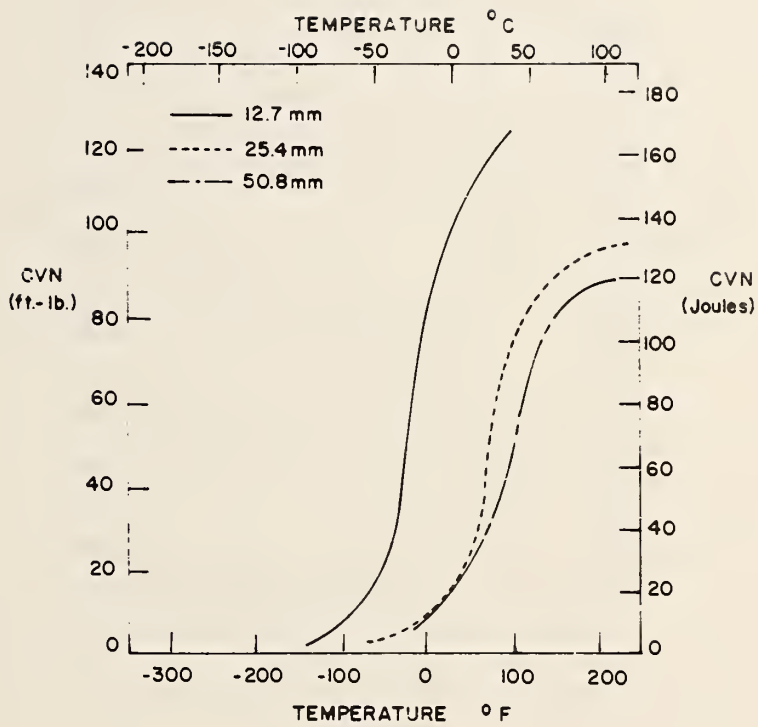


Figure 4-10 CVN results A242 steel.

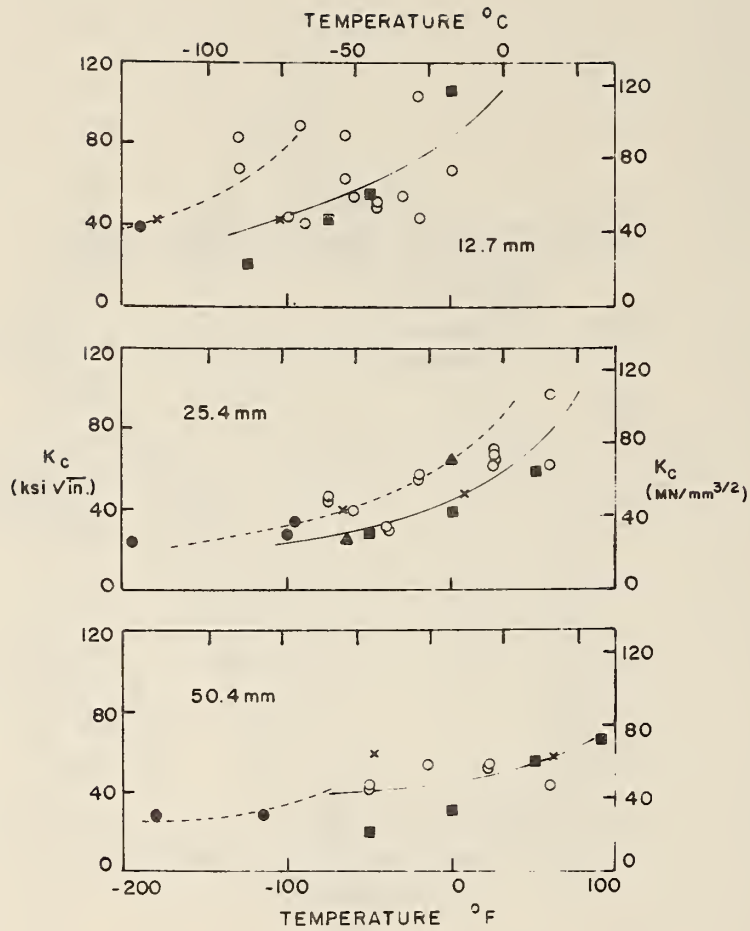


Figure 4-11 K data A242 steel ---  $\Delta$  = R values, o = dynamic K values,  $\bullet$  = static K values, and  $\blacksquare$  = estimate from Equation 4.5, x point of maximum valid K.

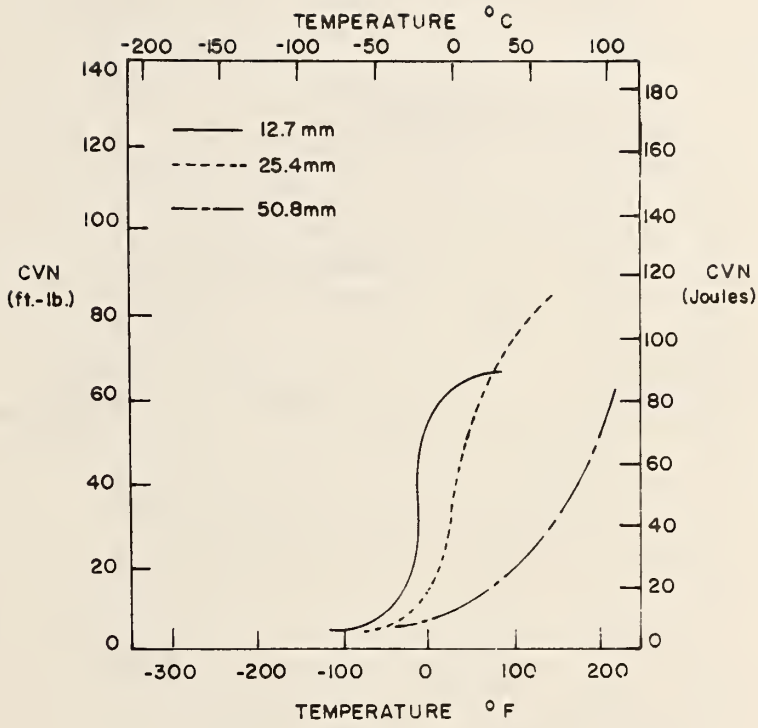


Figure 4-12 CVN results A440 steel.

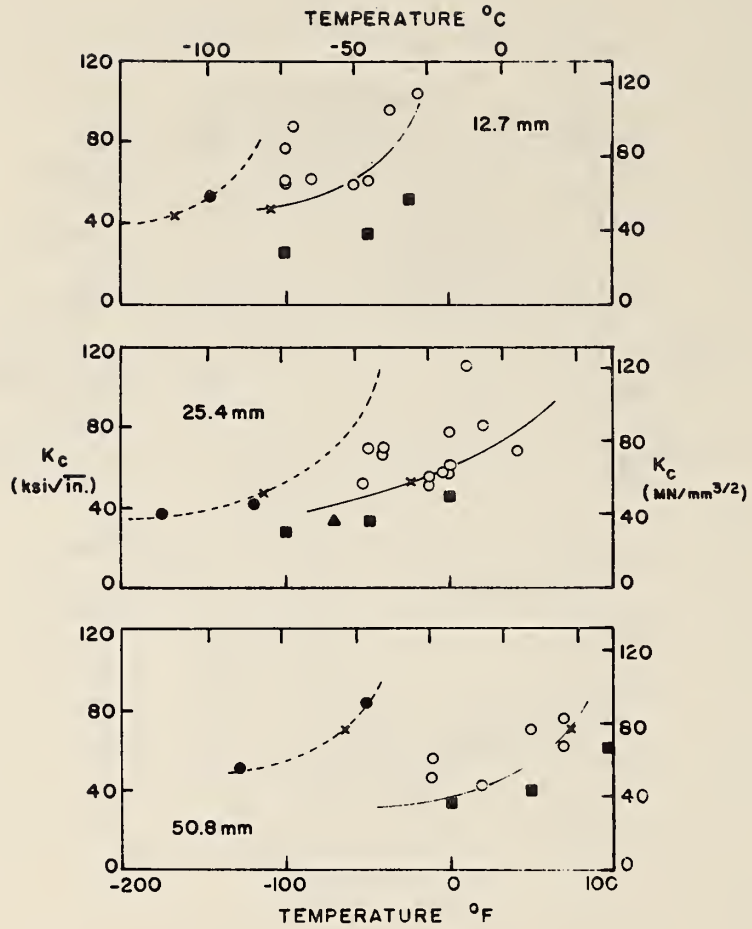


Figure 4-13 K data A440 steel --  $\Delta$  = R values, o = dynamic K values, ● = static K values, ■ = estimate from Equation 4.5, x point of maximum valid K.

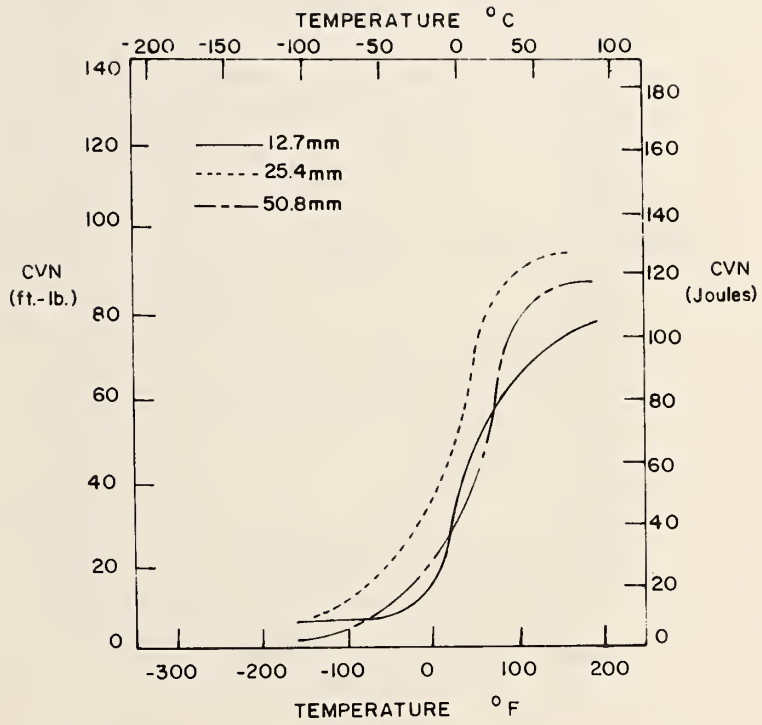


Figure 4-14 CVN results A588 steel.

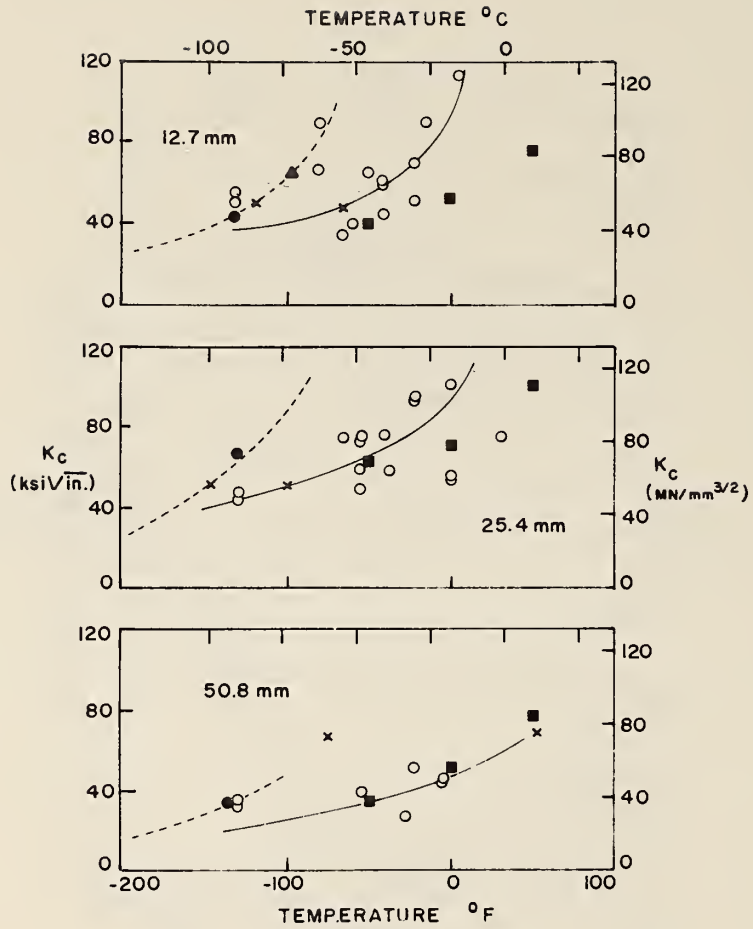


Figure 4-15 K data A588 steel --  $\Delta$  = R values, o = dynamic K values, ● = static K values and ■ = estimate from Equation 4.5, x point of maximum valid K.

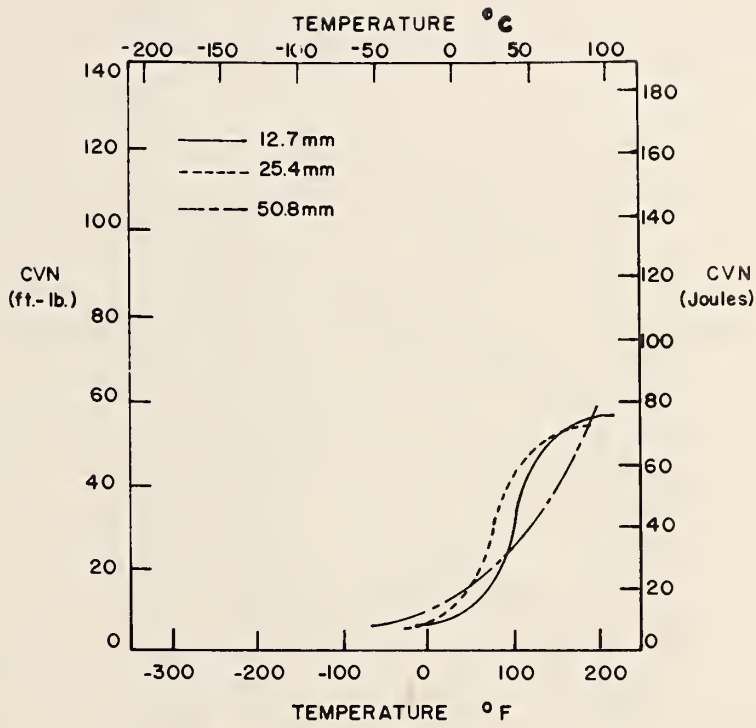


Figure 4-16 CVN results SAE1035 steel.

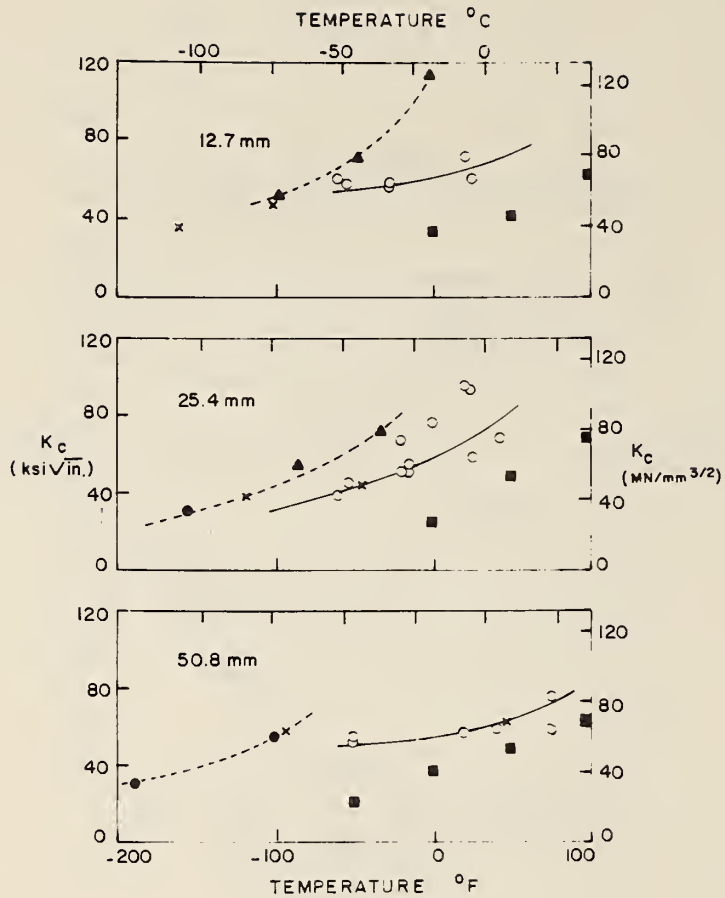


Figure 4-17 K data SAE1035 steel --  $\Delta$  = R values,  $\circ$  = dynamic K values,  $\bullet$  = static K values, and  $\blacksquare$  = estimate from Equation 4.5,  $\times$  point of maximum valid K.



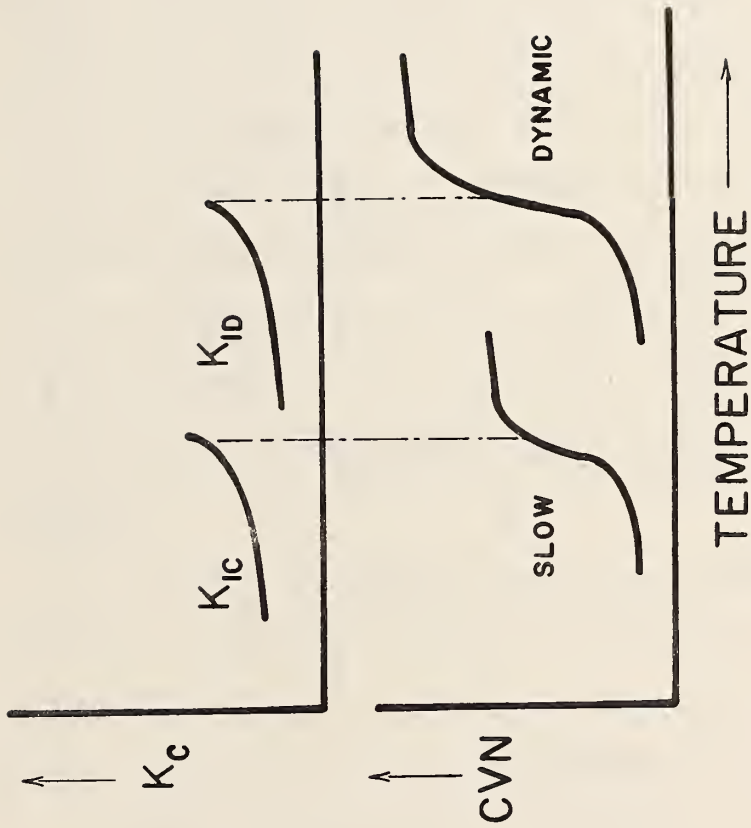


Figure 4-18 Correspondence between CVN and K temperature transition regions.

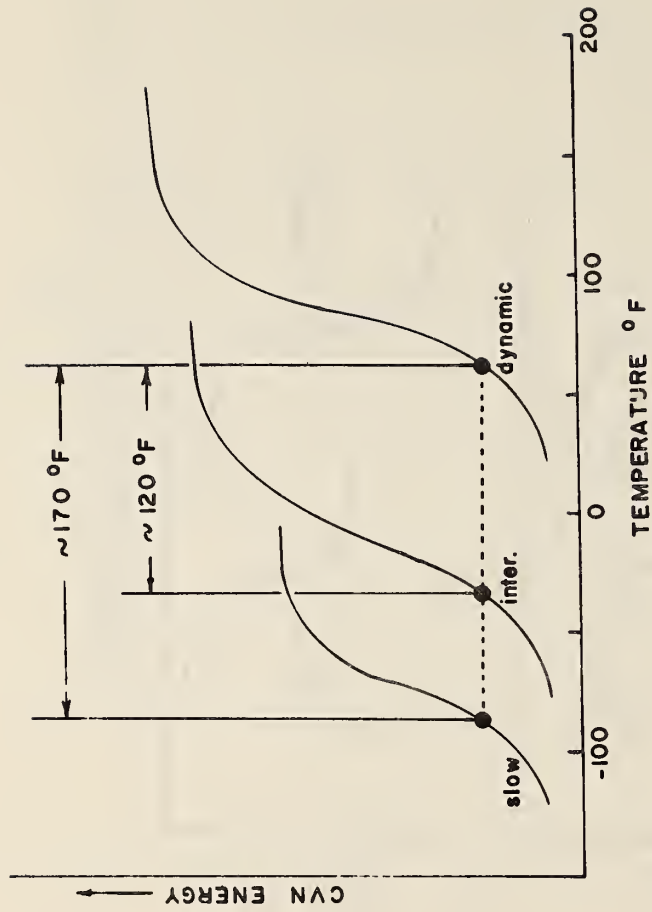


Figure 4-19 Typical K response for a 36 KSI (248 MN/m<sup>2</sup>) steel.

## CHAPTER 5. BRIDGE FAILURE EXAMPLES

### 5.1 INTRODUCTION

During the past 10 to 15 years a number of bridges or bridge-like structures have sustained fracture failures either during fabrication and erection or in actual service. It is the general purpose of this chapter to present a brief discussion of two of these events. These discussions will be used to highlight the application of the material presented in Chapters 1 through 4, and will attempt to be as factual as the actual failures and public information allow. In any post failure analysis certain assumptions must be made, for instance, as to the state of stress at the time of the failure event, the state of residual stress if any, any unusual environmental effects, etc. In spite of these uncertainties the analysis of failures presented here have attempted to be as accurate as scientifically possible.

### 5.2 A FRACTURE MECHANICS ANALYSIS OF THE BRYTE BEND BRIDGE FRACTURE

The Bryte Bend Bridge, Figure 5-1, crosses the Sacramento River about three miles from the city of Sacramento, California. The crossing is a part of Interstate Route 880 and permits through traffic to bypass the metropolitan area.

The bridge consists of twin parallel structures with an overall length of 4050 ft. (1234 m) and with 55 ft. (16.8 m) vertical clearance between low steel and mean high water, Figure 5-2. Each bridge carries three lanes of traffic plus shoulders. Approach spans are a series of 146 ft. (44.4 m) long simple spans. The main

river section consists of four continuous spans of 281 - 370 - 370 - 281 ft. (85.6 - 112.8 - 112.8 - 85.6 m) of the 370 ft. (112.8 m) spans, Figure 5-3.

The superstructure is a trapezoidal steel box supported on reinforced concrete piers. The box varies in depth from 8 ft.- 1 inch (2.5 m) for the approach spans to 14 ft.- 1 inch (4.3 m) for the river spans. The change in depth occurs in a transition span at either end of the continuous river spans, Figure 5-4. The exterior webs of the box were sloped 1:2, Figure 5-5, to reduce the width of the compression flanges in the continuous spans and to improve overall appearance. The boxes were designed with the top open. Conventional girder flanges were welded to the tops of the box sides and to a single longitudinal web plate stiffening the center of the box. The bottom plate of the box is longitudinally stiffened with a series of vertical plates.

The bridge was fabricated from plates of A36, A441 and an A517 type steel. The A36 steel was used in all areas of low stress. The A441 steel was used for the maximum positive moment section and the A517 type steel was used for the maximum negative moment section at the river piers. All fabrication was by welding.

In the region of high negative moment over the piers the A517 type steel was used to reduce the size of the members. The A517 type steel flanges were 30 inches (762 mm) wide and 2-1/4 inches (57 mm) thick.

While the composite concrete deck was being placed in June, 1970, a brittle fracture occurred across one of the outer flanges

at Pier 12, as shown in Figure 5-6. It initiated at the intersection of a 1/2 inch (12.5 mm) thick lateral attachment welded to the 2-1/4 inch (57 mm) thick flange as shown in Figure 5-7. The fracture propagated across the entire 30 inch (762 mm) wide flange and about 4 inches (101 mm) down into the web where it was arrested, Figure 5-8. The fracture surface was a classic herringbone type brittle fracture, with the herringbone patterns pointing back toward the crack origin and very small shear lips.

The nominal yield strength of this material was 100 ksi (690 MPa) and the design stress was 45 ksi (310 MPa). At the time the crack propagated the dead load stress was about 28 ksi (193 MPa) and the ambient temperature was about 60F (15.5C).

Analysis of the fracture surface indicated that a weld crack about 0.2 inches (5 mm) deep, Figure 5-9, was present in a residual stress field such that sometime during the fabrication or erection, the weld crack initiated. As the initial weld crack propagated out of the residual stress field, it arrested at a distance of about 1.3 inches (33 mm) from the edge of the plate. The extent of this 1.3 inch (33 mm) crack is shown as the rusted area in Figure 5-9 and is semi-circular. During pouring of the concrete deck, as the dead load stress was increased to about 28 ksi (193 MPa), complete fracture of the top flange occurred.

$K_{IC}$  tests of material from the flange plate that failed showed that at the service temperature of +60F (15.5C), and slow loading rates, the  $K_{IC}$  value was 55 ksi $\sqrt{in}$ . (60.5 MPa $\sqrt{m}$ ). This was a valid  $K_{IC}$  test that met all the requirements of ASTM Test

Method E399. A schematic of the test specimen and record is shown in Figure 5-10. The actual test specimen is shown in Figure 5-11, and the actual load-displacement record is shown in Figure 5-12. Note that the fracture surface is flat with very small shear lips, similar to that of the actual fracture surface, Figure 5-8. The  $K_{Ic}$  value of  $55 \text{ ksi}\sqrt{\text{in}}$  ( $60.5 \text{ MPa}\sqrt{\text{m}}$ ) at +60F was considerably lower than would be expected for this material and is not representative of A514-517 steels.

The stress-flaw size relation for  $K_{Ic} = 55 \text{ ksi}\sqrt{\text{in}}$  ( $60.5 \text{ MPa}\sqrt{\text{m}}$ ) is shown in Figure 5-13 using a simple edge-crack relation. It was assumed that sometime during transportation or erection, the 0.2 inch (5 mm) crack initiated. For a  $K_{Ic}$  of  $55 \text{ ksi}\sqrt{\text{in}}$  ( $60.5 \text{ MPa}\sqrt{\text{m}}$ ) and an initial flaw size of 0.2 inches (5 mm), crack extension would be expected in the vicinity of a high residual stress field, e.g. 70-100 ksi (483-690 MPa). After this crack propagated out of the residual stress region it arrested at about 1.3 inches (33 mm) as was shown in Figure 5-9. As the dead load stress was increased, the combination of an applied stress of 28 ksi (193 MPa) and the 1.3 inch (33 mm) deep crack caused the stress intensity  $K_I$  to reach the critical stress intensity for this material [ $55 \text{ ksi}\sqrt{\text{in}}$  ( $60.5 \text{ MPa}\sqrt{\text{m}}$ ), Figure 5-13] and complete failure of the flange resulted under static-loading conditions. As the crack propagated into the thinner (tougher) web plate, and the load was transferred to other members in the structure, the crack arrested.

Analysis of  $K_{Ic}$  values of A514-517 steels indicated that a  $K_{Ic}$  value of  $150 \text{ ksi}\sqrt{\text{in}}$  ( $165 \text{ MPa}\sqrt{\text{m}}$ ) is more representative of these

steels. This value is compared with the value of  $55 \text{ ksi}\sqrt{\text{in}}$  ( $60.5 \text{ MPa}\sqrt{\text{m}}$ ) in Figure 5-14 showing that even at the maximum design stress of 45 ksi (310 MPa), the critical crack size is about 3 inches (76 mm) for the more typical A514-517 steel. Actually the critical crack size would be even larger than 3 inches (76 mm) because elastic-plastic plane-stress behavior ( $K_{IC}$ ) would govern rather than  $K_{IC}$ . Thus if the flange material had had the level of notch toughness normally found in these steels, failure should not have occurred.

Repair was accomplished by jacking the entire structure into a zero-stress condition, cutting out the material in the vicinity of the failure and replacing it with material with a much higher level of notch toughness. The notch toughness of the replacement plate was insured from various correlations between toughness tests, including the upper-shelf CVN-impact- $K_{IC}$  correlations.

Because the toughness of other A517 type plates in similar negative moment regions in the structure was questioned, and because it did not appear feasible to remove these plates completely and replace them using field welding, additional plates were bolted to the original plates as shown in Figure 5-15. The structure was jacked into a zero stress condition before the additional plates were added, and thus the design stress in the original plates was reduced considerably, thereby increasing the critical crack size at the lower design stress level markedly. Also, and more importantly, multiple-load paths were established to carry the entire load,

in the event that additional fractures should occur throughout the life of the structure.

A close-up of the replacement plates as bolted to the original plates in the negative moment regions over the piers is presented in Figure 5-16. An overall view of the plates as extended back into the zero stress region is shown in Figure 5-17.

The Bryte Bend Bridge was opened to traffic in October, 1971 and has been in continuous successful operation since that time.

The brittle fracture of the Bryte Bend Bridge raised several extremely important issues of importance to bridge engineers. Two of the most important are listed below with pertinent comments.

1. Implied vs. Guaranteed notch toughness

If notch toughness is important, is it necessary to specify certain minimum toughness requirements or can the engineer rely on generic properties of various classes of steels? It would appear that even though the engineer should be able to expect certain minimum mechanical properties for a particular grade of steel, notch toughness values should be specified where desired because of their greater sensitivity to thermo-mechanical history. Essentially this is the position AASHTO has taken by the development of the 1974 material toughness requirements for bridge steels, and is the direction other code writing



bodies have taken.

Although difficult to establish quantitatively, a lower level of notch toughness apparently lowers the weldability of the steel. Thus not only is the critical crack size for a steel having low notch toughness relatively small, but the probability of cracks forming is greater because of the poorer weldability. Thus, it is desirable to have some minimum level of notch toughness, such as that specified by AASHTO. The question of how much notch toughness is necessary for a particular structural application depends on many factors such as service history, design, fabrication, consequences of failure, etc.

2. Relative importance of the low notch toughness of the material compared with the severe geometry of the detail in determining the overall life of the Bryte Bend Bridge.

The original plans for the Bryte Bend Bridge called for the lateral attachment at the fracture origin to be connected only to the web, not to the flange. After discovery of the weld in the fabrication year, the stress range was checked and found to be acceptable by existing design standards. (The AISC Guide to 1974 AASHTO Fatigue Specifications classified this as a Category E detail with an allowable stress range of 12.5 ksi (86 MPa) for 500,000 cycles).

Because this was within the design allowable and because it was thought that cutting the lateral attachments free from the flange might have produced additional lateral loading, it was decided prior to the occurrence of the fracture to leave the attachments welded to the flange.

For steels with very low levels of notch toughness (e.g.  $K_{Ic} = 55 \text{ ksi}\sqrt{\text{in}}$  (60.5 MPa $\sqrt{\text{m}}$ ), for a steel with a yield strength of 100 ksi (690 MPa), or  $K_{Ic}/\sigma_{Ys} \cong .5$ ) the critical crack size at the design stress loading is very small, Figure 5-14. As shown schematically in Figure 5-18, which is a plot of flaw size vs. number of cycles of fatigue loading, this small critical crack size is noted as  $a_{cr}$  for plane strain behavior. For an initial flaw size of  $a_o$ , the number of cycles of fatigue loading necessary to reach  $a_{cr}$  is very small. (In the case of the Bryte Bend Bridge, for  $a_o = 1.3$  inches (33 mm), the fatigue life was essentially zero).

If the Bryte Bend Bridge had been fabricated from a steel with more typical levels of notch toughness (e.g. 35 ft. lb. (47J) minimum CVN impact value as now required by AASHTO),  $a_{cr}$  would have been higher, i.e., elastic-plastic behavior, Figure 5-18. Thus there would have been considerable improvement in the fatigue life due to a moderate improvement in notch

toughness, Region III.

Recent tests at Lehigh University of beams with lateral attachments fabricated from A514 steel with normal levels of notch toughness have since verified this behavior. In these tests the fatigue life of Category E details similar to that found in the Bryte Bend Bridge had satisfactory fatigue lives. In fact, after 2,000,000 cycles of loading, during which time cracks of 1-1/4 or 7/16 inches (32-11 mm) depth were produced, testing temperatures below -140F (-95.6C) were necessary to cause brittle fractures. Even for flaws of this depth, the calculated remaining fatigue lives (after the initial 2,000,000 cycles which produced fatigue cracks greater in size than the 0.2 inch (5 mm) deep weld crack in the Bryte Bend Bridge) were over 500,000 cycles.

In summary, had the Bryte Bend Bridge been fabricated from A517 type steels with normal levels of notch toughness, the service life should have been satisfactory even with the severe Category E detail. Subsequent tests as part of the FHWA Research program at Lehigh verify this point. However, it is obviously preferable to minimize the use of severe details such as Category E ones. This usually can be done easily during the design stage.

### **5.3 ANALYSIS OF CRACK GROWTH IN THE QUINNIPIAC RIVER BRIDGE**

In November 1973 a large crack was discovered in a fascia girder of the suspended span of the Quinnipiac River Bridge near

New Haven, Connecticut. Figure 5-19 is a photograph showing the bridge profile. The crack was discovered approximately 34 ft. (10.4 m) from the left or west end of the suspended span. The suspended span is 165 ft. (50.3 m) long. The structure is noncomposite and the girders are 9 ft. - 2.75 in. (2.8 m) deep at the crack location.

Figure 5-20 shows the crack that developed in the girder web. The crack propagated to the mid-depth of the girder and as shown in Figure 5-21 had penetrated the bottom flange surface when discovered.

The structure was opened to traffic in 1964. Thus it had experienced approximately nine years of service at the time the crack was discovered.

Two studies were undertaken on this cracked structure. One involved the use of the FHWA Magnetic Crack Definer to ascertain the locations of the crack tips. A detailed study was also made of the causes of crack growth after removing the crack surfaces so that a determination could be made as to how and why the crack had formed. To accomplish this latter task, half of the fracture surface was removed for visual examination. Figure 5-22 shows a schematic of the materials that were removed at the cracked cross-section. They included a flange piece with a small portion of the web, two web pieces, and the left and right pieces of the longitudinal stiffener adjacent to the crack.

The Quinnipiac River Bridge had an existing crack which was visually apparent as shown in Figure 5-20 and Figure 5-21. The FHWA

Magnetic Crack Definer (MCD) as well as dye-penetrent was used to define the ends of the crack in the flanges so that crack arrest holes could be drilled at the crack tips. On the basis of this examination holes were drilled at the apparent crack tips with the center of the hole placed at the estimated crack tip. Subsequent field inspection with visual examination revealed that the crack had extended beyond the hole radius by at least one-half inch. Neither the dye-penetrent nor Magnetic Crack Definer had adequately defined the location of the crack tip. Care must be exercised at the time of discovery of such cracks to insure that the end of the crack is defined if it is desired to drill such arrest holes.

Examination Fracture Surface and Material. The fracture surfaces and material characteristics were evaluated in order to ascertain the reason for crack formation and growth. Figure 5-23 shows the flange-web fracture surface (flange piece from Figure 5-22). Figure 5-24 is a photograph which shows the web-longitudinal stiffener intersection at which the crack originated. The ends of the longitudinal stiffener at the fracture location are shown in Figure 5-25. Examination of the fracture surfaces indicated that the fracture had initiated at the web stiffener intersection. The fracture surfaces indicated that a butt weld in the longitudinal stiffener had been made at this location but had never been completely fused, as is apparent from Figure 5-26. Close examination revealed that only a surface pass had been made and the reinforcement removed by grinding. The surfaces of this portion of the

fracture were severely corroded from their exposure to the environmental conditions.

Replicas were made at the web-longitudinal stiffener intersection (see Figure 5-29) so that the fracture surface could be examined by transmission electron microscopy. Visual examination at low magnification indicated that fatigue crack growth was very probable in the web. The fracture surface in the web on each side of the longitudinal stiffener indicated that a cleavage or "brittle fracture" had occurred after the crack penetrated the web thickness. As can be seen in Figure 5-23 the cleavage fracture extended throughout the depth of the fractured web and penetrated some distance into the flange before it had arrested.

Examination at the web-stiffener intersection confirmed that fatigue crack growth had occurred. Fatigue crack growth striations were observed adjacent to the longitudinal web stiffener break. Figures 5-20 and 5-29 show photographs at high magnification (49,000X) of replicas of the fracture surface. The fatigue crack striations are apparent. Estimates of the rate of crack propagation were made on the basis of the striation spacing. These indicated that crack growth rates between  $7 \times 10^{-7}$  and  $2 \times 10^{-6}$  in./cycle ( $1.8$  and  $5.1 \times 10^{-5}$  mm/cycle) were occurring in the region examined (see Figure 5-27).

A detailed examination was also made of the fracture surface near the flange web intersection. Replicas were made and examined under the electron microscope. These revealed that the cleavage fracture extended about 1 in. (25.4 mm) into the flange

(see Figure 5-30). The crack appeared to assume a semielliptical shape as shown schematically in Figure 5-31. Subsequent crack growth appeared to be due to cyclic loading. However, no fatigue crack growth striations were detected on the fracture surface of the flange available for study. Other portions of the fracture surface in which fatigue is likely were destroyed by the drilled holes.

Standard ASTM Type A Charpy V-notch (CVN) specimens were fabricated from both the web and flange material. A standard tensile specimen was taken from the web material. The tensile coupon provided a yield strength of 36.8 ksi (252 MPa), an ultimate strength of 60.9 ksi (417 MPa) with a 43% reduction in area and 32% elongation in an 8 in. (203 mm) gage length.

Fourteen CVN specimens were taken from the flange adjacent to the fracture surface and twenty were taken from the web. The results of these tests are summarized in Figure 5-32. Both flange and web satisfied the toughness requirements for Group 2 of the 1974 interim AASHTO Specifications. The average CVN impact value for the web was 20 ft.-lbs. (27 J) at 40°F. (4°C). The flange provided an average value of 35 ft.-lbs. (47 J) at 40°F (4°C). In Figure 5-32, the LS specimens are cut longitudinal to the rolling axis of the flange but are notched in the plate surface. The LT specimens are also cut longitudinal to the rolling axis of the flange but are notched transverse to the plate surface.

It is apparent from Figure 5-32 that the web impact absorption decreased significantly at temperatures near 0°F (-18°C). Using

the  $K_{Ic}$  - CVN correlations suggested in References 4 and 5,  $K_{Ic}$  values in the range of 25-30 ksi $\sqrt{\text{in}}$  (27.5-33.0 MPa $\sqrt{\text{m}}$ ) result, for the minimum service temperature.

Analysis of Crack Growth. From examination of the fracture surfaces, it was apparent that crack growth had occurred in the Quinnipiac River Bridge in a number of stages and modes. These are illustrated schematically in Figure 5-31.

Stage I corresponded to the initial fabrication condition. Apparently during fabrication a very crude partial penetration weld was placed across the width of the longitudinal stiffener. It is probable that this cracked during transport or erection and constituted the initial crack condition. This would result in a large initial crack,  $a_i$  equal to 4.5 in. (114 mm) long.

Under normal truck traffic, Stage II of crack growth could occur. The electron microscope studies of the fracture surface have shown that fatigue crack growth striations exist. The crack growth rate was evaluated from the striation spacing yielding crack growth rates between  $7 \times 10^{-7}$  and  $2 \times 10^{-6}$  in./cycle (1.8 and  $5.1 \times 10^{-5}$  mm/cycle) near the mid-depth of the web in the Stage II zone. The corresponding  $\Delta K$  values would be between 10-20 ksi $\sqrt{\text{in}}$  (11-22 MPa $\sqrt{\text{m}}$ )<sup>1,2)</sup> as defined by Equation 5-2.

An estimate of the time required to propagate the crack through the web thickness was made assuming the crack penetrated the web as an edge crack. The stress intensity factor was assumed to be defined by

$$K = 1.12 \sigma \sqrt{\pi a} \sqrt{\sec \frac{\pi a}{2t}} \quad (5-1)$$



where  $a$  was the initial 4.5 in. (114 mm) long edge crack. The root-mean-square stress range was approximated from the gross vehicle weight distribution given in reference 3 assuming a value  $\alpha = 0.7$  for the stress range reduction factor. This results in  $S_{rRms} \approx 1.95$  ksi (13.4 MPa) in the flange versus the design stress range  $S_r^D = 4.35$  ksi (29.9 MPa). The stress at the longitudinal stiffener is about 60% of the maximum flange stress. Hence, at the crack  $S_{rRms} \approx 1.17$  ksi (7.3 MPa). The cyclic life was estimated from the crack growth relationship given in References 1 and 2 which showed that

$$da/dN = 2 \times 10^{-10} \Delta K^3 \quad (5-2)$$

The life was estimated by integrating the crack growth relationship as the crack penetrated the web

$$N = \frac{10^{10}}{2} \int_{a_i}^{a_f} \frac{da}{\Delta K^3} \quad (5-3)$$

This yielded about 15,000,000 cycles of random cyclic stress. The average daily truck traffic crossing the bridge was estimated to result in about 1,600,000 random stress cycles per year, corresponding to the  $S_{rRms} = 1.17$  ksi (7.3 MPa). This corresponds to an ADTT of about 4,300 trucks per day. This rate of loading would result in crack propagation through the web thickness in about ten years. The estimated life is in reasonable agreement with the performance of the bridge. The structure was subjected to cyclic stress from 1964 until discovery in 1973 a nine year interval.

After the fatigue crack penetrated the web a through thickness crack results and the stress intensity is defined as

$$K = \sigma \sqrt{\pi a} \quad (5-4)$$

Since two continuous fillet welds connected the longitudinal stiffener to the web the stress at the crack would equal the yield point due to residual tensile stresses. This would result in a K value of about  $40 \text{ ksi}\sqrt{\text{in.}}$  ( $44 \text{ MPa}\sqrt{\text{m}}$ ). The fracture toughness  $K_{Ic}$  can be estimated from the CVN values given in Figure 5-32. At  $0^\circ\text{F}$  ( $-18^\circ\text{C}$ ) a value of about  $25\text{-}30 \text{ ksi}\sqrt{\text{in.}}$  ( $27.5\text{-}33.0 \text{ MPa}\sqrt{\text{m}}$ ) results. Considering the possible beneficial effect of a slower strain rate still results in a K value that exceeds the fracture toughness of the girder web. It is visually apparent in Figures 5-23 and 5-24 that a cleavage fracture occurred. Observations of the fracture surface (see Figure 5-23), indicated that the crack arrested near the bottom of the flange.

The crack ran out of a high residual tensile stress region in the flange before arresting. Figure 5-30 shows an electron micrograph of the lower left-hand corner of the flange (see Figure 5-23) and shows a cleavage fracture mode still existing at that level. It is probable that the "brittle fracture" that occurred during Stage III (see Figure 5-31) occurred during the period of December 1972 - March 1973, when the material toughness would be decreased by low temperature. After Stage III of crack growth, subsequent cyclic loading during the balance of 1973 would result in fatigue crack propagation and enlargement of the flange crack until its discovery in November 1973.

It should be noted that substantial increases in fracture toughness would not have materially affected the behavior of this

girder. The random truck loading would have continued to grow the web crack in a stable manner until a critical crack length was reached.

## REFERENCES

1. J. W. Fisher, P. A. Albrecht, B. T. Yen, D. J. Klingerman, and B. M. McNamee, "Fatigue Strength of Steel Beams with Welded Stiffeners and Attachments," NCHRP Report 147, 1974, 85 pp.
2. M. A. Hirt and J. W. Fisher, "Fatigue Behavior of Welded Beams," Highway Research Record No. 400, 1972, pp. 4-15.
3. J. W. Fisher, "Guide to 1974 AASHTO Fatigue Specifications," American Institute of Steel Construction, 1974.
4. J. M. Barsom, "Investigation of Toughness Criteria for Bridge Steels," USS Research Laboratory Technical Report 97.018-001(5), February 1973.
5. J. M. Barsom and S. T. Rolfe, "Correlations Between  $K_{IC}$  and Charpy V-Notch Test Results in the Transition - Temperature Range," ASTM STP 466, ASTM, 1970.

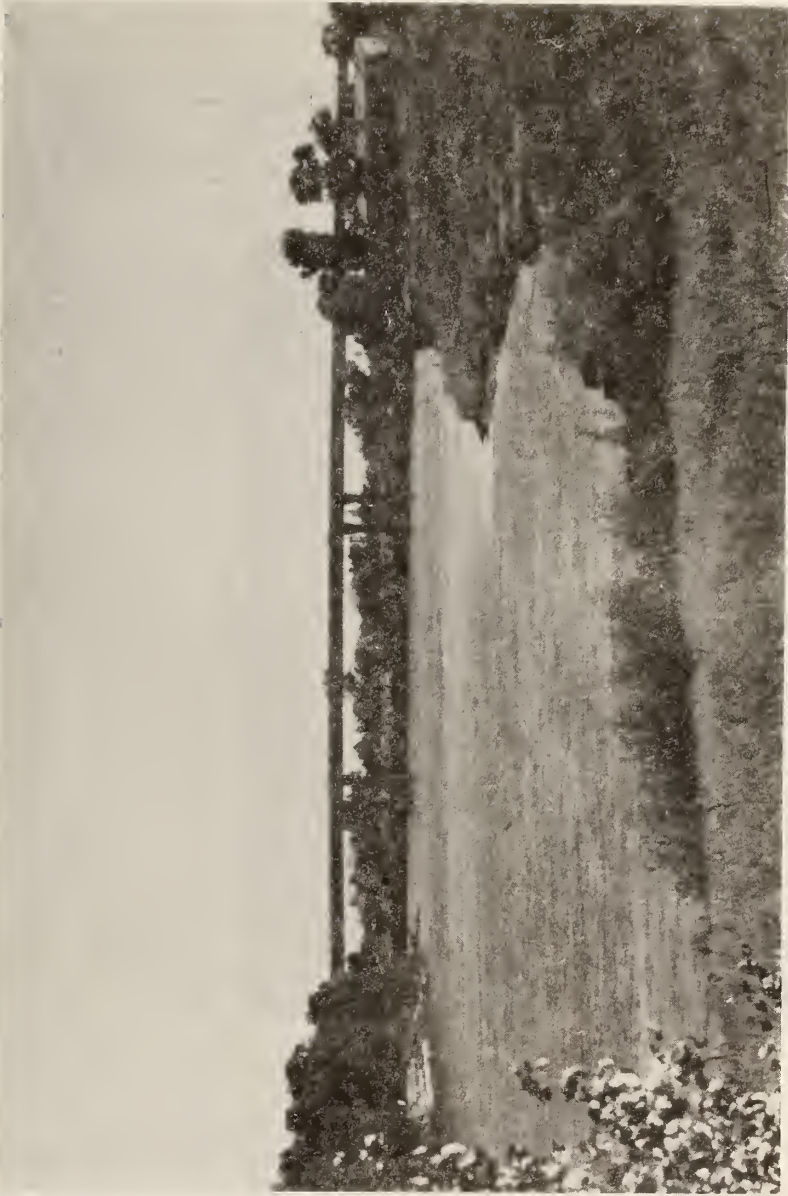


Figure 5-1 Overall view of Bryte Bend Bridge.



Figure 5-2 View of twin structures over river.

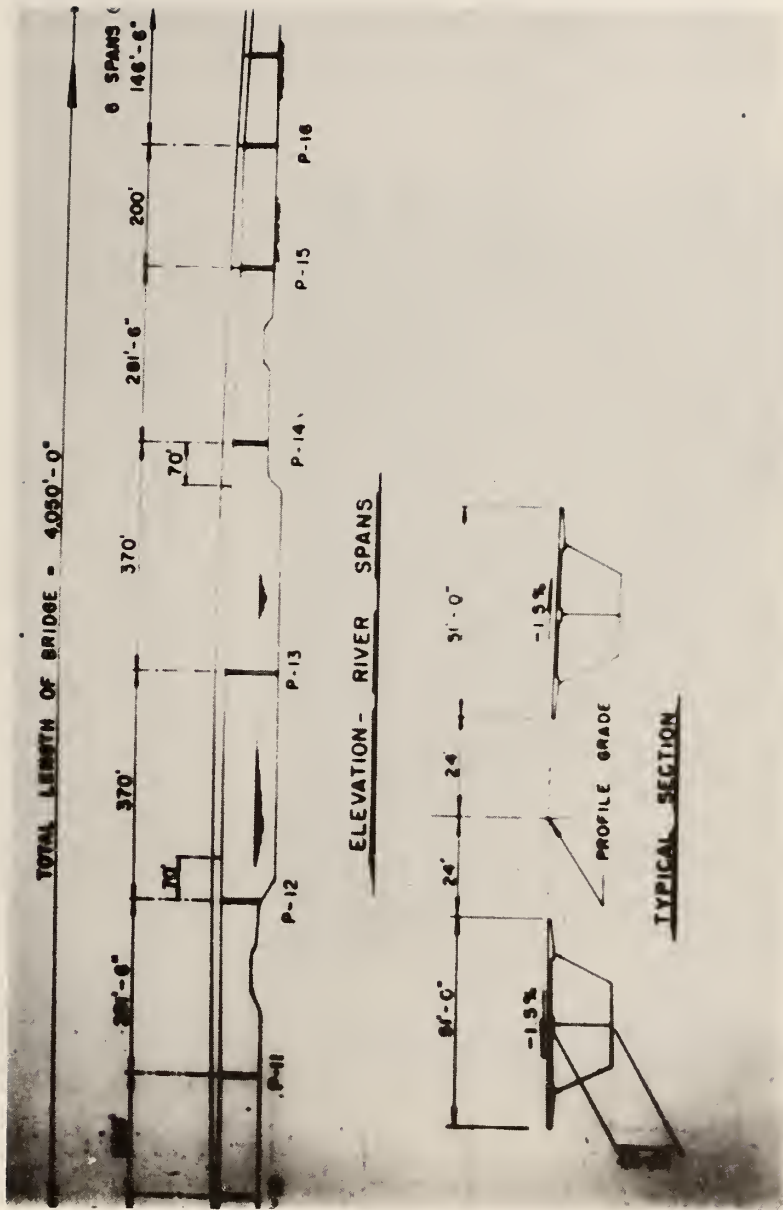


Figure 5-3 Section and elevation of 4050 ft. (1234 m) long structure.

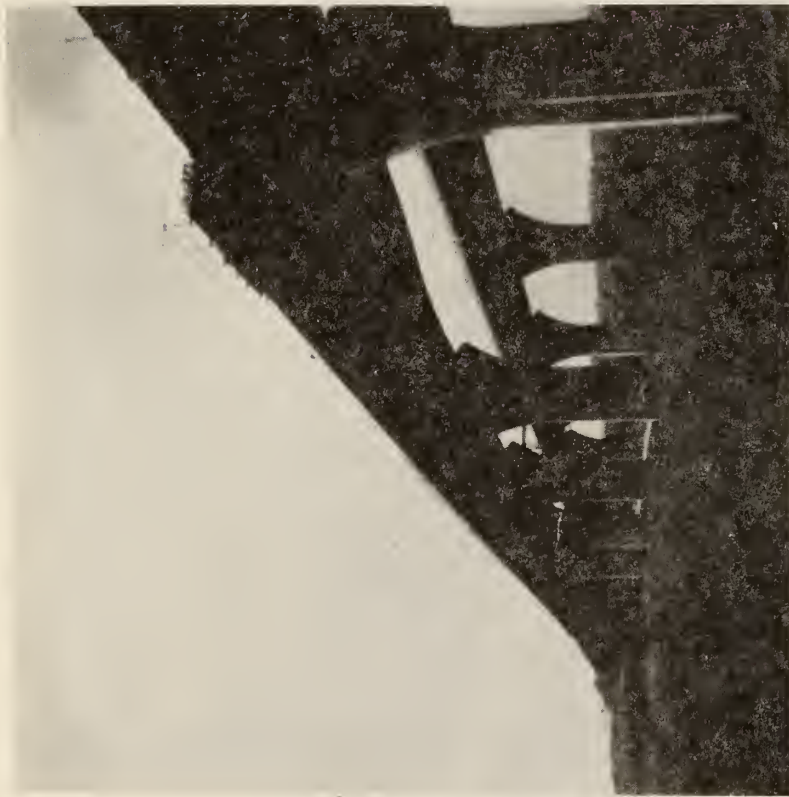


Figure 5-4 Transition region between simple approach spans and continuous bridge structure.





Figure 5-5 Cross-section of box girder.



Figure 5-6 Plan view of brittle fracture in flange.

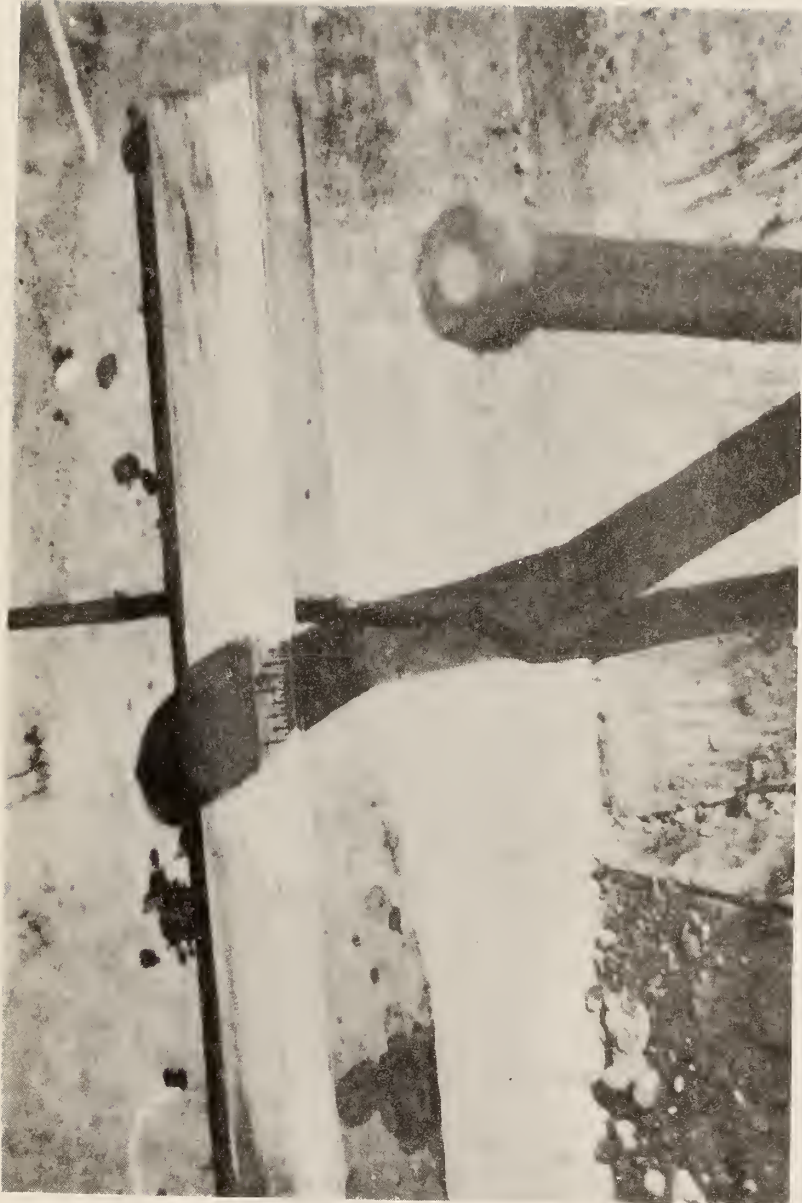


Figure 5-7 Brittle fracture origin at intersection of lateral attachment and flange plate.

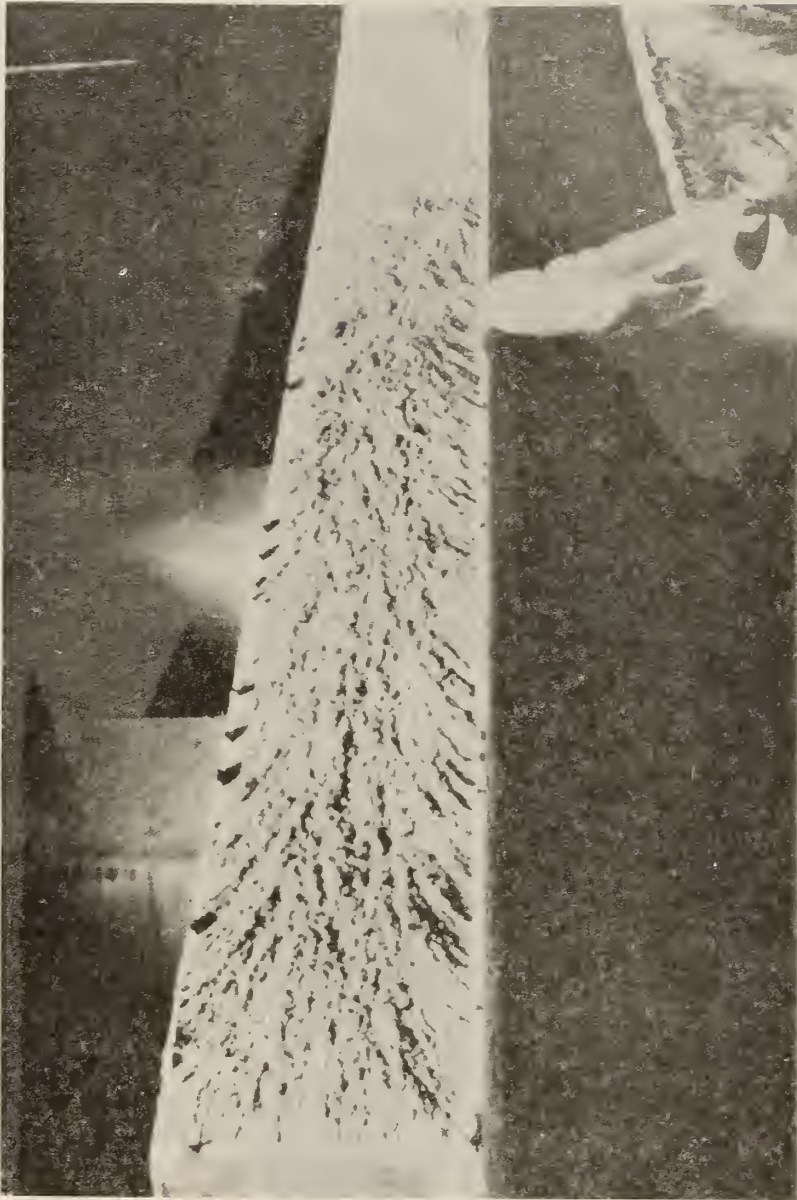


Figure 5-8 Brittle fracture surface showing classic herringbone pattern and small shear lips.



Figure 5-9 Origin of fracture showing 0.2-inch (5 mm) deep weld crack and 1.3 inch (33 mm) deep crack.

# $K_{Ic}$ TEST

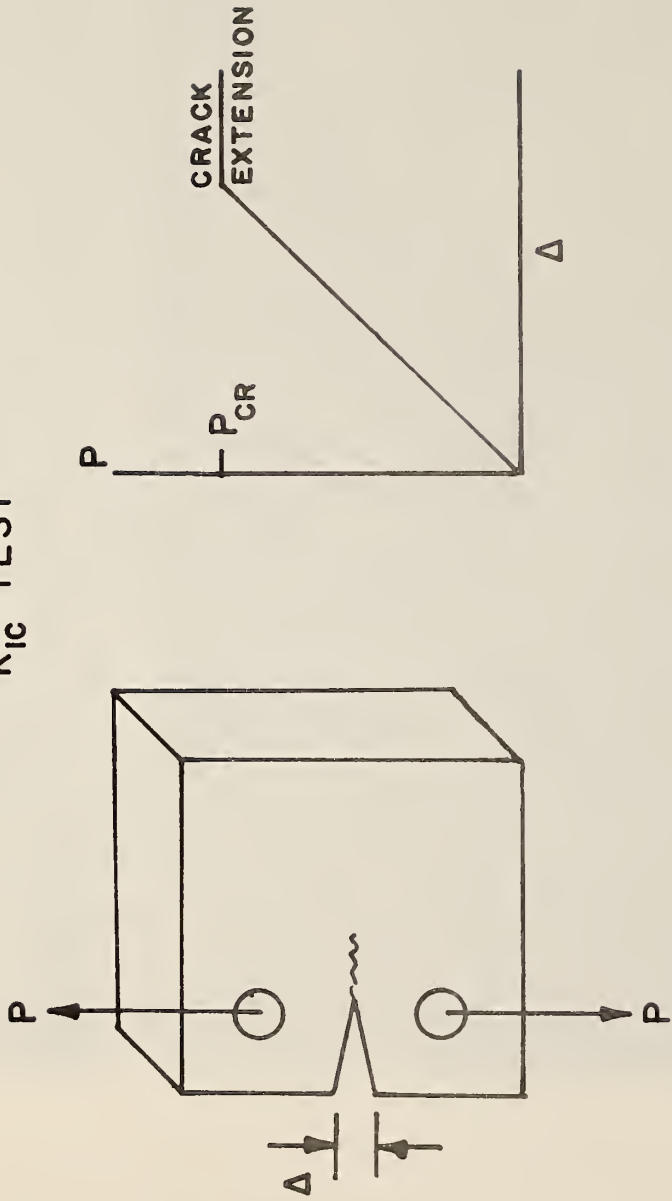


Figure 5-10 Schematic of  $K_{Ic}$  test specimen and P- $\Delta$  test record.

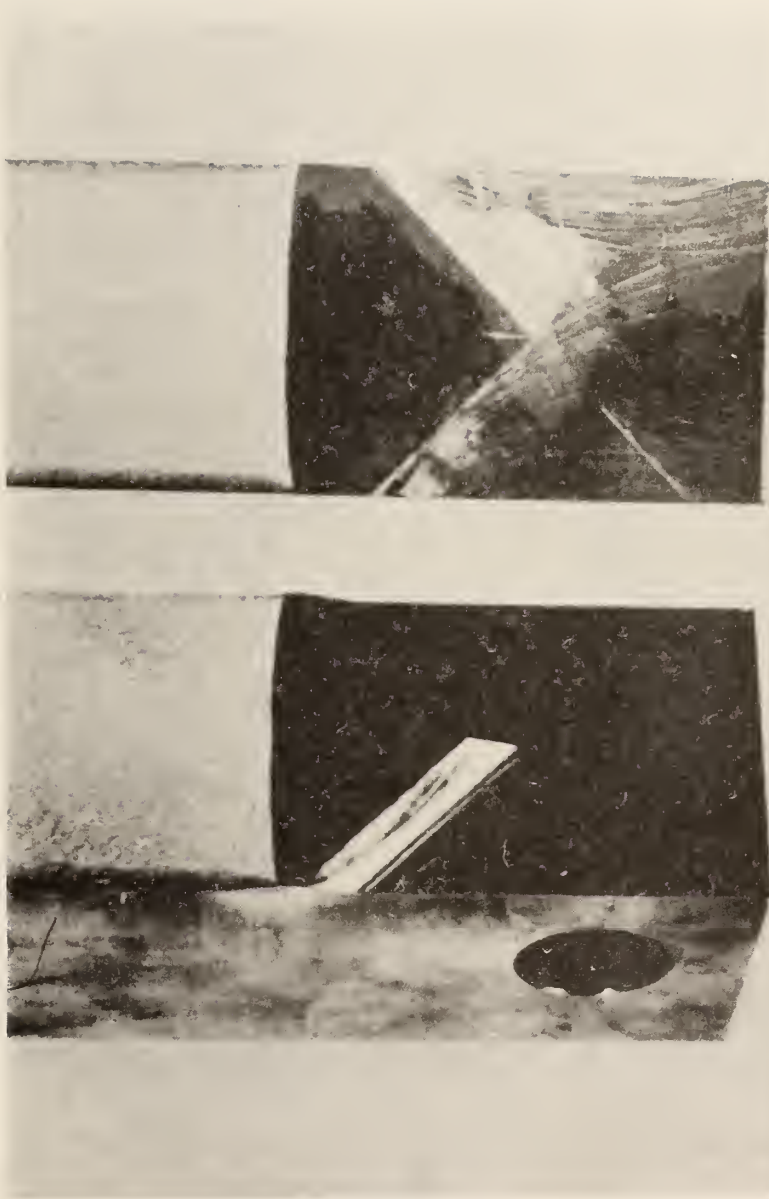


Figure 5-11 Actual fracture surface of  $K_{Ic}$  test specimen.

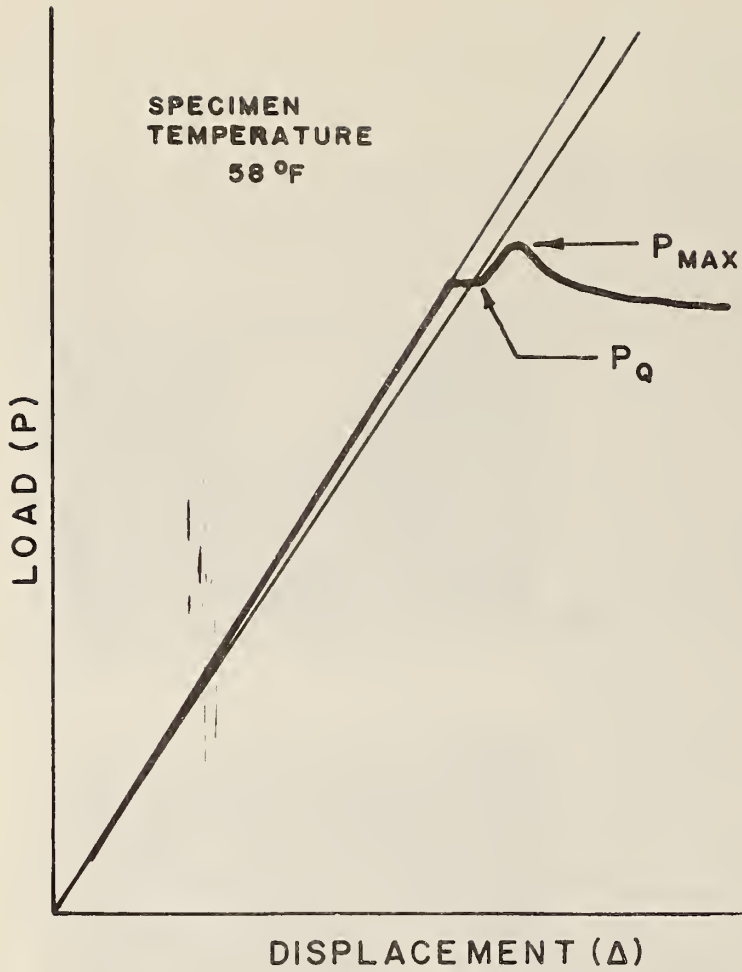


Figure 5-12 Actual P-Δ test record for  $K_{Ic}$  test specimen  
 —  $K_{Ic} = 55 \text{ ksi}\sqrt{\text{in.}}$  (60.5 MPa $\sqrt{\text{m}}$ ).



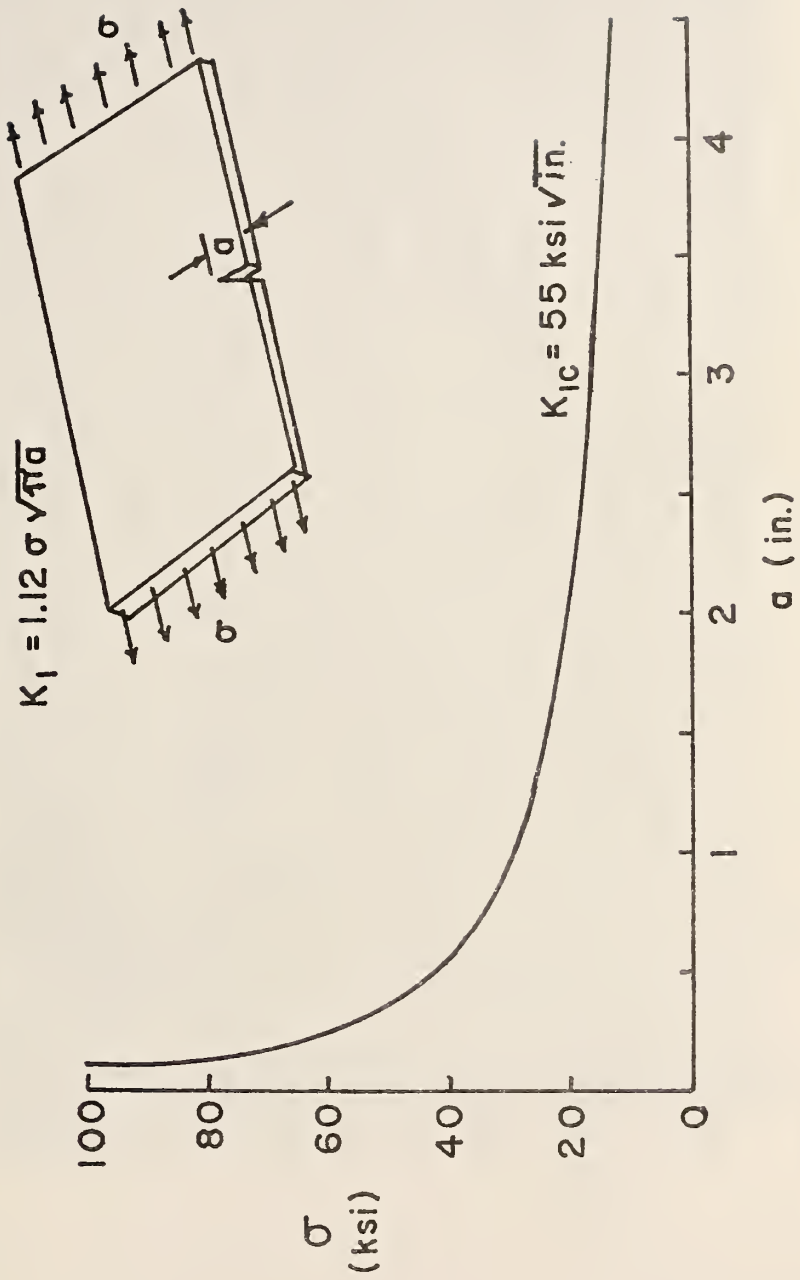


Figure 5-13 Stress-Flaw-Size relation for edge crack in steel with  $K_{IC} = 55 \text{ ksi} \sqrt{\text{in.}}$  ( $60.5 \text{ MPa} \sqrt{\text{m}}$ ).

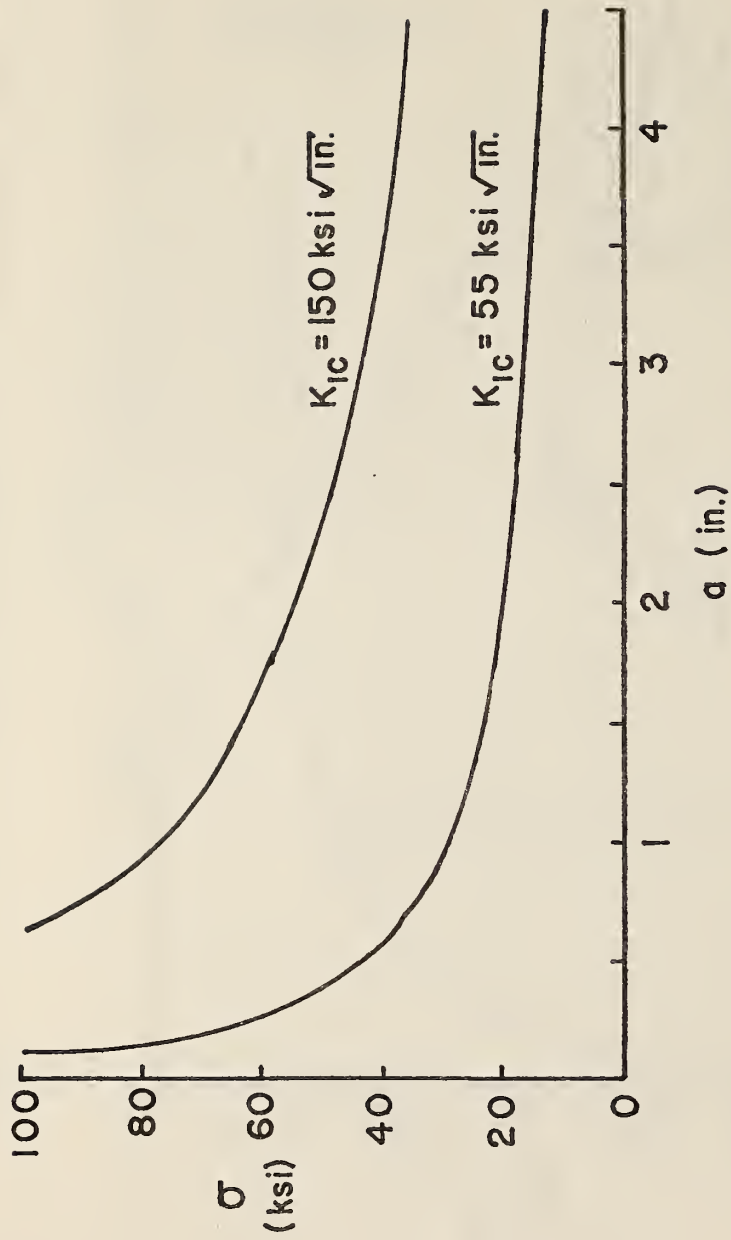


Figure 5-14 Stress-Flaw-Size relation for edge crack in steel with  $K_{IC} = 55$  and  $150 \text{ ksi}\sqrt{\text{in.}}$  ( $60.5$  and  $165 \text{ MPa}\sqrt{\text{m}}$ ).



Figure 5-15 Schematic showing location of additional flange plates.

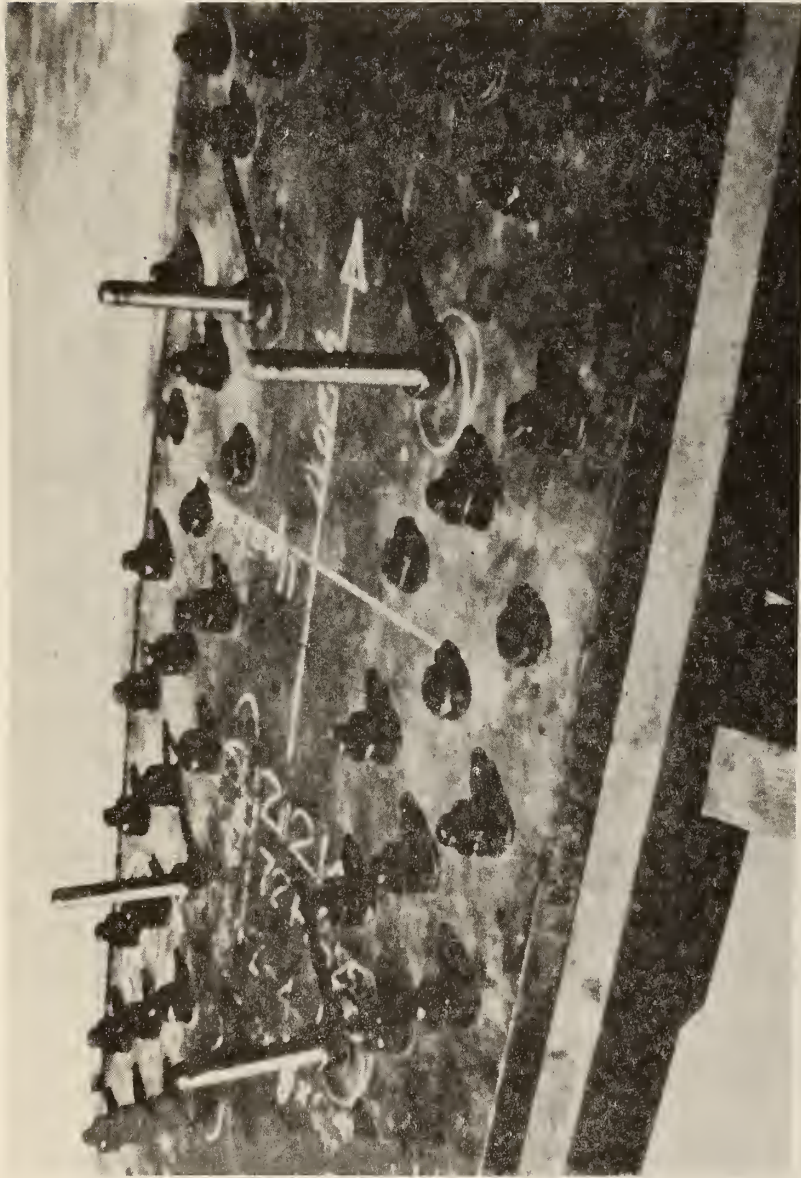


Figure 5-16 Closeup of additional plates attached to original flange plates.

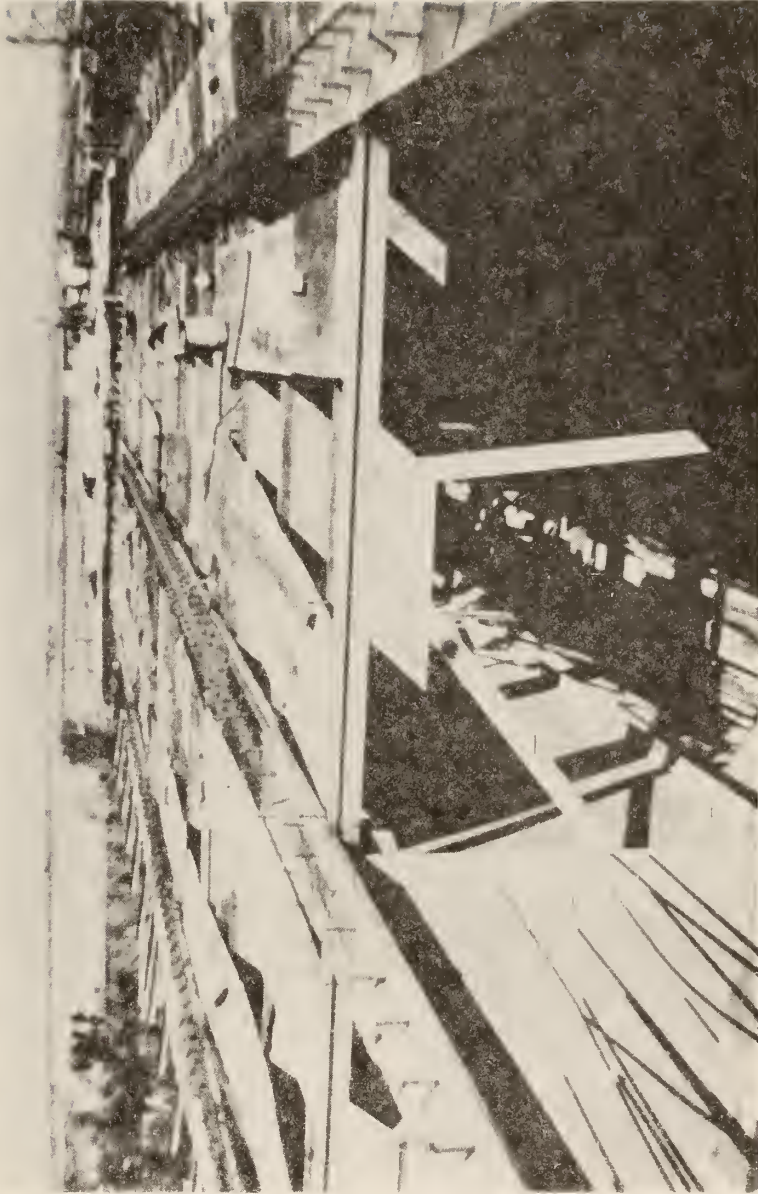


Figure 5-17 Overall view of additional plates extending back to zero stress region.

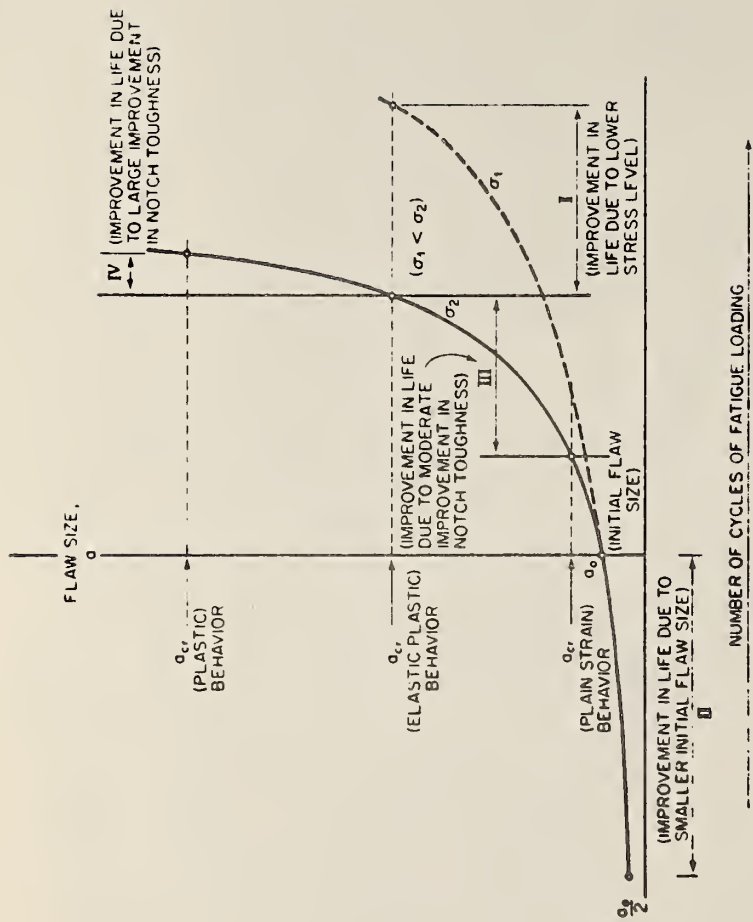


Figure 5-18 Schematic showing flaw size-fatigue life relations for various critical crack sizes.



Figure 5-19 Profile of Quinpiac River Bridge.



Figure 5-20 Crack in web of Fascia Girder.





Figure 5-21 Crack on bottom of beam flange.

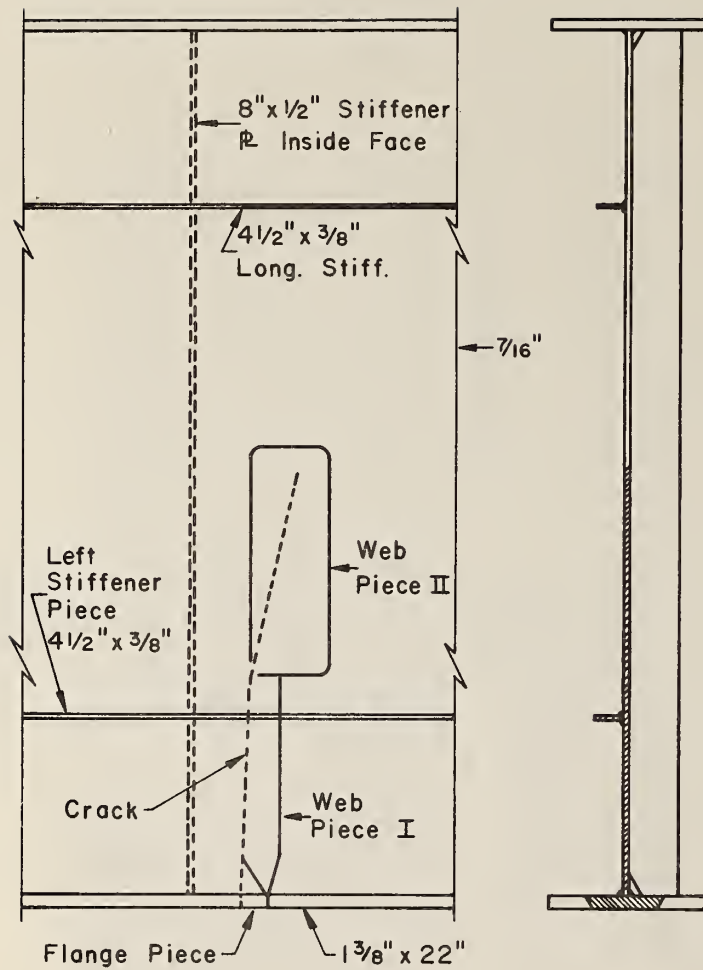


Figure 5-22 Schematic of girder showing sections removed for examination at crack.

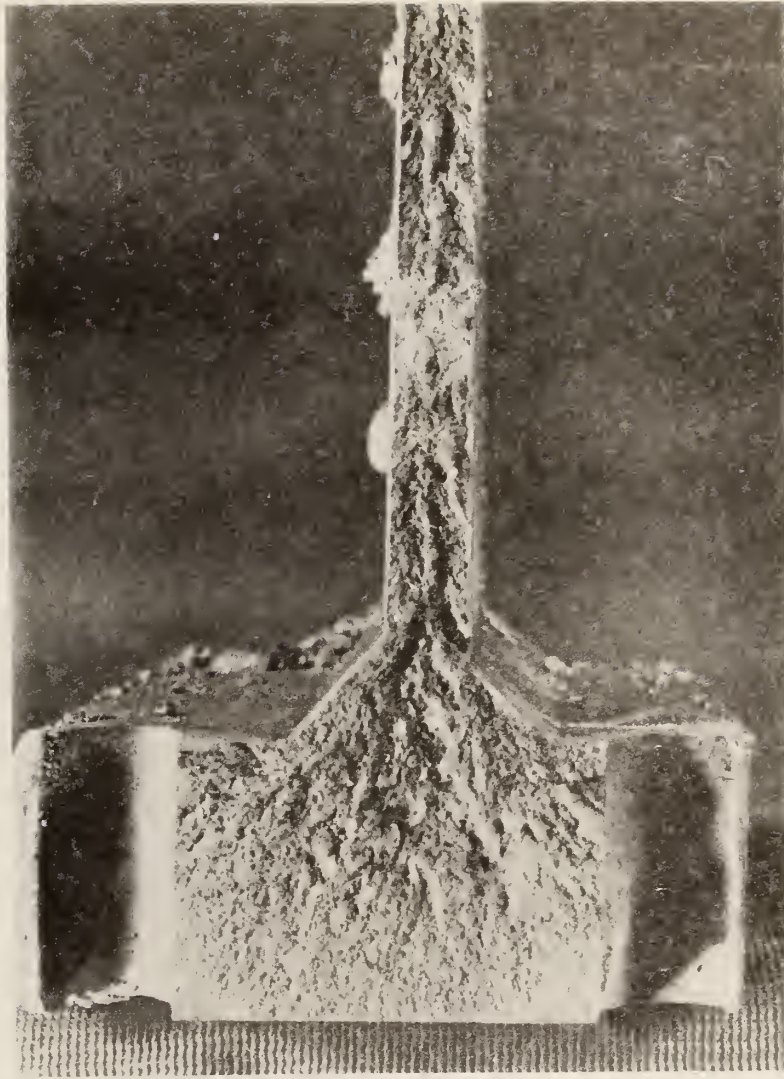


Figure 5-23 Fracture surface at flange-web junction.

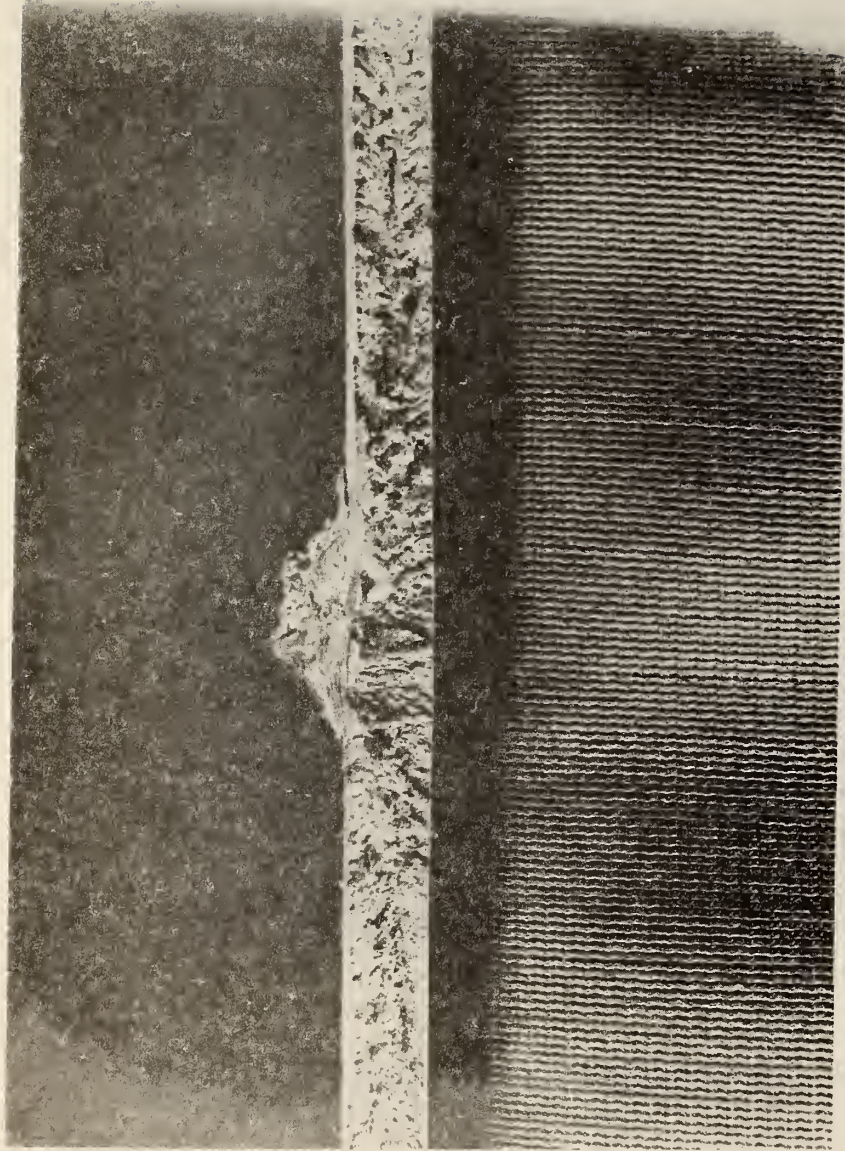


Figure 5-24 Fracture surface of web near longitudinal stiffener.

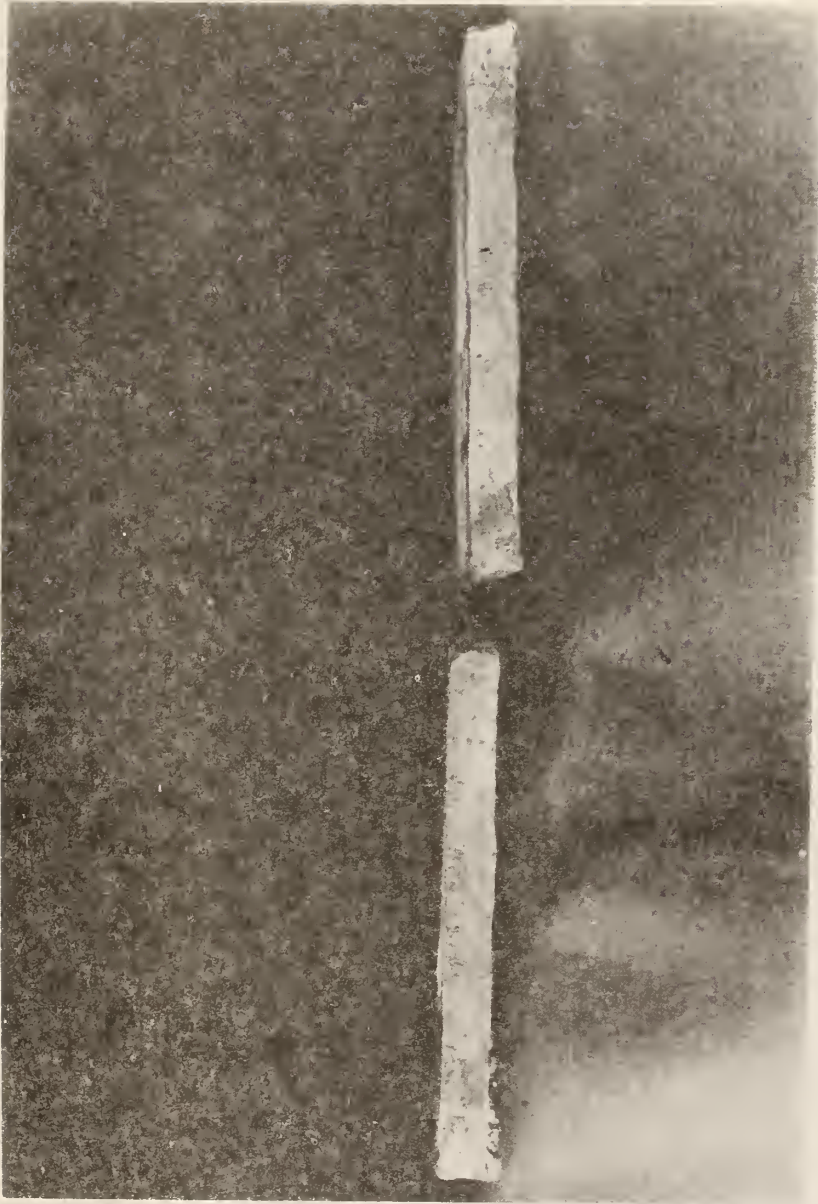


Figure 5-25 Ends of longitudinal stiffener at crack.



Figure 5-26 Fracture surface of longitudinal stiffener showing lack of penetration of transverse weld.

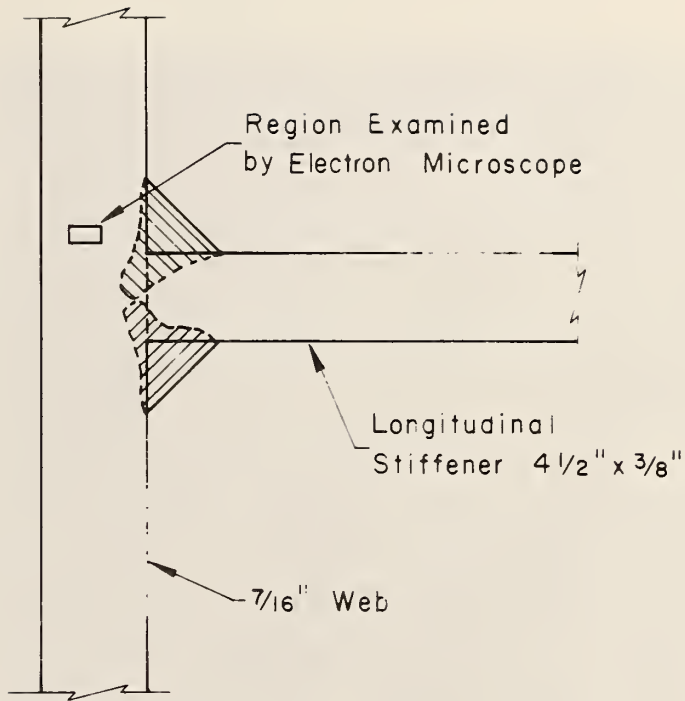


Figure 5-27 Schematic showing location examined by electron microscope.



Figure 5-28 Crack growth striations nearest longitudinal stiffener - 49125X.





Figure 5-29 Crack growth striations nearer web surface - 49125X.



Figure 5-30 Cleavage in flange near bottom surface - 4300X.

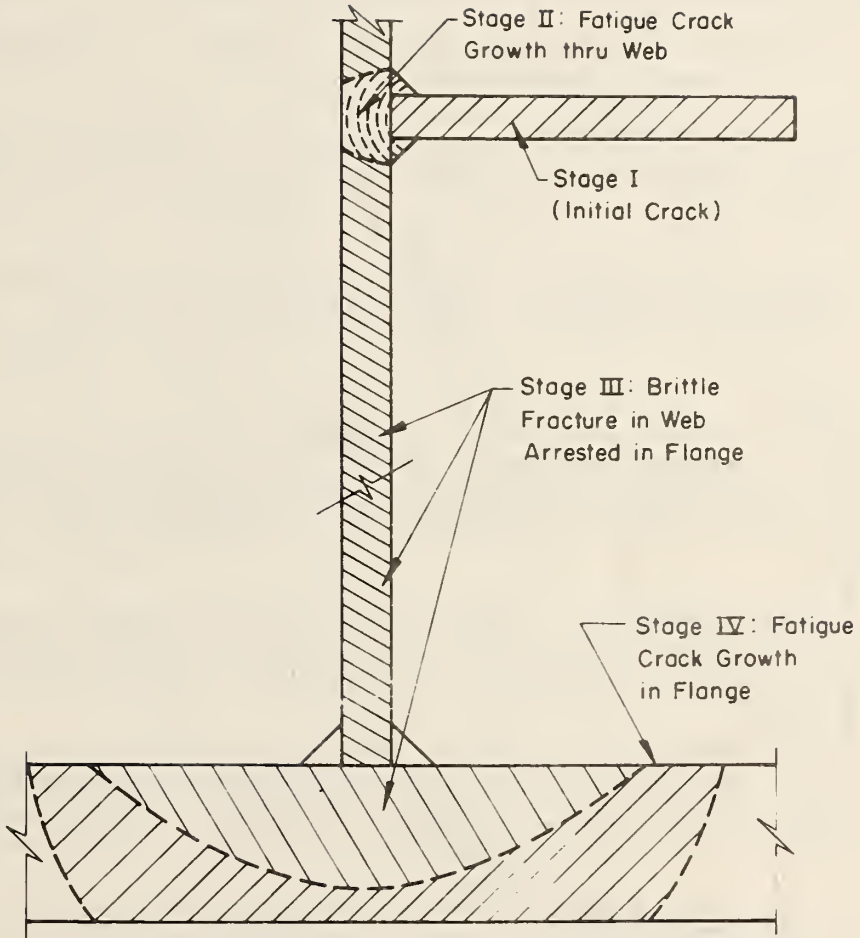


Figure 5-31 Schematic of crack growth stages.

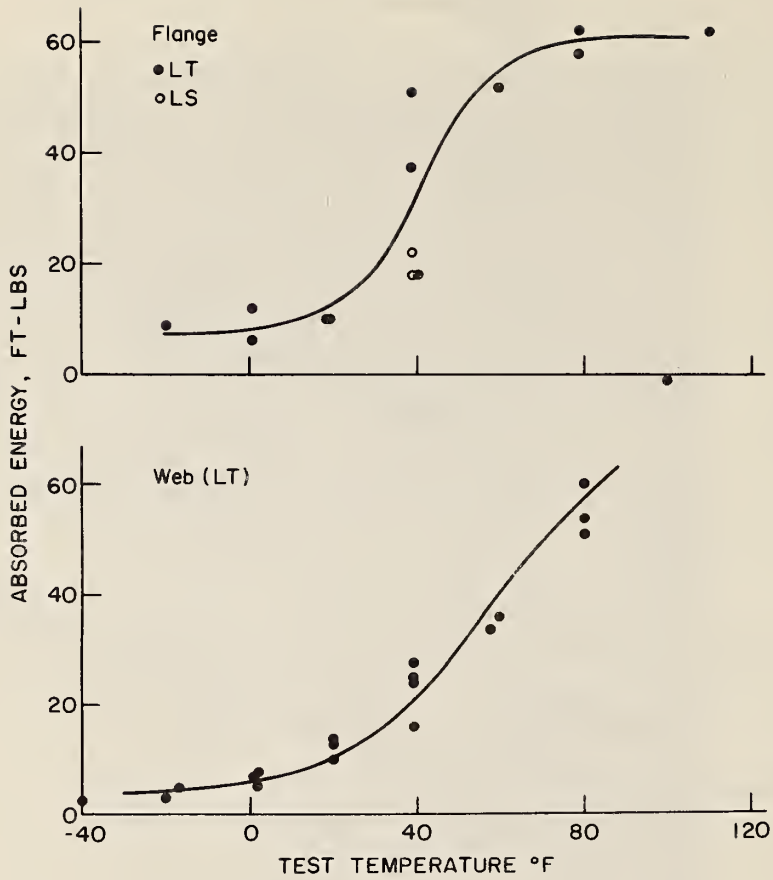


Figure 5-32 CVN results for web and flange adjacent to crack.

## GLOSSARY OF TERMS

1. Brittle Fracture is a type of catastrophic tensile failure in structural materials that usually occurs without prior plastic deformation and at extremely fast speeds.
2. Ductile Fracture is a type of fracture which is generally preceded by general yielding and large plastic deformations.
3. Toughness is defined as the ability of a smooth member to absorb energy, usually when loaded slowly.
4. Notch toughness is defined as the ability of a material to absorb energy in the presence of a flaw, usually when loaded dynamically.
5. To measure toughness, conduct a standard round bar tension test and record stress (psi) vs strain (in/in). The area under this stress-strain curve is the toughness of the material in psi.
6. To measure notch toughness, conduct an impact test of a notched bar and record the amount of energy the specimen absorbed (ft-lbs). Using the CVN impact test, the amount of energy absorbed is a measure of the notch toughness of the material in ft-lbs.
7. Fracture Mechanics is a method of quantitatively characterizing fracture behavior in structural parameters familiar to the engineer, namely stress and crack size.
8.  $K_I$  is the stress intensity factor for a mode I type crack opening and is dependent on crack geometry, flaw size, and stress level.  $K_I$  is a mathematical calculation and is not dependent on material properties.
9.  $K_{Ic}$  is the critical stress intensity factor for a mode I type crack opening and is a material property, at a given temperature and loading rate. It is a minimum value for thick plates.
10.  $K_{Ic}$  is the critical stress intensity factor for plane stress conditions and is a function of temperature, loading rate, and plate thickness.  $K_{Ic}$  approaches the minimum value for thick plates, namely  $K_{Ic}$ .
11. Yield strength,  $\sigma_{ys}$ , is the yield stress of a particular material while  $\sigma_{nominal}$  is some stress used for design or analysis which is usually below  $\sigma_{ys}$ .

12. Flaw size, a, is the measurement of the defect, such as a flaw or fatigue crack in a structural element.
13. Plane strain is the triaxial stress condition occurring in thick plates when stress is applied in one direction and strains are induced not only in the direction of the applied stress but also in the other two mutually perpendicular directions, according to Poisson's Ratio. Thick plates.
14. Plane stress is the biaxial stress condition occurring in most thin plates when the stress acting transversely to the plane of the plate is essentially zero. Thin plates.
15. The three levels of structural performance are as follows:
  - (1) Plane-strain behavior, which refers to fracture under elastic stresses with little or no shear lip development and it is essentially brittle.
  - (2) Plastic behavior, which refers to ductile fracture under general yielding conditions accompanied usually, but not necessarily with large shear lips.
  - (3) Elastic-plastic behavior, which refers to a mixed mode type of failure because it is a combination of the first two types of behavior.
16. Sub-critical crack growth is the cracking or crack growth in a material where the flaw size is below the critical flaw size for that material. This can occur by fatigue, stress corrosion, or a combination of the two.
17. A fracture criterion is a standard against which the expected fracture behavior of a structure can be judged.
18. A fracture control plan is a detailed procedure used to:
  - (1) identify all the factors that may contribute to the fracture of a structural detail or the failure of the entire structure.
  - (2) assess the contribution of each factor and the synergistic contribution of these factors to the fracture process.
  - (3) determine the relative efficiency and trade-offs of various methods to minimize the possibility of fracture.
  - (4) assign responsibility for each task that must be undertaken to ensure the safety and reliability of the structure.

19. Stress intensity range,  $\Delta K$  is the difference between the minimum and maximum  $K_I$  values applied during fatigue. Analagous to the fatigue stress range,  $\Delta\sigma$ , except that the flaw size,  $a$ , must be known also.







TE662

.A3

no. FHWA-RD-

78-68

BORROWE

Form DOT F 172  
FORMERLY FORM DC

## FEDERALLY COORDINATED PROGRAM OF HIGHWAY RESEARCH AND DEVELOPMENT (FCP)

The Offices of Research and Development of the Federal Highway Administration are responsible for a broad program of research with resources including its own staff, contract programs, and a Federal-Aid program which is conducted by or through the State highway departments and which also finances the National Cooperative Highway Research Program managed by the Transportation Research Board. The Federally Coordinated Program of Highway Research and Development (FCP) is a carefully selected group of projects aimed at urgent, national problems, which concentrates these resources on these problems to obtain timely solutions. Virtually all of the available funds and staff resources are a part of the FCP, together with as much of the Federal-aid research funds of the States and the NCHRP resources as the States agree to devote to these projects.\*

### *FCP Category Descriptions*

- 1. Improved Highway Design and Operation for Safety**

Safety R&D addresses problems connected with the responsibilities of the Federal Highway Administration under the Highway Safety Act and includes investigation of appropriate design standards, roadside hardware, signing, and physical and scientific data for the formulation of improved safety regulations.
- 2. Reduction of Traffic Congestion and Improved Operational Efficiency**

Traffic R&D is concerned with increasing the operational efficiency of existing highways by advancing technology, by improving designs for existing as well as new facilities, and by keeping the demand-capacity relationship in better balance through traffic management techniques such as bus and carpool preferential treatment, motorist information, and rerouting of traffic.
- 3. Environmental Considerations in Highway Design, Location, Construction, and Operation**

Environmental R&D is directed toward identifying and evaluating highway elements which affect the quality of the human environment. The ultimate goals are reduction of adverse highway and traffic impacts, and protection and enhancement of the environment.
- 4. Improved Materials Utilization and Durability**

Materials R&D is concerned with expanding the knowledge of materials properties and technology to fully utilize available naturally occurring materials, to develop extender or substitute materials for materials in short supply, and to devise procedures for converting industrial and other wastes into useful highway products. These activities are all directed toward the common goals of lowering the cost of highway construction and extending the period of maintenance-free operation.
- 5. Improved Design to Reduce Costs, Extend Life Expectancy, and Insure Structural Safety**

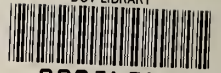
Structural R&D is concerned with furthering the latest technological advances in structural designs, fabrication processes, and construction techniques, to provide safe, efficient highways at reasonable cost.
- 6. Prototype Development and Implementation of Research**

This category is concerned with developing and transferring research and technology into practice, or, as it has been commonly identified, "technology transfer."
- 7. Improved Technology for Highway Maintenance**

Maintenance R&D objectives include the development and application of new technology to improve management, to augment the utilization of resources, and to increase operational efficiency and safety in the maintenance of highway facilities.

\* The complete 7-volume official statement of the FCP is available from the National Technical Information Service (NTIS), Springfield, Virginia 22161 (Order No. PB 242057, price \$45 postpaid). Single copies of the introductory volume are obtainable without charge from Program Analysis (HRD-2), Offices of Research and Development, Federal Highway Administration, Washington, D.C. 20590.

DOT LIBRARY



00056361

